DISCLAIMER NOTICE

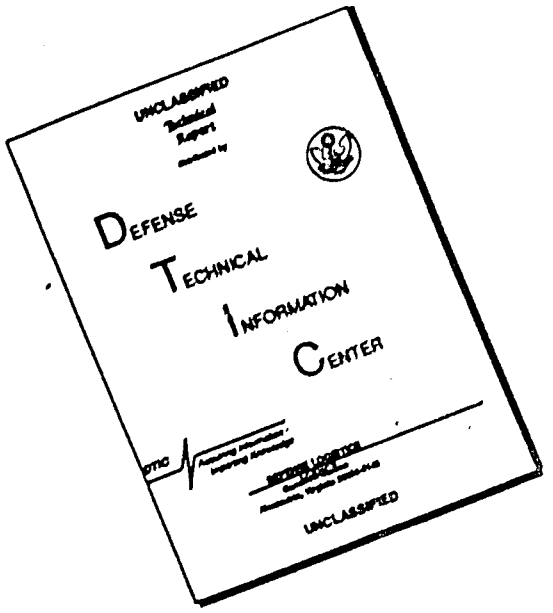

THIS DOCUMENT IS BEST QUALITY AVAILABLE. THE COPY FURNISHED TO DTIC CONTAINED A SIGNIFICANT NUMBER OF PAGES WHICH DO NOT REPRODUCE LEGIBLY.

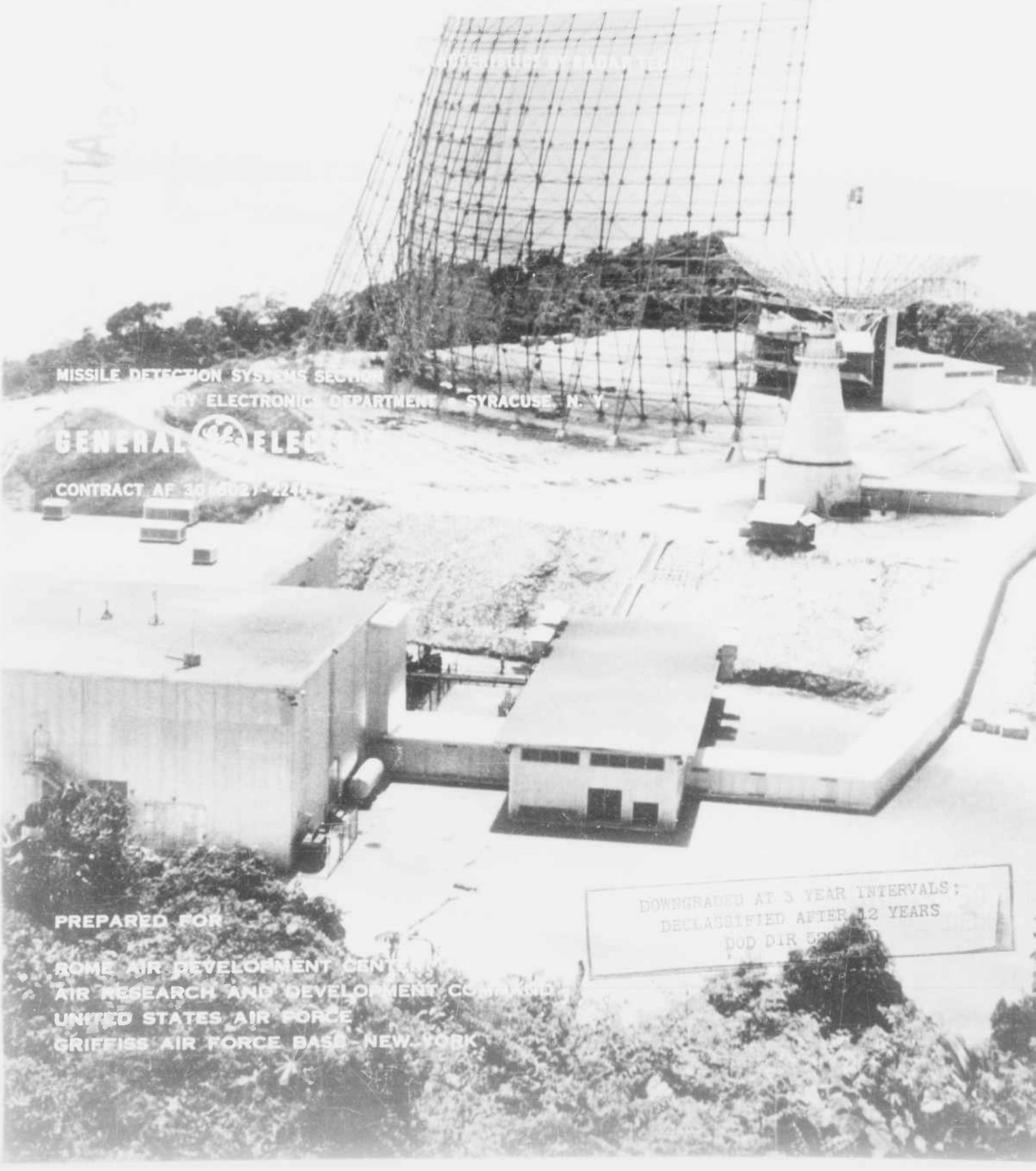

RADC-TN-61-140

RADC TRINIDAD TEST SITE
QUARTERLY TECHNICAL NOTE
VOLUME IV
A STUDY OF IONOSPHERIC AND LUNAR CHARACTERISTICS BY RADAR TECHNIQUES

Phase I, Item 9
Contract No. AF30(602)-2244

Prepared by

Missile Detection Systems Section
HEAVY MILITARY ELECTRONICS DEPARTMENT
General Electric Company
Syracuse, New York

31 October 1960

For

Rome Air Development Center
AIR RESEARCH AND DEVELOPMENT COMMAND
United States Air Force
Griffiss Air Force Base
Rome, New York

TABLE OF CONTENTS

LIST OF ILLUSTRATIONS

LIST OF ILLUSTRATIONS-continued

LIST OF ILLUSTRATIONS-continued

RADC TRINIDAD TEST SITE
QUARTERLY TECHNICAL NOTE
VOLUME IV
A STUDY OF IONOSPHERIC AND LUNAR CHARACTERISTICS
BY RADAR TECHNIQUES

I. INTRODUCTION

A. GENERAL

The first radio reflections from the moon, using conventional radar techniques, were recorded at a frequency of 111.5 megacycles at moonrise and moonset by the U.S. Army Signal Corps.[1] A more complete description of the Signal Corps results are described by DeWitt and Stodola.[2] In order to obtain the required sensitivity, a receiver bandwidth of about 50 cps, transmitter pulse length of 0.25 second and a transmitter peak power of three kilowatts were used. The experimental results showed that the returned echo amplitude was often times less than the theoretically computed one and, on occasions, could not be detected. In addition, the signal amplitude under went unexpected fluctuations having periods of several minutes which were attributed to anomalous ionospheric refraction.

At approximately the same time as the Signal Corps observations, Bay also reported that radar contact had been made with the moon at a frequency of 120 megacycles.[3] These measurements indicated a power reflection coefficient, for the moon's surface, of the order of 0.1.

Kerr, Shain and Higgins[4] of Australia performed the moon reflection experiment at 21.5 megacycles, during moonrise and moonset, mainly to study the characteristics of low angle propagation through the ionosphere. Their records[5] indicated a rather slow amplitude fluctuation rate which also was attributed to ionospheric refraction phenomena. The rapid amplitude fluctuations having periods of a few seconds were explained by assuming that the moon's surface consisted of many random scatterers in relative motion, brought about by the moon's libration. This phenomenon, together with the evidence that the received pulse was stretched out several times the length of the (one-millisecond) transmitted pulse, showed that the moon was a "rough" reflector at their frequency.

The first successful transmissions at UHF using the moon as a relay station were accomplished by Sulzer, Montgomery and Gerks.[6] CW radio signals at a frequency of 418 megacycles were relayed from Cedar Rapids, Iowa to Sterling, Virginia. It was found that the signal was subject to severe fading, its amplitude varying from the receiver noise level to occasional peaks as high as 10 db above the noise.

Measurements of radar-lunar echoes by Evans[7] at 120 megacycles, by Trexler[8] at 198 megacycles and by Yaplee, Bruton, Craig and Roman[9] at 2860 megacycles revealed that radar reflection takes place within a small area at the center of the moon's surface, the radius of which is approximately one-third the radius of the moon. These results confirmed that the moon appeared to be a quasi-smooth reflector at radio wave frequencies.

The characteristics of lunar echoes such as libration fading of the order of two to three cps and pulse lengthening to approximately one lunar radius have recently been noted by investigators operating in the 400 to 440-mc frequency range.[10, 11] The latter phenomenon indicated the possibility that the rear portion of the moon behaved as a rough scatterer.

The employment of radar techniques to reflect signals off the moon's surface for studing the characteristics of the ionosphere by means of the Faraday effect was first reported by Browne[12] and Evans.[13, 14] Their equipment consisted of a 10-kw peak power transmitter, operating with a 30-millisecond pulse length and a pulse repetition frequency of 0.6 pulses per second, and an antenna whose size was approximately 250 square meters. The degree of rapid echo amplitude fading was found to be due to the moon's libration and was a function of the position of the moon in its orbit. By comparing the slow signal amplitude fading on two close spaced frequencies, 120.0 megacycles ± 0.6 per cent, which was due to the rotation of the plane of polarization by the ionosphere, Evans[13, 14] was able to deduce the ionospheric electron content during periods when the moon crossed the meridian at Manchester, England.

Bauer and Daniels[15] performed similar measurements at a frequency of 151.11 megacycles employing a bistatic radar system operating between Belmar, New Jersey and Urbana, Illinois. The absolute values of the total electron

content were evaluated from these measurements.

The lunar observations of Hill and Dyce[16] at Menlo Park, California on 106.1 megacycles, however, did not permit an accurate determination of the electron content because of the ambiguity in resolving the number of polarization rotations of the wave.

B. STATEMENT OF PROBLEM

The analytical results of the radar-lunar measurements conducted at the U.S. Air Force Trinidad Test Site, WIF, (107.7° N, 61.6° W) during the period between January and July 1960 are herein reported. The objectives of the experimental program were to determine (1) the diurnal and also seasonal variation of the electron content in the ionosphere (2) the reflectivity characteristics of the moon's surface.

Transmissions were made at a frequency of approximately 425 megacycles utilizing linear (horizontal) polarization while the reflected lunar signals were simultaneously received on both the transmitted and orthogonal polarizations.

The moon was automatically tracked from moonrise to moonset on two of the experimental measurements while partial lunar orbits were observed on four other occasions. The date of observation of one of the partial lunar orbits corresponded to the time when the moon was at its maximum southern declination. The remaining five observations were conducted during the time when the moon was at its maximum northern declination.

II. THE DETERMINATION OF THE ELECTRON CONTENT IN THE IONOSPHERE

A. INTRODUCTION

Prior to the advent of rockets, space vehicles and high-powered radars, the determination of the characteristies of the ionosphere such as the distribution of electron density with height and the electron content was accomplished by vertieal incidence pulse sounders and radio star methods.[17] With the availability of these new techniques, the state of knowledge of the structure and composition of the ionosphere has been greatly enhanced.

Electron density profiles above the maximum ionization of the F-layer are readily obtainable from radio wave transmissions emanating from rockets[18, 19, 20, 21, 22,] and satellites[23, 24] from r-f probe-satellite measurements[25, 26] and by means of incoherent scattering of radio waves by free electrons.[27, 28, 29]

Radio signals from satellites undergoing doppler frequency changes,[30,31] and Faraday rotation effects[23, 24, 32] can be analyzed to yield the electron content in the ionosphere. In addition, the ionospheric electron eontent can also be deduced from radar reflections from the moon which display Faraday rotation fades.[13,14,15 16, 33]

In this section, the theory of analysis of radar-lunar amplitude data for determining the electron content in the intervening medium is briefly discussed.

B. FARADAY ROTATION

When a linearly polarized electromagnetie wave is propagated through an ionized medium immersed in a magnetic field, the plane of polarization undergoes a rotation. This phenomenon eommonly referred to as the Faraday effect is known to take place for radio waves traversing the ionosphere.

It can be shown (see Appendix A) that the amount of rotation experienced by a linearly polarized wave traversing a two-way path in the ionosphere can be represented by the function

$$\phi = \frac{4.7233 \times 10^{4}}{f_o^{2}} \int_{h_1}^{h_2} f(h)\, H \cos\theta\, N\, dh \qquad (1)$$

where $\emptyset$ is the rotation in radians, f_o is the transmission frequency in cps, H is the magnetic field intensity in gauss, N is the electron density in electrons per cubic centimeter, dh is the height differential in centimeters, and θ is the propagation angle, i.e., the angle between the direction of the earth's magnetic lines of force and the direction of electromagnetic propagation.

The function, f(h), which is basically the secant of the angle between the ray path and the zenith, is given by

$$f(h) = \frac{r_o + h}{\left[(r_o + h)^2 - (r_o \operatorname{Cos} E)^2\right]^{1/2}} \tag{2}$$

where r_o is the radius of the earth and E is the elevation angle of the antenna beam.

Equation (1) is representative of the quasi-longitudinal mode of propagation. For frequencies in the 425-mc range, this relationship is valid for $0° \leq \theta \leq 89°$.

It should be noted that, for transmissions to the moon, the total angular rotation, $\emptyset$, is ambigous in that

$$\emptyset = n\pi \pm \Delta\emptyset \tag{3}$$

where n is a positive integer. The parameter, $\Delta\emptyset$, is the acute polarization angle normally indicated in a radar-lunar measurement and is defined by

$$\Delta\emptyset = \operatorname{Tan}^{-1}\left[\frac{A_o}{A_T}\right] \tag{4}$$

where A_o and A_T are the amplitudes of the signals received on the orthogonal and transmitted polarization channels, respectively.

One method for resolving the ambiguity of the complete number of polarization rotations is to employ two closely spaced frequencies. From the lunar-echo amplitude fading patterns recorded at the two frequencies it is possible to infer the electron content in the ionosphere. This technique was employed by Evans.[13, 14]

Since only one frequency was available in the Trinidad radar-lunar experiment, it was necessary to consider various methods for resolving the ambiguity problem. It was shown in a preliminary analysis of the experimental data that it was possible, by a process of elimination, to arrive at a somewhat reasonable solution to the polarization ambiguousness.[33] This was based on the correlation of the ionospheric electron content, deduced from the radar-lunar amplitude data, with the electron content up to the F-layer maximum derived from vertical incidence ionospheric soundings.

The analysis of the data presented in this study has been modified to some extent from the earlier published results.[33] That is, instead of indirectly arriving at a solution to the ambiguity problem by a process of elimination, theoretical estimates are made of the expected angular rotation along various earth-moon paths. These data, in turn, are compared with the experimental observations. The measured angluar rotation as defined by Equation (3) which best correlates with the theoretical calculation is then selected for the parameter to be used in evaluating the electron content along the ray path.

For all lunar orbits traversing paths north of Trinidad, i.e., moonrise occurring at an azimuth angle less than 90 degrees and moonset at an azimuth angle greater than 270 degrees, the electron density profiles evaluated from vertical incidence ionospheric sweep frequency soundings recorded at the National Bureau of Standards' Puerto Rico station were employed in the computation of the theoretical Faraday rotation. The electron densities deduced from the National Bureau of Standards ionospheric sounder station, Bogota, Colombia, were used in the analysis of the lunar southerly orbital path, i.e., moonrise occuring at an azimuth angle greater than 90 degrees and moonset at an azimuth angle less than 270 degrees. The loci of points of the lunar orbits, as projected on the earth's surface from 100-km and 500-km altitudes, are illustrated in Figure 1.

The virtual height versus frequency records of the Puerto Rico ionospheric sounder were converted into true height versus electron density profiles by means of the Budden matrix technique[34], the coefficients of the matrix being furnished by E.R. Schmerling of the Ionosphere Research Laborabory, the Pennsylvania State University. The ionosonde data recorded at Bogota were

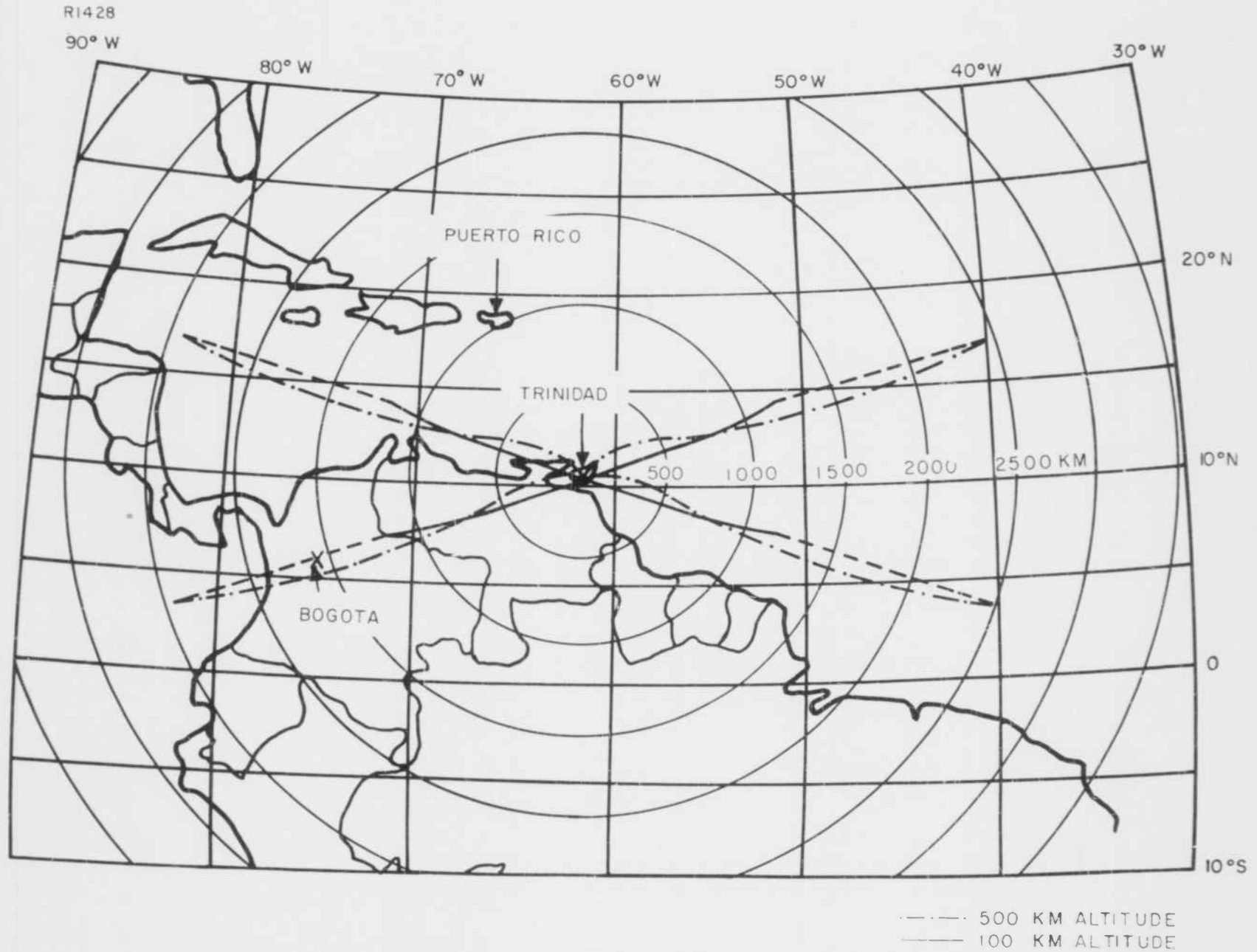

Figure 1. Locus of Points of the Moon's Orbit at Maximum Declination as Viewed from Trinidad

reduced to true height-electron density profiles by J.W. Wright of the Central Radio Propagation Laboratory, National Bureau of Standards.

Since sweep frequency sounders are capable of only yielding the characteristics of the ionosphere up to the height of maximum ionization of the F-layer, it was necessary to postulate a model above this region for the Faraday calculations. As a first approximation, it was assumed that, above the F-layer maximum, the distribution of electron density with height (under equilibrium conditions followed a Chapman model expressed by the function

$$N = N_m e^{1/2\left[1 - Z - e^{-Z}\right]} \tag{5}$$

where N_m is the electron density at the level of maximum ionization and Z is the normalized height.

The normalized height is given by

$$Z = \frac{h - h_m}{H'} \tag{6}$$

where h_m is the height of maximum ionization. The scale height, H', which is the height of the homogeneous atmosphere at a given temperature, is defined by

$$H' = \frac{KT}{mg} \tag{7}$$

where K is Boltzmann's constant (1.38×10^{-16} erg/degree Kelvin); T, the temperature in degrees Kelvin; m, the mean molecular mass of air (4.8×10^{-23} gm); and g, the gravitational constant (980.2 cm/sec^2).

It should be noted that the scale height associated with the Chapman expression, Equation (5), is that of the neutral particles. In this study, a constant scale height of 80 kilometers was assumed for all the electron density distributions above the F region.

According to Equation (1), the magnitude of the angular rotation encountered by a linear polarized wave transmitted through the ionsophere is proportional to H Cos θ where H is the magnetic field intensity and θ is the propagation angle.

It can be shown [35] that

$$\theta = \cos^{-1}\left[- \cos e \sin I - \sin e \cos I \cos (\gamma - D) \right] \qquad (8)$$

where I and D are the magnetic inclination and declination angles, respectively. These parameters specify the direction of the total magnetic intensity vector in space.

The angle, γ, is the geographic azimuth bearing of the observer's location measured with respect to the subionospheric point, i.e., the location on the earth's surface directly underneath the particular point in space. The angle, e, is simply given by

$$e = \sin^{-1}\left[\frac{r_o}{r_o + h} \cos E \right] \qquad (9)$$

where h is the height of the point in space above the earth's surface; r_o and E are previously defined in Equation (2).

The calculations of H and θ, as reported in the preliminary results of the Trinidad data[33], were based on the assumption that the earth's magnetic field may be approximated by a centered magnetic dipole having a geomagnetic pole at 78.6° N and 70.1° W.

The technique employed in evaluating H and θ in this report is as follows: the parameters, H, I and D have been scaled in 2.5-degree and 5.0-degree latitude and longitude steps over the whole earth's surface from isomagnetic maps issued by the U.S. Navy Hydrographic Office and the Canadian Department of Mines and Technical Surveys. The ground-observed magnetic data, scaled from these maps, are stored in matrix form in an IBM-7090 digital computer. Linear interpolation is used for obtaining the values of the magnetic field elements at other geographic locations.

When traversing a path in the ionosphere, the angles I and D at the subionospheric point are assumed to be invariant at all heights. The magnetic field intensity at the point in space, on the other hand, is derived from the surface value which is assumed to decrease inversely as the cube of the distance

from the earth's center.

It is believed that this method for determining H and θ is far more accurate than that obtained by assuming a dipole model for the earth's magnetic field. The evaluation of the magnetic field elements based on spherical harmonic expansion[36,37] is another method which could be employed. However, utilization of such a sophisticated technique is believed not warranted in the Faraday rotation problem.

C. ELECTRON CONTENT DETERMINATION BY RADAR-LUNAR TECHNIQUE

Once the ambiguity of the total number of rotations defined by Equation (3) is resolved, it is then readily possible to determine the total electron content in the ionosphere.

For transmissions to the moon, Equation (1) can be modified to the form.

$$\emptyset = \frac{4.7233 \times 10^{4}}{f_o^2} \left[\int_o^{h_m} f(h)\, H \cos\theta\, N\, dh \; + \; \overline{\left[f(h)\, H \cos\theta \right]}_{h_m}^{\infty} \int_{h_m}^{\infty} N\, dh \right] \qquad (10)$$

where h_m is the height of the F-layer maximum and

$$\overline{\left[f(h)\, H \cos\theta \right]}_{h_m}^{\infty}$$

is the average value of the function, $f(h)H \cos\theta$, between the limits of the height of the F-layer maximum and the distance to the moon. As a first approximation, it is valid to assume that

$$\overline{\left[f(h)\, H \cos\theta \right]}_{h_m}^{\infty} \approx \overline{\left[f(h)\, H \cos\theta \right]}_{h_m}^{1000\ \text{km}}$$

since the contribution of the integrated electron density to the angular rotation of the wave is considered to be negligible above a height of 1000 km.[38]

The value of f(h) H Cos θ as viewed from Trinidad is plotted as a function of height in Figure 2 for various azimuth-elevation orientations of the northern and southern lunar orbits. It is evident that, at low angles of elevation, the function can vary over quite a wide range. As the elevation angle is decreased, there is a noticeable reduction in the spread of its value as a function of height.

Because of the extreme variation in magnitude at low elevation angles, it is necessary to retain f(h)H Cos θ within the integral up to the F-layer maximum height. Above this height, the function can be approximated by an average value taken between the F-layer maximum and the 1000 km height limits.

The electron content above the F-layer maximum can be expressed in terms of the electron content below the F-layer maximum by the constant K where

$$\int_{h_m}^{\infty} N \, dh = K \int_{o}^{h_m} N \, dh \qquad (12)$$

According to Nisbet[39] and Nisbet and Bowhill[22], a description of the ionosphere in terms of the constant K is not ideal since the electron content below the F-layer maximum, determined from ionograms may be in error due to an underestimation of 20 to 40 km of the true height of the F-layer maximum. The existence of this error which is prevalent during the night was disclosed from rocket measurements. The daytime observations of electron density profiles by Nisbet were in good agreement with those obtained from the true - height scaling of ionograms.

In concurrence with Evans and Taylor[40], the use of the ratio K will be maintained in this study because of the lack of a substitute parameter to describe the variations of electron content in the ionosphere.

Ross[31] has proposed that the simplest parameter that can be readily determined for describing electron content measurements is the equivalent slab

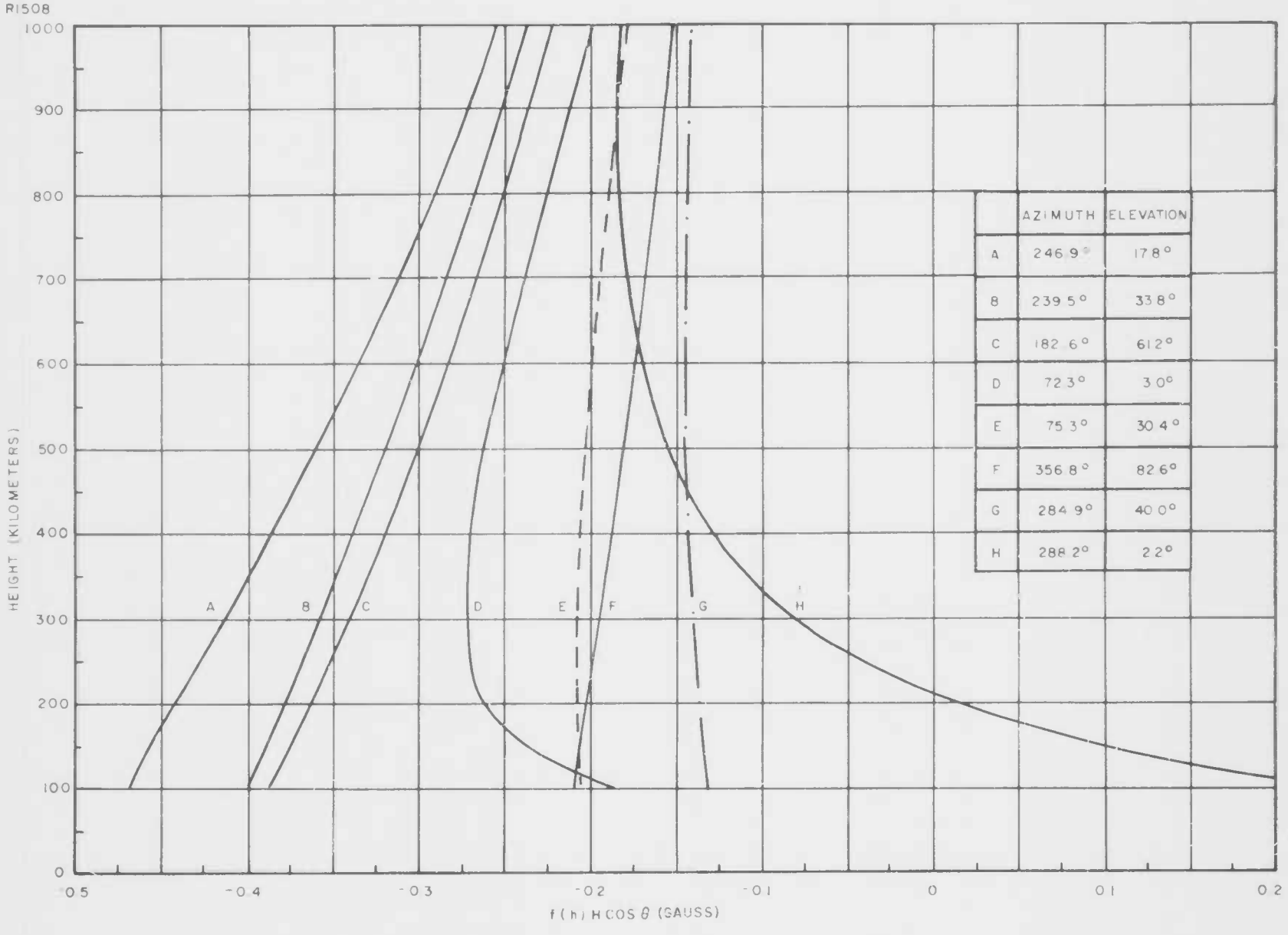

Figure 2. The Function, f(h) H Cos θ, as Viewed from Trinidad

thickness of the total ionosphere, τ, given by

$$\tau N_m = \int_0^{h_m} N \, dh + \int_{h_m}^{\infty} N \, dh \qquad (13)$$

where N_m is the maximum electron density of the F-layer. The first integral is the electron content below the peak of the F-layer evaluated from vertical incidence sounders while the second is the electron content deduced from Faraday rotation measurements (Equation (10)). It should be noted that τ is essentially the equivalent slab thickness of the F-layer.

Wright[41] has shown that, if the electron density distribution in the ionosphere is of the Chapman form, the total integrated electron content can then be expressed by

$$(4.133)\, H' N_m = \int_0^{\infty} N \, dh \qquad (14)$$

This relationship can be used to calculate the scale height, H', from the experimental data.

It is seen from Equations (13) and (14) that, for an assumed Chapman distribution of electrons, the equivalent slab thickness is simply related to the scale height by a constant factor of 4.133.

III. THE CHARACTERISTICS OF RADIO WAVES REFLECTED FROM THE MOON

A. INTRODUCTION

The characteristics of the moon as a radar target are determined almost entirely by the surface structure of the moon. Although large scale irregularities such as mountains and valleys are known to exist from optical observations, the small scale irregularities having dimensions of the order of a wavelength greatly influence the reflection of radio waves from its surface.

In addition to surface roughness, the relative velocity of the moon with respect to the earth and lunar libration are also important factors which contribute to the characteristics of the resultant echo. The results of such effects are evident by variations in pulse amplitude fading, pulse broadening, and doppler frequency shift.

In this section, reflection laws governing the scattering of radiation from various surfaces as determined by optical means are applied to radio signals reflected by the moon. The probability distribution of the amplitude of radar-lunar echoes and the doppler frequency spread due to the moon's libration are also briefly discussed.

B. LUNAR REFLECTION LAWS

According to the radar equation, the power returned from a target, which reflects radiation isotropically, is given by, for a monostatic system,

$$P_r = \frac{P_t G^2 \lambda^2 \sigma}{(4\pi)^3 R^4} \qquad (15)$$

where P_r is the received power; P_t, the transmitted peak power; G, the gain of the antenna relative to an isotropic antenna; R, the radar-target range; λ, the transmission wavelength; and, σ, the target cross sectional area.

For an idealized spherical target whose dimensions are large compared with wavelength and whose surface is smooth and perfectly reflecting, its cross section is merely the geometric projected area given by

$$\sigma_g = \pi r^2 \qquad (16)$$

where r is the radius of the sphere.

When the target is not a totally reflecting body, the cross section is modified to

$$\sigma_s = \pi r^2 \rho \tag{17}$$

where ρ is the power reflection coefficient of the surface.

It is evident from the Fresnel diffraction theory that the amplitude of a spherical wave returned from a smooth body is equal to one-half that due to the first Fresnel zone acting alone. This applies to an aperture with an infinite number of zones. Since the first Fresnel zone has a radius of $(R\lambda/2)^{1/2}$, in the case of the moon (if it were a smooth body), only a small portion of the moon's surface would contribute to the received reflected energy. The first Fresnel zone occupies a portion of the moon nearest to the observer so that a pulse reflected from the moon would not be extended by reflections from the rear portions of the moon. In general, it can be stated that a pulsed electromagnetic wave incident on a smooth sphere is reflected without any distortion, i.e., pulse width of the reflected wave is identical to that of the incident wave.

With regard to a spherical target whose surface is comparatively rough, the equivalent echoing area, σ_r, is given by

$$\sigma_r = \pi r^2 \rho q \tag{18}$$

where q is the directivity of the target. The magnitude of the directivity factor is dependent upon the scattering law applicable to the rough surface.

Although the radiation is scattered in all directions, there is a greater increase in the amount of energy scattered back in the echoing direction for a rough sphere than for a smooth sphere of the same geometric size.

The two scattering laws considered in this report are the Lambert and the Lommel-Seeliger law.

The Lambert law, which applies to the scattering from a diffuse surface having irregularities on the order of a wavelength, states that the scattered energy in any direction is proportional to the cosine of the angle between the incident ray and the normal to the surface and to the cosine of the angle between the scattered ray and the normal.

In applying the Lambert law to the scattering from a rough sphere, it is shown in Appendix B that, for an incident pulse of finite length, the received reflected power at any instant of time is merely the sum of all the energy contributions from a finite band around the sphere. The received power, assuming reflection back in the direction of the radiating source, can be represented by the function

$$P_r = \frac{8\, P_t G^2\, \lambda^2\, \sigma_s}{(4\pi)^3\, R^4} \int_{\theta_1}^{\theta_2} \mathrm{Sin}\,\theta\, \mathrm{Cos}^2\,\theta\, d\theta \qquad (19)$$

where θ is the angle measured from the radial line passing through the point of tangency containing the incident wave front and the sphere. The limits of integration are, for the condition $t \geq T$,

$$\theta_1 = \mathrm{Cos}^{-1}\left[\frac{r - \frac{c}{2}(t-T)}{r}\right] \qquad (20)$$

and

$$\theta_2 = \mathrm{Cos}^{-1}\left[\frac{r - \frac{ct}{2}}{r}\right] \qquad (21)$$

where T is the pulse width and t is the travel time of the leading edge of the pulse along the moon's surface measured from the point of tangency. When $T \geq t$, $\theta_1 = 0$ while θ_2 remains unchanged.

It is evident from Equations (15) and (19) that, for a pulse width greater than 11.6 milliseconds, i.e., time required to travel a distance of twice the radius of the moon, the signal power received from a rough-surfaced moon, obeying Lambert's law, would be 8/3 times greater than that from a smooth moon.[42]

In other words, the directivity factor, described in Equation (18), for the Lambert case, is equal to 8/3.

The Lommel-Seeliger law refers to scattering taking place from a rough surface having irregularities that are large compared with wavelength. The energy scattered from all regions of the surface is the same. Thus, when considering radio wave reflection from such a surface, the received power is only proportional to the cosine of the angle between the incident ray and the normal to the surface.

As shown in Appendix B, the received power can then be expressed by

$$P_r = \frac{4 P_t G^2 \lambda^2 \sigma_s}{(4\pi)^3 R^4} \int_{\theta_1}^{\theta_2} \sin\theta \cos\theta \, d\theta \qquad (22)$$

It follows, therefore, that for pulse lengths greater than 11.6 milliseconds, twice the power is received from a moon, approximating Lommel-Seeliger scattering than from a smooth moon.

With regard to the effect of scattering from a rough surface on the pulse shape, since all portions of a rough body contribute to the total reflected signal, the returned echo would be extended in length, i.e., the pulse lengthening being equal to the time it takes the wave to travel from the nearest surface to the limb and then back again to the surface. Since the radio-depth of the moon is 11.6 milliseconds, a pulse of length, T, incident on a rough moon, would be elongated to a length, T + 11.6 milliseconds, after reflection.

C. STATISTICAL DISTRIBUTION OF THE AMPLITUDE OF LUNAR ECHOES

1. Random Fading

The rapid fluctuations of radar pulses reflected from the moon's surface are usually attributed to the libration which is defined as the oscillatory motion of the moon about an axis which itself changes with time. There are three principle causes of libration: (1) libration in latitude; this results from the fact that the axis of rotation of the moon is tilted about

6.5 degrees to the plane of revolution. Thus, from a fixed position on the earth varying amounts of the moon's northern hemisphere and southern hemisphere are visible; (2) libration in longitude; this is due to the fact that the period of rotation of the moon is constant, but the speed along the orbit varies in accordance with Kepler's second law for planets; (3) diurnal libration; this is the result of the rotation of the earth. As the earth rotates, the position of the moon relative to an observer on the earth is continually changing.

The effect of the moon's libration on the reflected signal can be explained by assuming that the moon's surface consists of a random number of scatterers. The amplitude of the reflected pulse, as observed on the earth's surface, is the resultant of the signals reflected from each of the scattering elements. Since the moon undergoes an apparent rocking motion,or libration, the signals scattered from various parts of its surface are continuously undergoing random changes in phase and amplitude which, in turn, produce fluctuations in the resultant signal.

For surface irregularities which scatter incident radiation with random phases and amplitudes, the probability of occurrence of any resultant signal is therefore given by the Rayleigh probability distribution law. The concept of the Rayleigh distribution is maintained provided that the number of scattering areas is large, i.e., at least on the order of 10 or greater.

The probability, $P(R)\,dR$, of finding an amplitude between R and $(R + dR)$ is therefore given by

$$P(R)\,dR = \frac{R}{\Psi} e^{-\frac{R^2}{2\Psi}} dR \qquad (23)$$

where R is the amplitude of the resultant scattered signal at any instant of time and Ψ is a constant defined in terms of the first or second moments of R by

$$\bar{R} = \left(\frac{\pi \Psi}{2}\right)^{1/2} \qquad (24)$$

or

$$\bar{R^2} = 2\Psi \qquad (25)$$

It can be readily shown that ψ can also be expressed by

$$R_m = (\psi)^{1/2} \tag{26}$$

where R_m is the most probable value of R, i.e., the value of R when P(R) is a maximum.

It should be noted that the distribution of the amplitude of random noise emerging from a bandpass filter, as discussed by Rice[43], follows the Rayleigh law.

2. Random Fading Contaminated with a Steady Signal

The condition in which a steady signal is superimposed on a signal which is the resultant of elementary contributions originating from random scattering areas is of considerable interest since it approximates a possible situation prevailing in the lunar reflection of radio waves.

The steady signal corresponds to a specularly reflected wave coming from the first Fresnel zone or from a relatively small number of smooth surface areas in the region of the first Fresnel zone. The random signal is caused by the lunar libration or by random surface irregularities. If the number of smooth surface areas becomes very large, it is possible for the signals reflected by these areas to undergo cancellation and reinforcement. Thus, instead of specular reflection taking place, a random type noise could result.

The probability density distribution function that describes the envelope of resultant signal can be written as, according to Rice's theory of random noise[43],

$$P(V) = \frac{V}{\psi} e^{-\frac{V^2 + B^2}{2\psi}} I_o\left(\frac{VB}{\psi}\right) \tag{27}$$

where B is the amplitude of the steady signal; V, the envelope of the resultant amplitude comprised of the steady signal (B) and the random signal (R); ψ, constant defined by Equations (24), (25), or (26).

The parameter, $I_o(VB/\psi)$, is the modified Bessel function of the first

kind of zero order, given by

$$I_o\left(\frac{VB}{\psi}\right) = \sum_{n=0}^{\infty} \frac{1}{n!\ n!} \left(\frac{VB}{2\psi}\right)^{2n} \tag{28}$$

During $B = b\sqrt{\psi}$, it follows that, when b=0, Equation (27) simplifies to the Rayleigh distribution law.

When b>3, the Bessel function can be replaced by its asymptotic expression

$$I_o\left(\frac{bV}{\sqrt{\psi}}\right) \approx \left(\frac{\sqrt{\psi}}{2\pi\ b\ V}\right)^{1/2} e^{\frac{b\ V}{\sqrt{\psi}}} \tag{29}$$

and then Equation (27) simplifies to

$$P(V) \approx \frac{1}{\sqrt{2\pi\ \psi}} \left(\frac{V}{b\sqrt{\psi}}\right)^{1/2} e^{-\frac{(V - b\sqrt{\psi})^2}{2\psi}} \tag{30}$$

It is evident that, apart from the term $(V/b\sqrt{\psi})^{1/2}$, this distribution is Gaussian with a standard deviation of $\sqrt{\psi}$. When b is equal to or larger than two, the presence of a steady signal is indicated.

When applying Equation (27) to experimental data, it is necessary to obtain the value of ψ. If the data to be analyzed is in amplitude form, containing both steady and random signals, then according to Equation (24), ψ may be approximated by

$$\psi \approx \frac{2}{\pi}\ \overline{V}^{\,2} \tag{31}$$

It follows from Equation (25) that if the data is in the form of cross section, σ, or power,

$$\psi \approx \frac{\overline{\sigma}}{2} \tag{32}$$

It should be mentioned that the validity of the approximations for obtaining ψ from experimental data, Equations (31) and (32), is improved for

$b < 2$.

In applying the theory of random noise to the study of the characteristics of the lunar surface, it would appear that, if the moon were completely smooth, b would be on the order of three or greater and if it were a rough body, b would most likely be zero. Assuming that the moon contained both rough and smooth regions, it could be expected that b would lie between zero and three. However, it should be mentioned that, for this particular situation, it would be difficult to determine the extent of the actual smooth and rough areas.

Specular reflection can contribute to the resultant signal when the surface normal is in the direction of the observation site; such areas are most likely contained on a cap of the moon closest to the earth. The specular returns can be highly perturbed either by rough scattering areas located in the near vicinity of smooth regions or by the presence of a large number of isolated smooth surfaces.

Another factor which must be considered in the analysis of lunar amplitude data is the time interval over which the probability distribution is applied. Since the lunar libration affects the reflected signal amplitude, the time over which any statistical analysis is applied should be small compared to the time variation of the libration rate.

In short, an evaluation of the probability density distribution of lunar echo amplitudes may not result in a true indication of the surface characteristics of the moon. Other factors such as pulse lengthening and the characteristics of the amplitude decay of the lengthened pulse should be examined concurrently.

D. DOPPLER EFFECTS OF LUNAR ECHOES

Radio waves reflected from the moon are found to exhibit both a doppler shift and a doppler spread in the transmission frequency.

The doppler shift is brought about by the fact that the orbit of the moon around the earth is elliptical. Thus, there is a component of the moon's orbital velocity directed toward the center of the earth. Since the earth is also

rotating, there is an additional velocity component along the earth-moon line-of-sight, its magnitude being a function of the latitude of the observation site and the moon's position on the celestial sphere. The resultant of these two velocity components produces the frequency shift in the reflected echo.

For a monostatic system, the doppler shift imposed on a radar signal reflected from the moon's surface is given by

$$f_d = - \frac{2 \dot{R} f}{c} \tag{33}$$

where f_d is the difference between the apparent reflected frequency and the transmitted frequency, f; $\dot{R}$, the time rate of change of the distance between the observation site and the surface of the moon; c, the free space velcoity.

According to Fricker[44], the relative velocity, $\dot{R}$, can be expressed by

$$\dot{R} = \frac{\dot{D}_o (D_o - r_o \operatorname{Cos} \psi) - D_o r_o \frac{d}{dt} (\operatorname{Cos} \psi)}{D} \tag{34}$$

where, as shown in Figure 3,

$$D = \left[D_o^2 + r_o^2 - 2 r_o D_o \operatorname{Cos} \psi \right]^{1/2} \tag{35}$$

and D_o is the distance from the center of the earth to the center of the moon; D, the distance from the observation site to the moon's center; r_o, the radius of the earth; and ψ, the angle between the line connecting the earth-moon centers and the radial line from the earth center to the observation site.

The terms in Equations (34) and (35) can be computed from the following relationships:

$$D_o = \frac{r_o}{\operatorname{Sin} \pi} \tag{36}$$

$$\dot{D}_o = - D_o \operatorname{Cot} \pi \frac{d \pi}{dt} \tag{37}$$

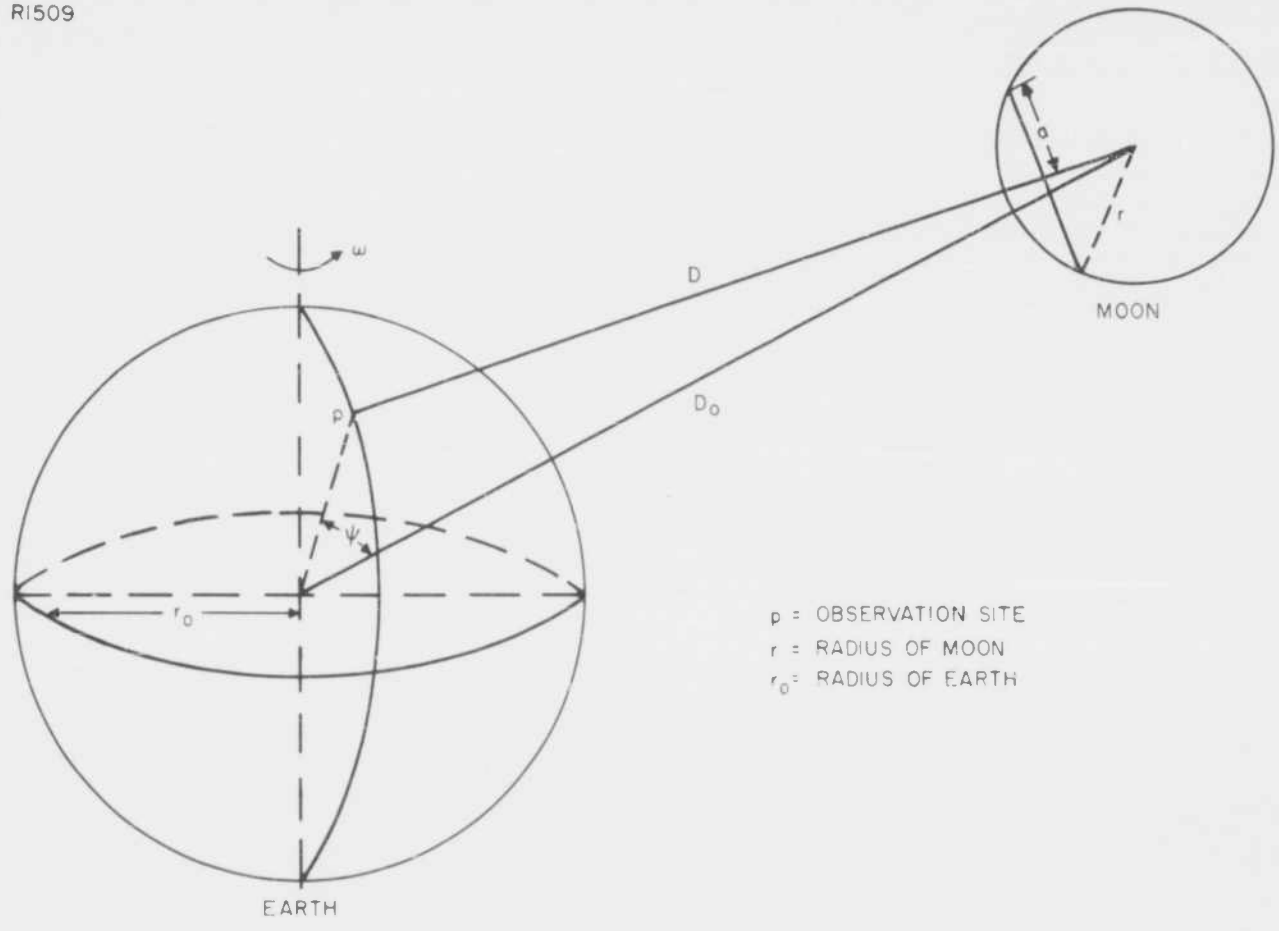

Figure 3. Earth-Moon Geometry

$$\frac{d}{dt}(\cos\psi) = \left[\cos\delta \sin\phi - \sin\delta \cos\phi \cos(\mathrm{LHA})\right]\frac{d\delta}{dt} - \cos\phi \cos\delta \sin(\mathrm{LHA})\frac{d}{dt}(\mathrm{LHA}) \tag{38}$$

$$\frac{d}{dt}(\mathrm{LHA}) = \omega - \frac{d}{dt}(\mathrm{RA}) \tag{39}$$

where Π is the horizontal parallax angle of the moon; δ, the declination of the moon; LHA, the local hour angle of the moon; RA, the right ascension of the moon; ϕ, the latitude of observation site; and ω, the angular velocity of the earth. The moon's celestial coordinates and the horizontal parallax are tabulated in the Nautical Almanac.

The libration of the moon causes a variation of range-rate in the radial distances from the observation site to points on the moon's surface. The differences in the velocity components from the various parts of the moon's surface give rise to a doppler spread in the reflected signal frequency. In addition, doppler spreading also results due to the movement of the observation site toward the center of the lunar disk. The total spread is the resultant of both these effects.

The total doppler spread, Δf_d, as derived by Fricker[44], can be given in terms of the function

$$\Delta f_d = \frac{2 f K r}{c}\left[\ell_{TB} \sin\nu - \ell_{TL} \cos\nu\right] + \frac{f K^2 r^2 \dot{R}}{c R^2} \tag{40}$$

where r is the radius of the moon; ℓ_{TB}, the total effective libration rate in latitude; ℓ_{TL}, the total effective libration rate in longitude; ν, the angle between a location on the perimeter of the moon and the moon's equator; and K, the fractional radius of the moon, i.e., K = a/r as illustrated in Figure 3.

The first term in this expression applies to the doppler spread due to the moon's libration while the second is that due to the motion of the observer. In general, the latter term can be neglected for libration rates greater than 10^{-7} radians per second.

When the motion of the observer is not taken into account, the maximum doppler spread occurs at an angle, ν_o, where

$$\nu_o = \mathrm{Tan}^{-1} \left[\frac{\ell_{TB}}{\ell_{TL}} \right] \tag{41}$$

The expressions defining the parameters, ν, ℓ_{TB} and ℓ_{TL}, are not presented in this report because of their complexity. Computational procedures for evaluating the terms are contained in Reference 44.

With regard to the effect of libration on lunar echoes, if the moon were a perfectly smooth body, the libration would produce a slight doppler spread within a Fresnel zone, its magnitude being directly proportional to the fractional radius, K, or dimensions of the zone and varying as a function of the angle, ν. Since the first few Fresnel zones, where K is very small, contribute to most of the energy of the reflected signal, the doppler spread would be expected to be insignificant. The amplitude of the echo would have a slight modulation with a bandwidth determined by the doppler spread over the contributing Fresnel zones.

For a moon consisting of smooth regions (such as the first few Fresnel zones) and rough scattering areas (such as mountains), it may be possible, by means of the libration effects, to reveal the existence of the scatterers. Since the lunar libration introduces a doppler spread and amplitude fluctuation in the reflected signal, the magnitude of the frequency components in the doppler spread or the dominant frequencies in the power density spectrum can be used to determine the fractional radius of the moon which best fits the experimental data. This parameter, in turn, can then be compared with photographs of the lunar face for correlation with known mountain ranges.

The feasibility of mapping the surface of the moon by means of doppler shift-power spectrum measurements has been demonstrated by Pettengill.[10]

IV. EXPERIMENTAL MEASUREMENTS

The experimental observations discussed in this report were conducted at Trinidad, WIF between January and July 1960 with a high-powered pulsed radar operating at a frequency of 425 megacycles, Linear (horizontal) polarization was employed on transmission while the reflected radar signals were simultaneously received on both the transmitted and the orthogonal (vertical) polarization.

Automatic tracking of the moon was accomplished by means of an orbit programmer which continuously positioned, in three-minute intervals, an 84-foot diameter steerable antenna so as to follow the theoretical path of the moon.

The theoretical geometric orientation of the moon, as viewed from Trinidad, for moonrise commencing on 12 January 1960 is shown in Figure 4. The method for determining the azimuth, elevation and time coordinates of a celestial body for tracking purposes is discussed in Appendix C.

The radar data pertaining to the lunar echo return were recorded in digital form on magnetic tape in order to facilitate data processing and analysis. In addition, photographic recordings were made of the various combinations of the amplitude, range and time coordinates schematically illustrated in Figure 5.

A tracing of a typical A-scope photograph of a radar-lunar echo recorded at Trinidad is shown in Figure 6. The upper trace is the horizontally polarized signal while the lower is the vertical. It is noted that the pulse return is stretched out to approximately 12 milliseconds in length and that the echo shapes of both polarizations are comparatively alike. The maximum radar cross section of 126.3 db above one square meter is obtained on horizontal polarization. This value compares reasonably well with the geometric projected lunar disk area of 129.8 db above one square meter (radius of moon = 1740 km). Assuming a smooth moon with a power reflection coefficient of 0.15, the theoretical echoing area should be on the order of 121.6 db above one square meter.

A lunar echo showing pulse distortion and also pulse lengthening is contained in Figure 7. For this particular example, the signal amplitude is only about 114 db above one square meter.

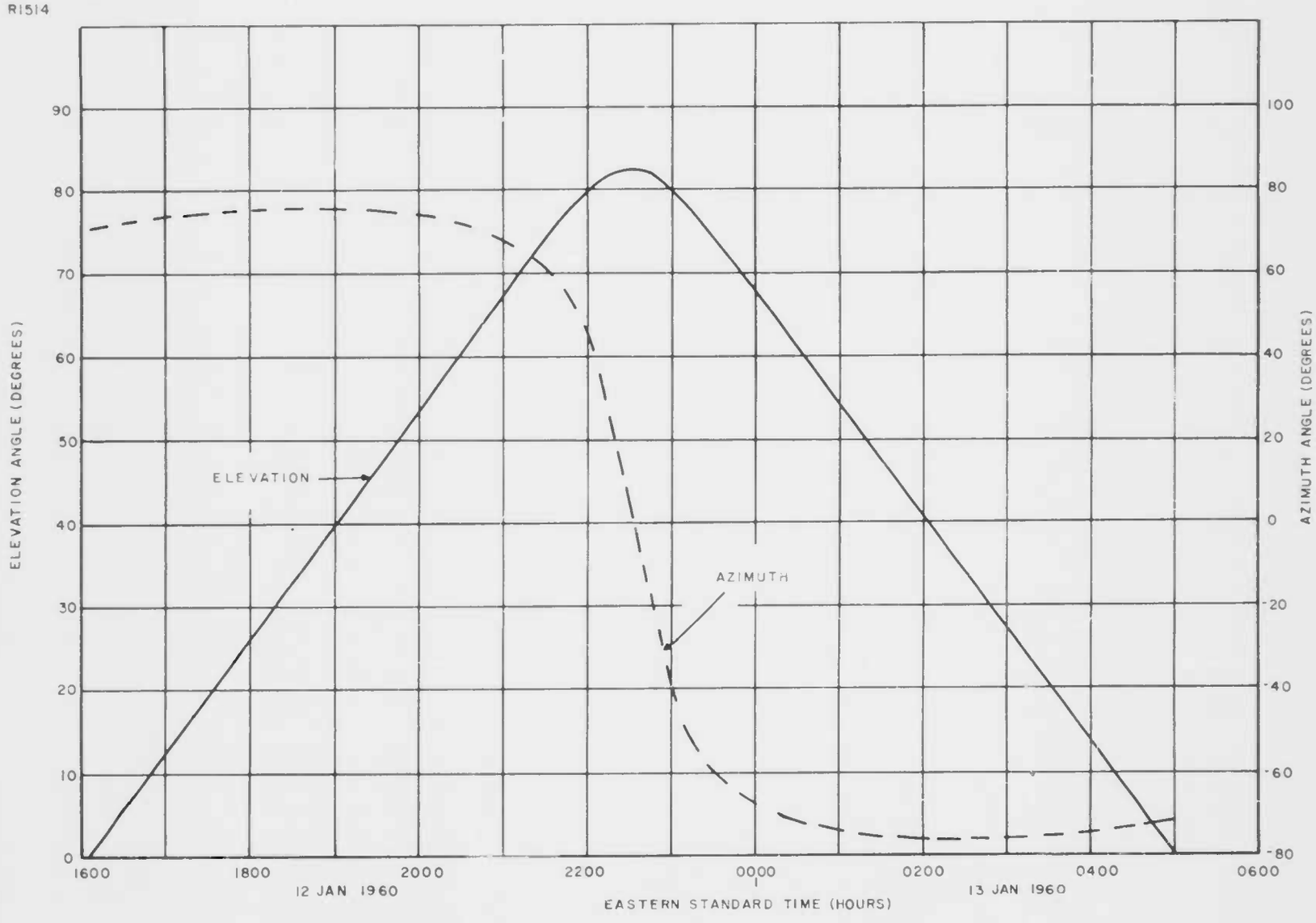

Figure 4. The Orbit of the Moon at Maximum Northern Declination as Viewed from Trinidad

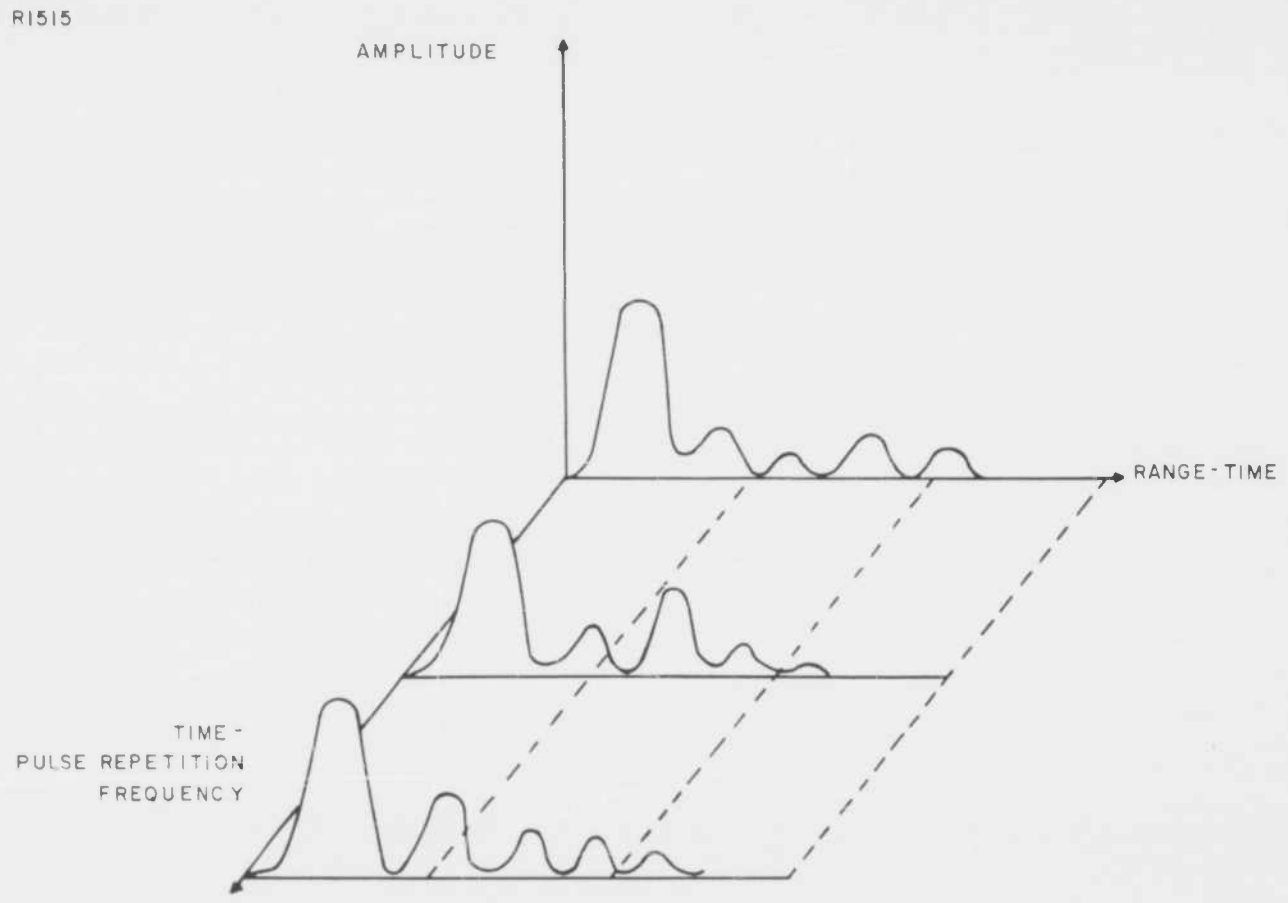

Figure 5. Spatial Coordinates of Lunar Echoes

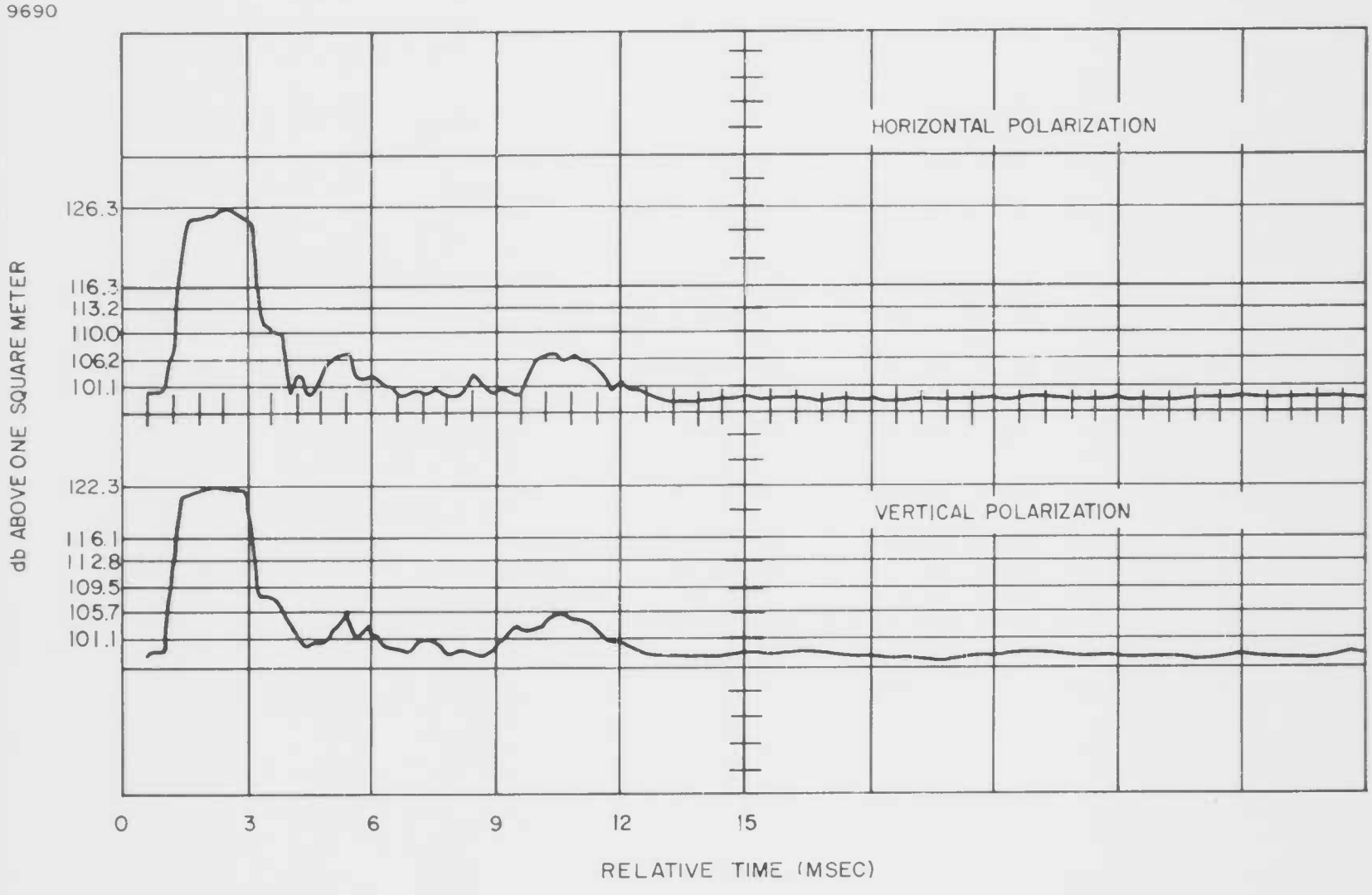

Figure 6. A Typical Lunar Echo Recorded at Trinidad at 425 Mc Showing Pulse Lengthening

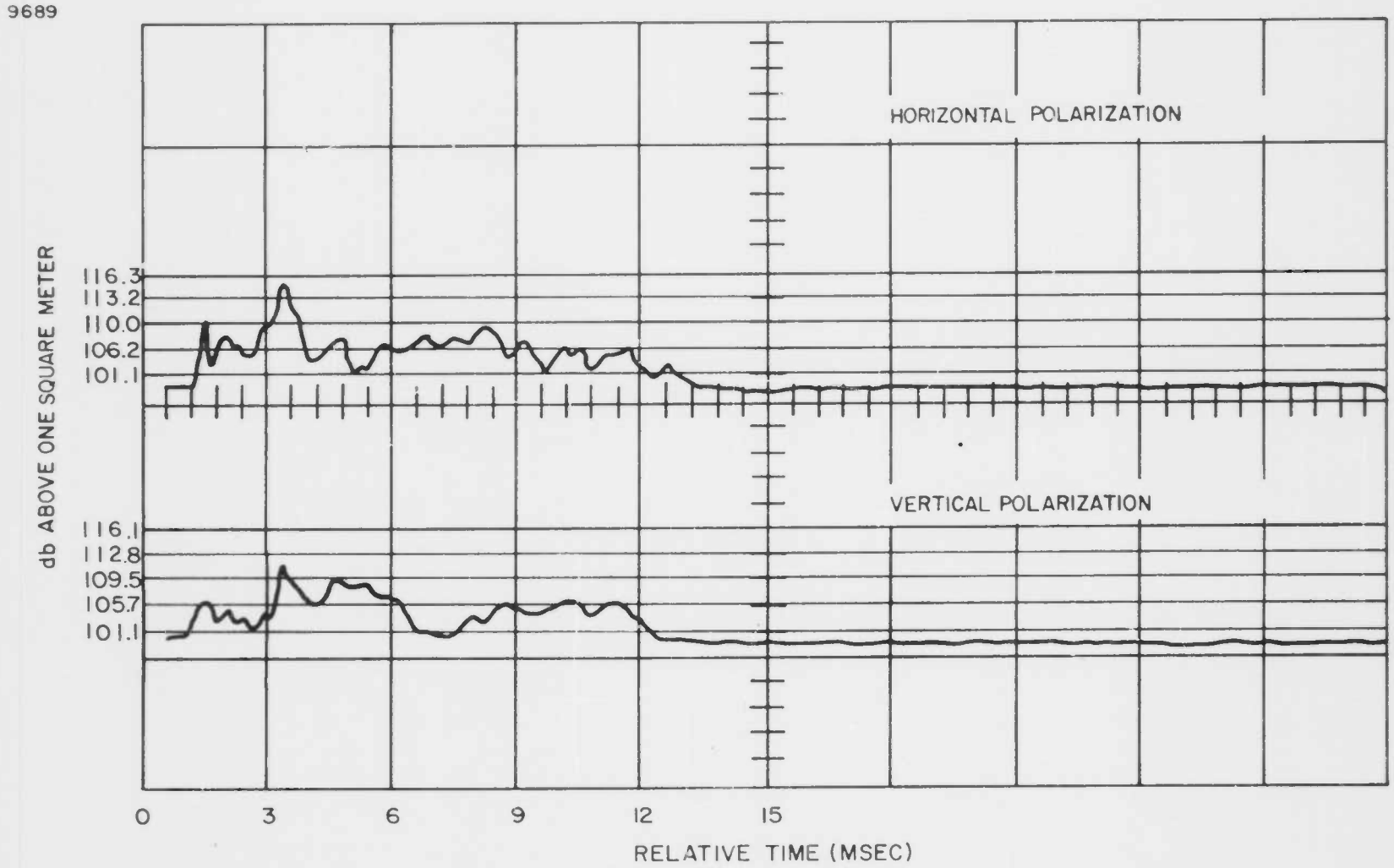

Figure 7. A Typical Lunar Echo Recorded at Trinidad at 425 Mc Showing Pulse Distortion

A selected sample of an amplitude vs. time film record of moon echoes displaying Faraday rotation is illustrated in Figure 8. It is noted that the reflected signal is predominantly oriented in the vertical polarization receiver channel during the period when horizontal polarization was employed on transmission.

An amplitude vs. time fading record illustrating the presence of lunar libration is shown in Figure 9. It is seen that the envelope of the back portions of the pulse returns exhibits a much higher fading rate than the front portion. It is interesting to note that the fading patterns of the main echo pulse (the large signal amplitude) observed on both polarizations are identical. The significance of this is that the polarization of the incident pulses on reflection from the front part of the moon is maintained, which implies that this region of the moon's surface appears reasonably smooth at a frequency of 425 megacycles. Depolarization of a signal should occur on reflection from a rough surface. It would follow that the amplitude fading patterns observed on orthogonal polarizations would be somewhat different.

A typical range vs. time photograph of lunar echoes, revealing pulse lengthening, is shown in Figure 10. The signal fading indicated by the reduction of the echo intensity in the back portion of the range scale is mainly due to the moon's libration.

The schedule of the radar-lunar observations performed at Trinidad is presented in Table 1. The total time of experimental measurements was 44-3/4 hours, of which less than 10 per cent (the March 1960 data) were conducted when the moon was at its maximum southern declination. The remaining observations were made during the time when the moon was at its maximum northern declination.

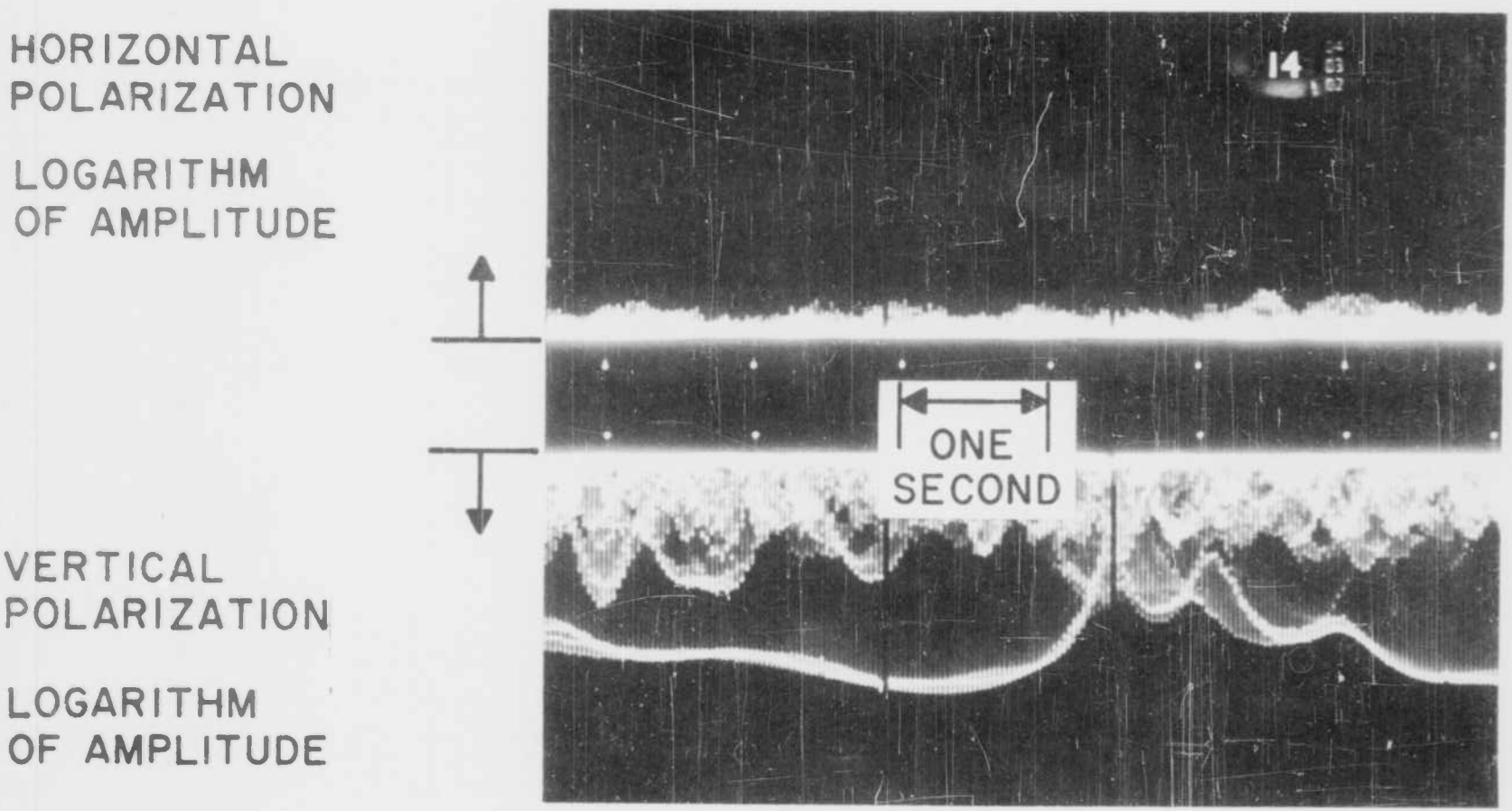

Figure 8. Amplitude vs. Time film Record of Lunar Echoes Recorded at Trinidad at 425 Mc Displaying Faraday Rotation, 8 February 1960, 1403 EST.

9848

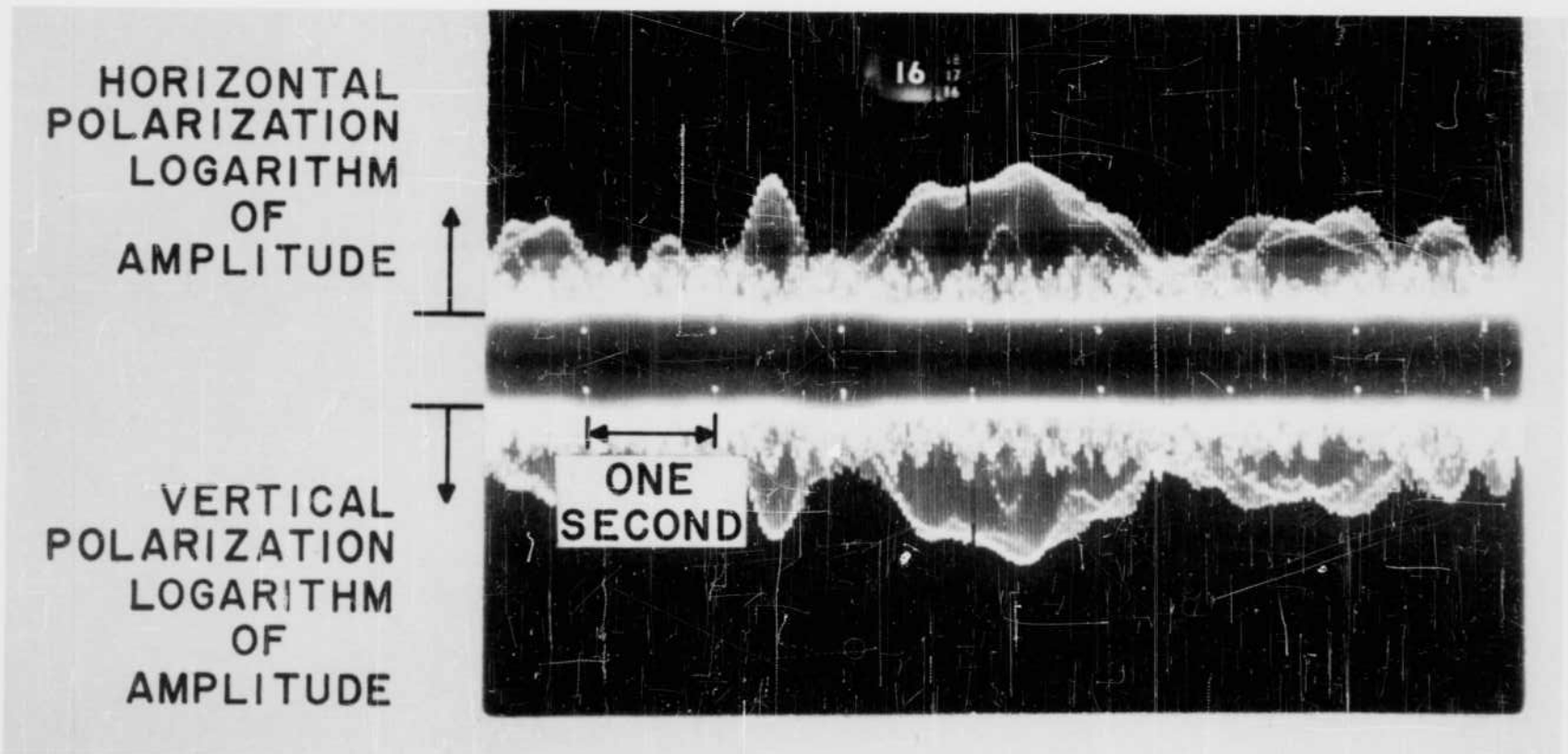

Figure 9. Amplitude vs. Time Film Record of Lunar Echoes Recorded at Trinidad at 425 Mc Displaying Lunar Libration, 12 January 1960, 1617 EST.

9846

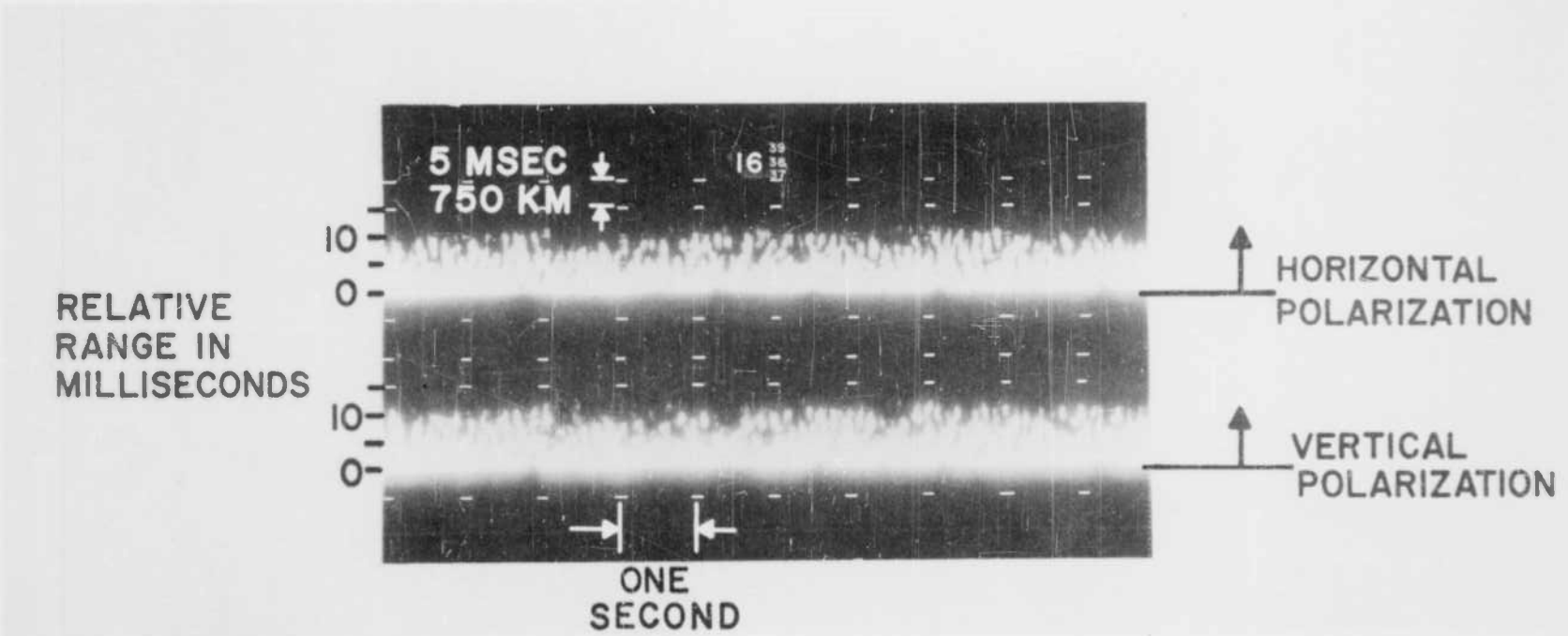

Figure 10. A Typical Range vs. Time Photograph of Radar-Lunar Echoes Recorded at Trinidad at 425 Mc 12 January 1960, 1617 EST.

TABLE 1

SCHEDULE OF RADAR-LUNAR OBSERVATIONS CONDUCTED AT TRINIDAD

Date	Coordinates of Moon at Beginning of Observation			Coordinates of Moon at End of Observation			Total Time of Lunar Observation (Hours)
	Time (EST)	Elevation Angle (Degrees)	Azimuth Angle (Degrees)	Time (EST)	Elevation Angle (Degrees)	Azimuth Angle (Degrees)	
12 January 1960	1615	1.5	71.9	2225	82.3	15.3	6-1/4
8 February 1960	1415	2.7	72.0	2100	79.1	314.7	6-3/4
19 March 1960	0415	61.1	175.4	0545	55.2	214.1	1-1/2
	0645	45.5	229.8	0900	17.8	246.9	2-1/4
4 April 1960	1145	4.7	73.4	1530	56.8	75.0	3-3/4
26 May 1960	0600	4.9	73.0	1730	12.4	286.3	11-1/2
20 July 1960	0215	0	71.6	1500	2.2	288.2	12-3/4

V. DATA ANALYSIS

A. CHARACTERISTICS OF THE IONOSPHERIC MEDIUM

1. Preliminary Analysis

In the initial planning of this experiment involving the moon, in studying, by means of radar techniques, the diurnal variation of the electron content in the ionosphere, it was revealed that, when the moon was at its maximum northern declination, its orbit, as viewed from Trinidad, intersected regions in the ionosphere where the direction of the magnetic field lines was perpendicular to the direction of propagation.[35] Since only one frequency was available for the experiment, it was believed that: (1) for the condition of perpendicularity with the magnetic field lines, the angular rotation of the plane of polarization of a linearly polarized wave (due to the Faraday effect) would be negligible for transmissions on an earth-moon path; (2) it would be quite feasible to resolve the ambiguity of the complete number of rotations of the plane of polarization by simply counting the maxima and minima of the polarization angle of the resultant signal.

The preliminary analysis of the experimental data indicated that, for transmissions through the entire ionosphere, the condition of completely transverse propagation is maintained in only a very small region in space. The Faraday rotation, even when the condition of perpendicularity of the propagation direction with the earth's magnetic field is satisfied, can still be appreciable.

The determination of the electron content in the ionosphere was, therefore, accomplished from the lunar-echo polarization data by an indirect method.[33] All possible solutions to the problem were considered and, by a process of elimination, based on the comparison of the estimated electron content with the electron content below the F-layer maximum deduced from ionospheric soundings at Puerto Rico, a reasonable solution was obtained.

The magnetic field strength and orientation employed in that analysis[33] were calculated on the assumption that the earth's magnetic field could be approximated by a magnetic dipole located at the center of the earth and having a geomagnetic pole at 78.6° N and 70.1°W.

A re-evaluation of the preliminary work resulted in a more direct method for solving the ambiguity in the polarization angle, i.e., by the comparison of the estimated theoretical angular rotation with the experimental measurements. In addition, the magnetic dipole model for the earth's magnetic field was replaced by the surface values.

The lunar orbit of the moon and the contours of perpendicularity with the earth's magnetic field as viewed from Trinidad are presented in Figure 11. It is seen that the magnetic field orientations based on the dipole model and surface data are slightly different. The latter is considered to be the more accurate representation.

2. Total Electron Content

The average acute angular rotation of the signals reflected from the moon during the observation of 12 January 1960 is presented by the $\phi = \Delta\phi$ and the A curve of Figure 12. Because of the inability of an antenna-receiver system to determine the true orientation of the incident radiation, it is necessary to examine the other possible values of the polarization angle defined by Equation (3) and also plotted in Figure 12.

The intersection of any two " ϕ " curves such as the $\phi = \Delta\phi$ and the $\phi = \pi - \Delta\phi$ curves at 1800 EST always occurs when the polarization of the received signal passes through either a 90-degree or a 0-degree angular rotation. It should be noted that an intersection could result either from a phase reversal or from a continuing monotonic phase change. For example, there are two possible paths which each of the ϕ curves could follow; the $\phi = \Delta\phi$ curve could have continued along the B path instead of the A path.

The theoretical estimate of the magnitude of the ionospheric Faraday rotation that could have occurred at the various azimuth-elevation orientations of the lunar orbit is also shown in Figure 12. These calculations are based on the true height-electron density profiles deduced from the vertical incidence ionospheric soundings taken at 15-minute intervals at Puerto Rico. Above the F-layer maximum, the electron density distribution is assumed to follow a Chapman model, as defined by Equation (5), having a constant scale height of 80 kilometers

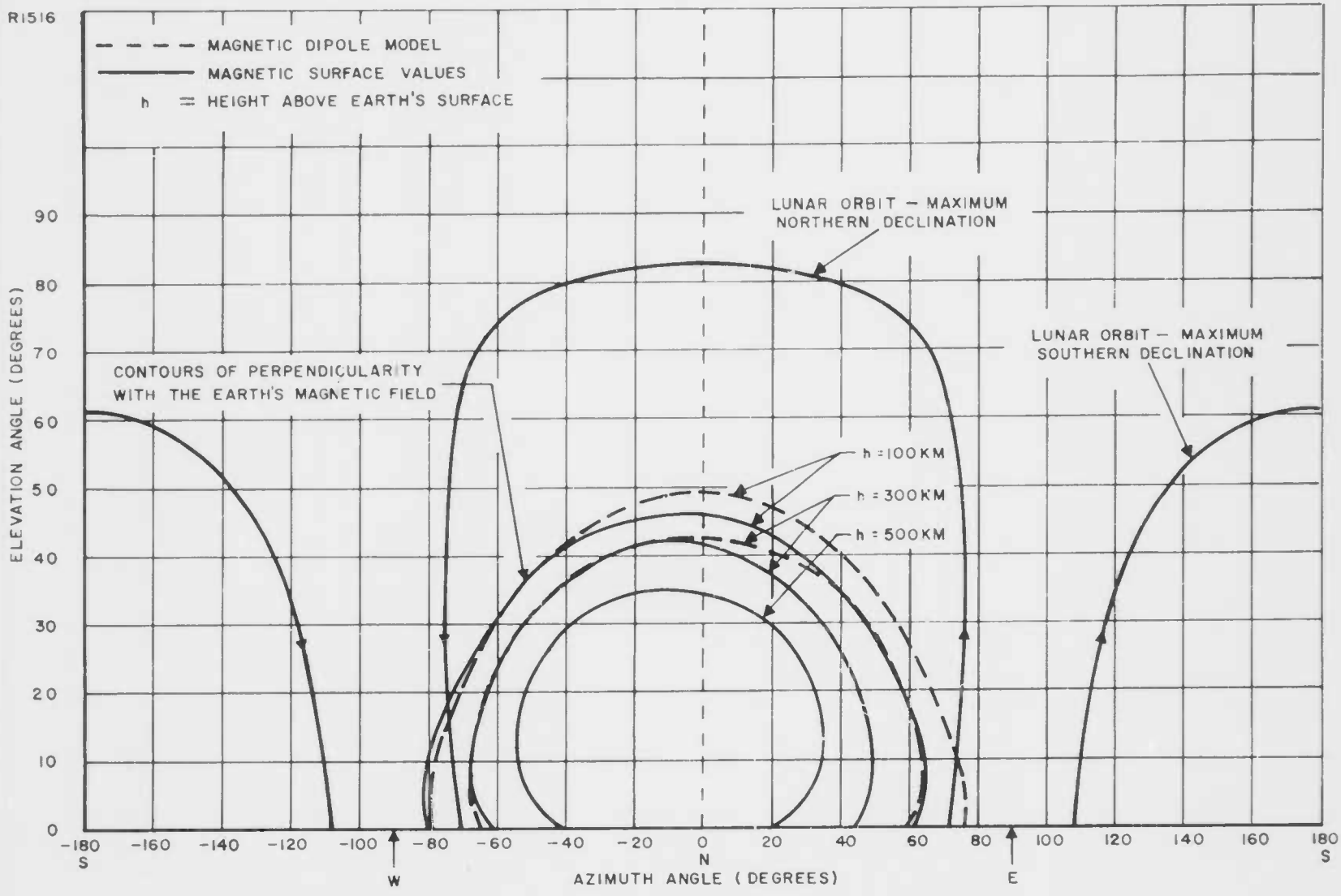

Figure 11. The Lunar Orbits and Contours of Perpendicularity With the Earth's Magnetic Field as Viewed from Trinidad

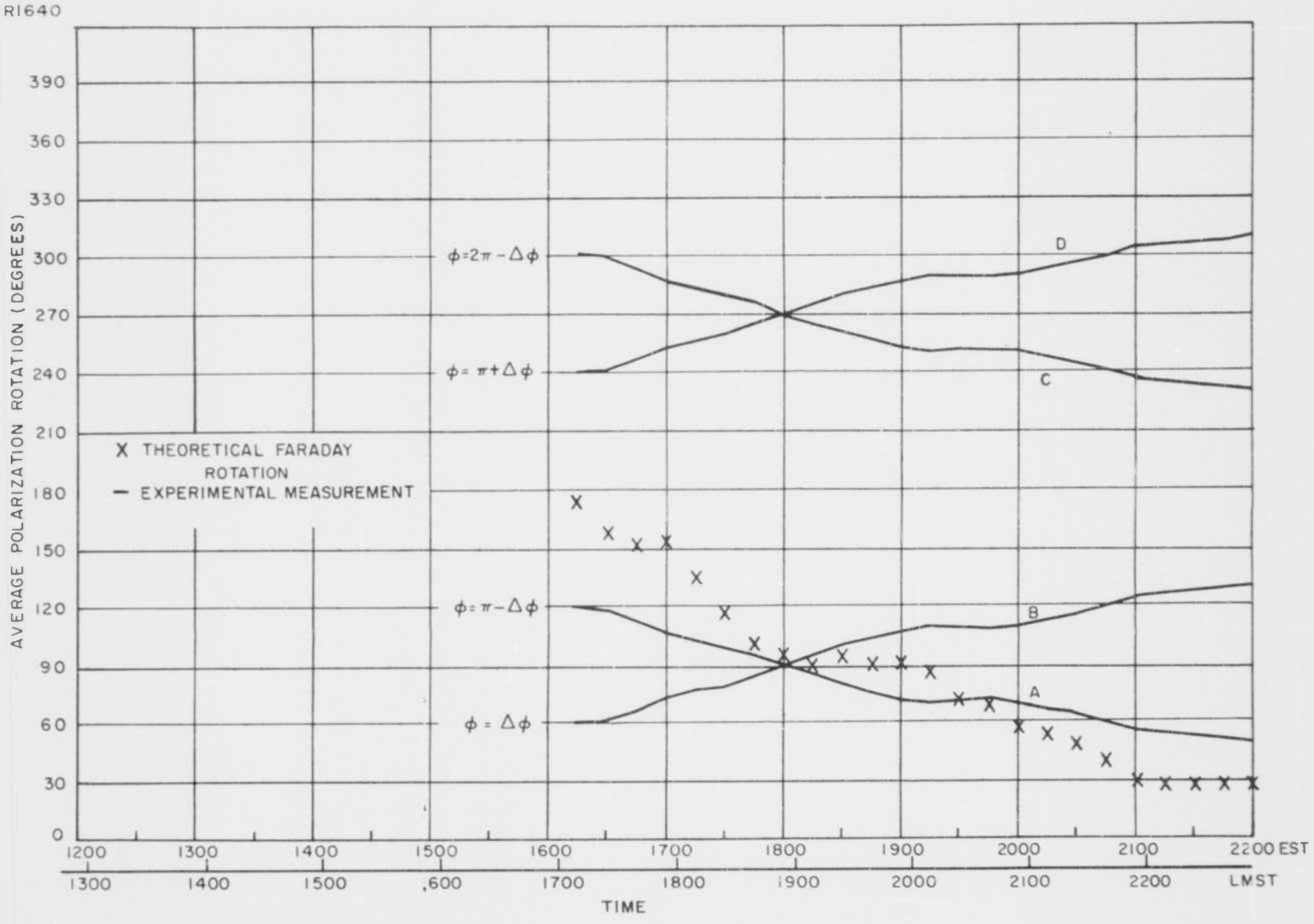

Figure 12. Average Faraday Rotation from Trinidad Radar-Lunar Observation, 12 January 1960

for the neutral particles.

It is quite evident that the theoretical calculations correlate to a high degree with the experimental data represented by the $\phi = \pi - \Delta\phi$ and the A curves. Thus, these two curves are chosen as the most likely correct solution to the ambiguity problem. It is of interest to note that a similar conclusion was arrived at in the early analysis of the radar-lunar data.[33]

The electron content in a one-square centimeter vertical column through the ionosphere is depicted in Figure 13. The experimental plot is derived from Equation (10) in conjunction with the values of ϕ specified by the $\phi = \pi - \Delta\phi$ and the A curves. It is seen that, in the late afternoon, the total electron content determined from the integration of the combined electron density profile (from ionospheric soundings) and a Chapman distribution is slightly higher than the experimental measurements, while in the early evening the reverse takes place. This would imply that, for this particular day, the scale height during the daytime should be less than 80 kilometers and that, during the evening, the ionosphere could perhaps be represented by a Chapman model with a constant scale height in excess of 80 kilometers.

The average Faraday rotation observed on 8 February 1960 is shown in Figure 14. It is seen that the acute polarization angle reaches a minimum at 1700 EST which would infer that the polarization of the received lunar echo at that time was the same as the transmitted polarization.

An examination of the theoretical angular rotation with the experimental measurements reveals that the $\phi = \pi - \Delta\phi$ and the A curves best correlate with the theoretical data.

A plot of the total electron content derived from the radar-lunar observations and from the Puerto Rico ionosonde data is given in Figure 15. It is evident that, as in the case of the 12 January results, a constant scale height of 80 kilometers above the F-layer maximum, assuming a Chapman model, is too low for the evening. The daytime data, on the other hand, are reasonably well correlated.

The average angular rotation measured on 19 March 1960 when the moon

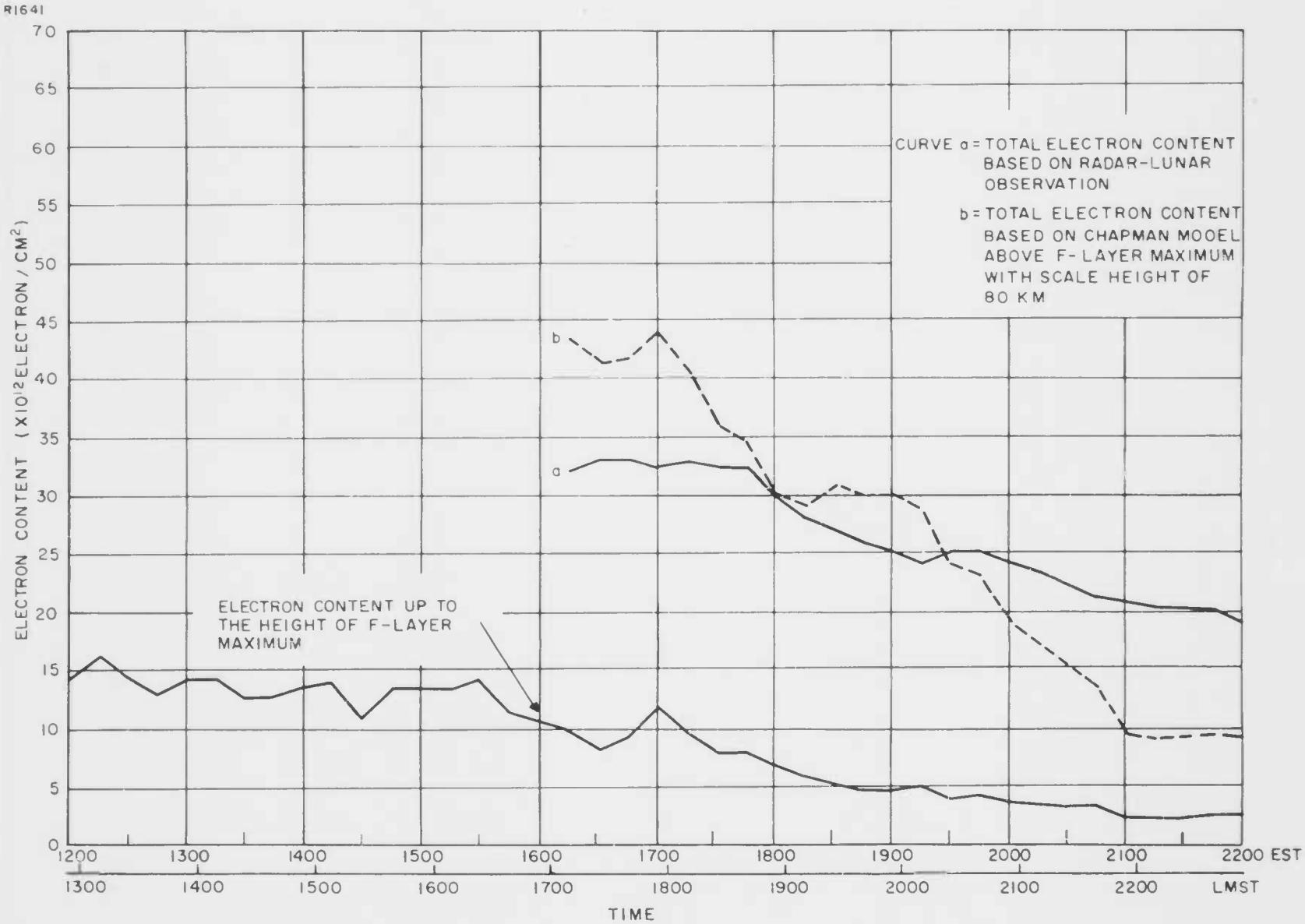

Figure 13. Comparison of the Measured Total Electron Content in a One Square Centimeter Vertical Column Through the Ionosphere with Theoretical Estimate, 12 January 1960

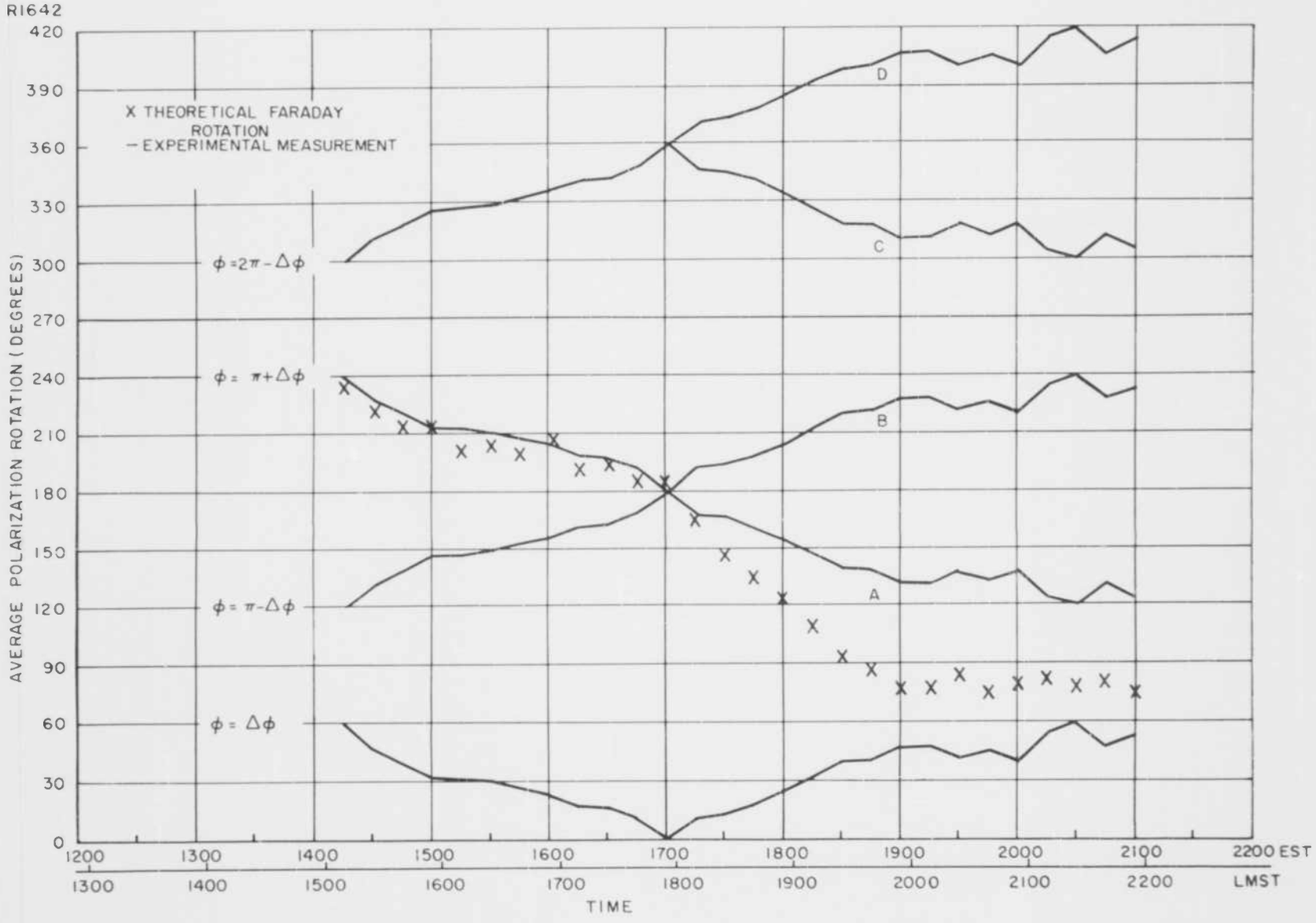

Figure 14. Average Faraday Rotation from Trinidad Radar-Lunar Observation, 8 February 1960

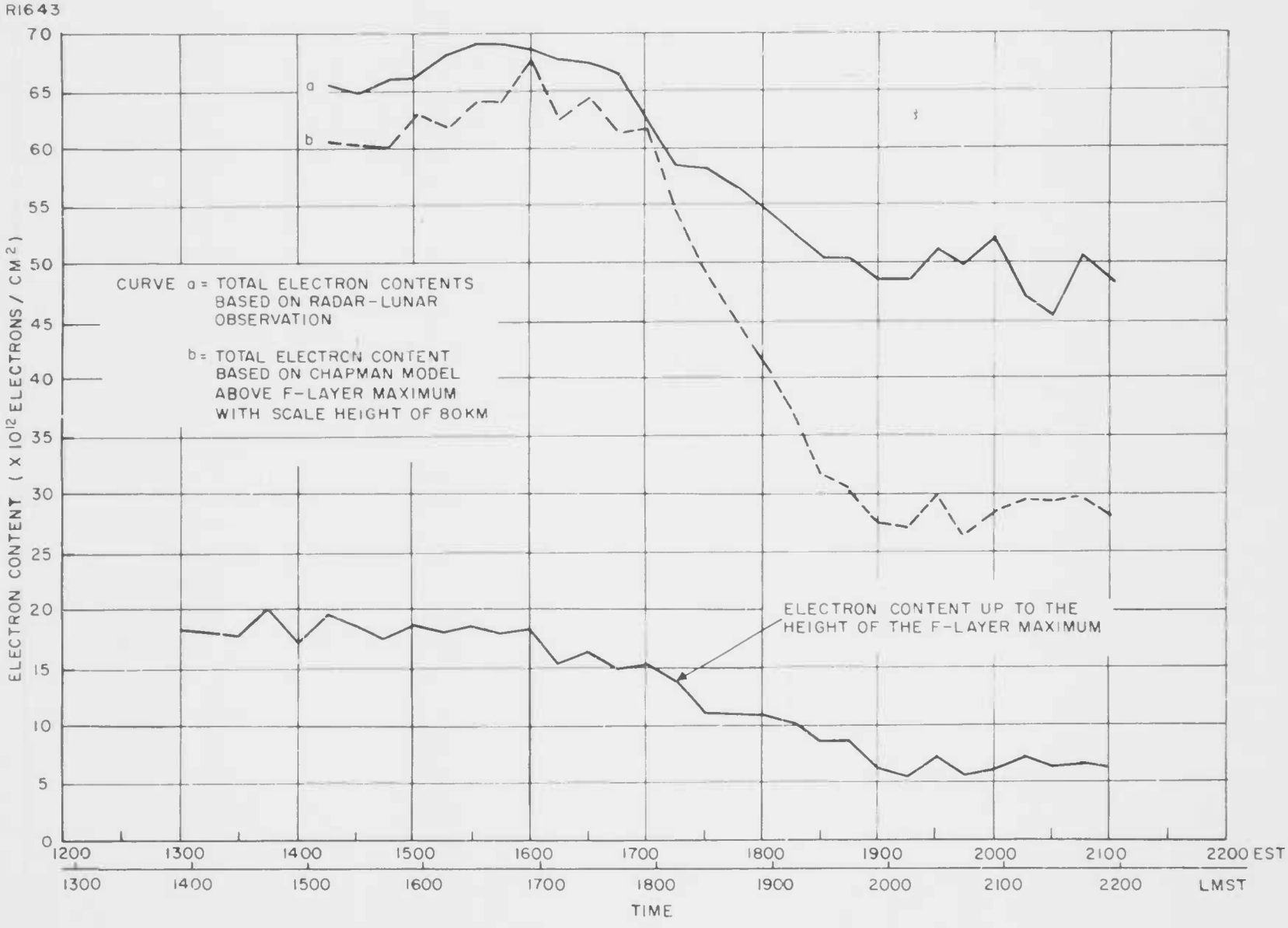

Figure 15. Comparison of the Measured Total Electron Content in a One Square Centimeter Vertical Column Through the Ionophere with Theoretical Estimate, 8 February 1960

traversed a southerly orbit, with respect to Trinidad, is shown in Figure 16. The theoretical computations are based on vertical incidence ionospheric soundings recorded at Bogota, Colombia and an assumed electron density distribution of the Chapman form with a scale height of 80 kilometers above the F-layer maximum. The conversion of the Bogota virtual height versus frequency records into true height versus electron density was performed by the National Bureau of Standards.

The dashed lines between 0545 and 0645 hours indicate missing experimental data. Based on the theoretical calculations, the measured angular rotation is assumed to have a value of 90 degrees at approximately 0615 hours. It is quite evident therefore, that the actual Faraday rotation encountered in the ionosphere can be described by the $\phi = \Delta\phi$, B and C' curves.

The variation of the total electron content deduced from an assumed angular rotation given by the $\phi = \Delta\phi$, B and C' curves is contained in Figure 17. The experimental measurement of the total electron content is found to be higher than that theoretically predicted for a part of the orbit.

The measured acute polarization angle for the 4 April 1960 lunar observation remained between approximately 24 and 48 degrees, as illustrated in Figure 18. It would appear from the theoretical rotational data that the correct solution to the ambiguity problem is most likely the $\phi = \pi - \Delta\phi$ curve.

In order to check the validity of this assumption, the electron content obtained from the various values of ϕ are plotted in Figure 19, together with the theoretical estimate. Both the $\phi = \pi + \Delta\phi$ and $\phi = 2\pi - \Delta\phi$ curves would indicate that the total ionospheric electron content was increasing during the time the electron content below the height of the F-layer maximum was commencing to decrease. This would require that the electron production above the F-layer maximum was continuing at a greater rate than the electron loss below the F-layer maximum. The mechanism governing this physical process is difficult to visualize.

The total electron content defined by the $\phi = \pi - \Delta\phi$ curve, on the other hand, closely resembles the variation of the integrated electron density below the F-layer maximum. It would appear from the theoretical data that the

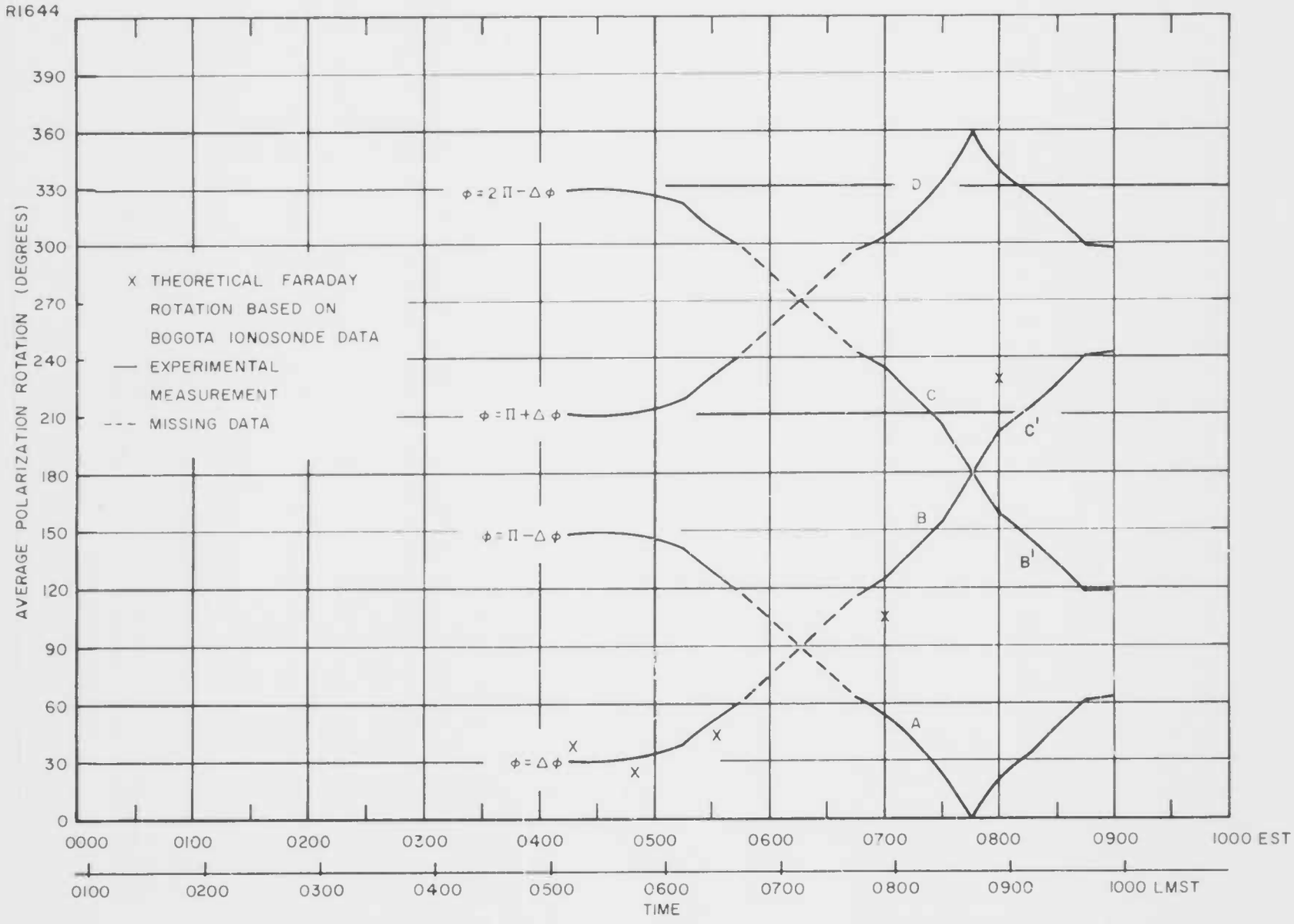

Figure 16. Average Faraday Rotation from Trinidad Radar-Lunar Observation, 19 March 1960

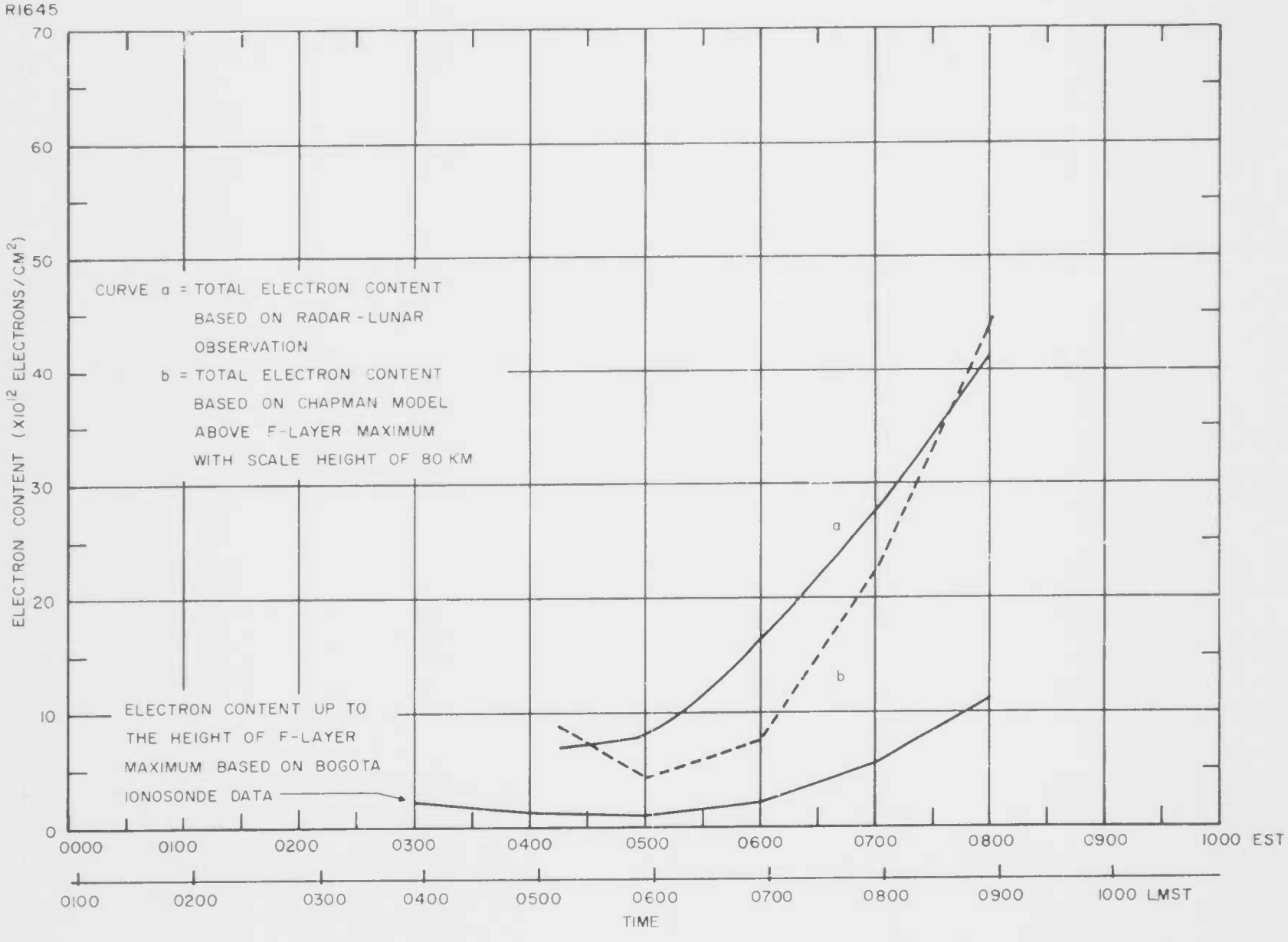

Figure 17. Comparison of the Measured Total Electron Content in a One Square Centimeter Vertical Column Through the Ionosphere with Theoretical Estimate, 19 March 1960

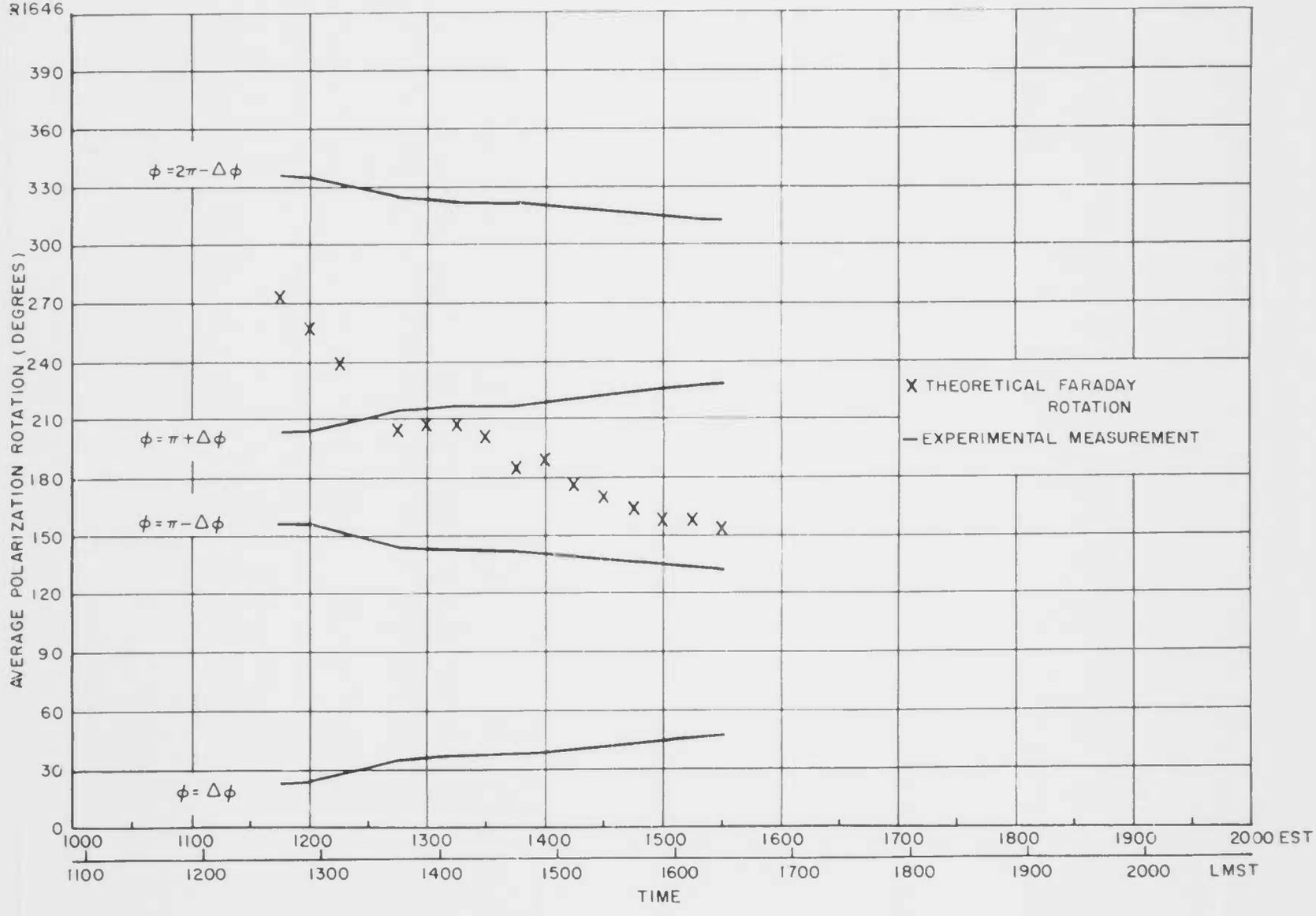

Figure 18. Average Faraday Rotation from Trinidad Radar-Lunar Observation, 4 April 1960

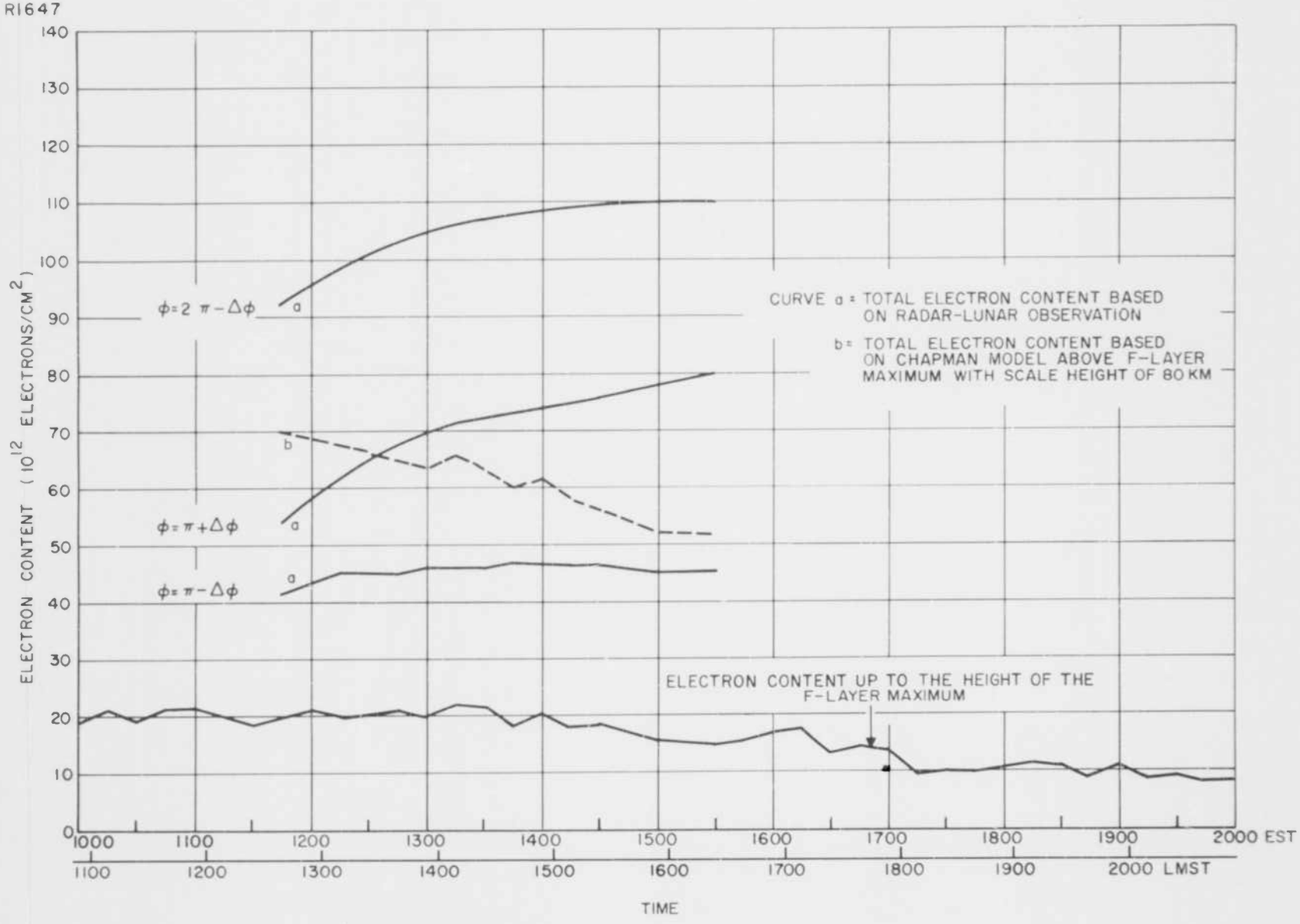

Figure 19. Comparison of the Measured Total Electron Content in a One Square Centimeter Vertical Column Through the Ionosphere with Theoretical Estimate, 4 April 1960

scale height for the region above the peak of the F-layer should be somewhat less than the 80 km value employed in the calculations.

The angular rotation data for the complete lunar orbit of 26 May 1960 is contained in Figure 20. It is quite obvious that the most acceptable diurnal variation of the polarization angle is given by the $\phi = \pi - \Delta\phi$, B and A' curves. There is also excellent agreement between the experimental and theoretical total electron contents as shown in Figure 21.

The polarization data acquired during the whole lunar orbit of 20 July 1960, are given in Figure 22. It is seen that the $\phi = \Delta\phi$, B and B' curves best fit the theoretical calculations.

An examination of Figure 23 reveals that, during the nighttime, the experimentally determined electron content is greater than the theoretical estimates. As noted previously, this would infer a scale height in excess of 80 kilometers for the region above the F-layer maximum.

A composite of all the total electron contents in a one-square centimeter vertical column through the ionosphere inferred from the lunar observations is depicted in Figure 24. There is evidence of a diurnal variation with the maximum ionization content appearing in the vicinity of mid-afternoon. The value of 7×10^{12} electrons/cm^2 in the early hours of the morning for the southerly lunar orbit of 19 March 1960 is a factor of about one-third times lower than the magnitude deduced for the northerly orbits. According to Wright[41], based on his study of electron density profiles in the F-layer along the 75°W geographic meridian, the electron density should maximize at about 5°N geographic latitude which is the region south of Trinidad. Insufficient radar-lunar data recorded during the time when the moon's coordinate was at the maximum southerly declination prevent a full analysis of this discrepancy.

From the excellent agreement found between the electron content determined from radar-lunar observations and that predicted on the basis of a simple Chapman model for the region above the F-layer maximum, it appears that the ionosphere may be represented, to a first approximation, by a Chapman model having a constant scale height of 80 kilometers or less for the daylight hours and perhaps 80 kilometers or more for the nighttime. Wright has suggested that a

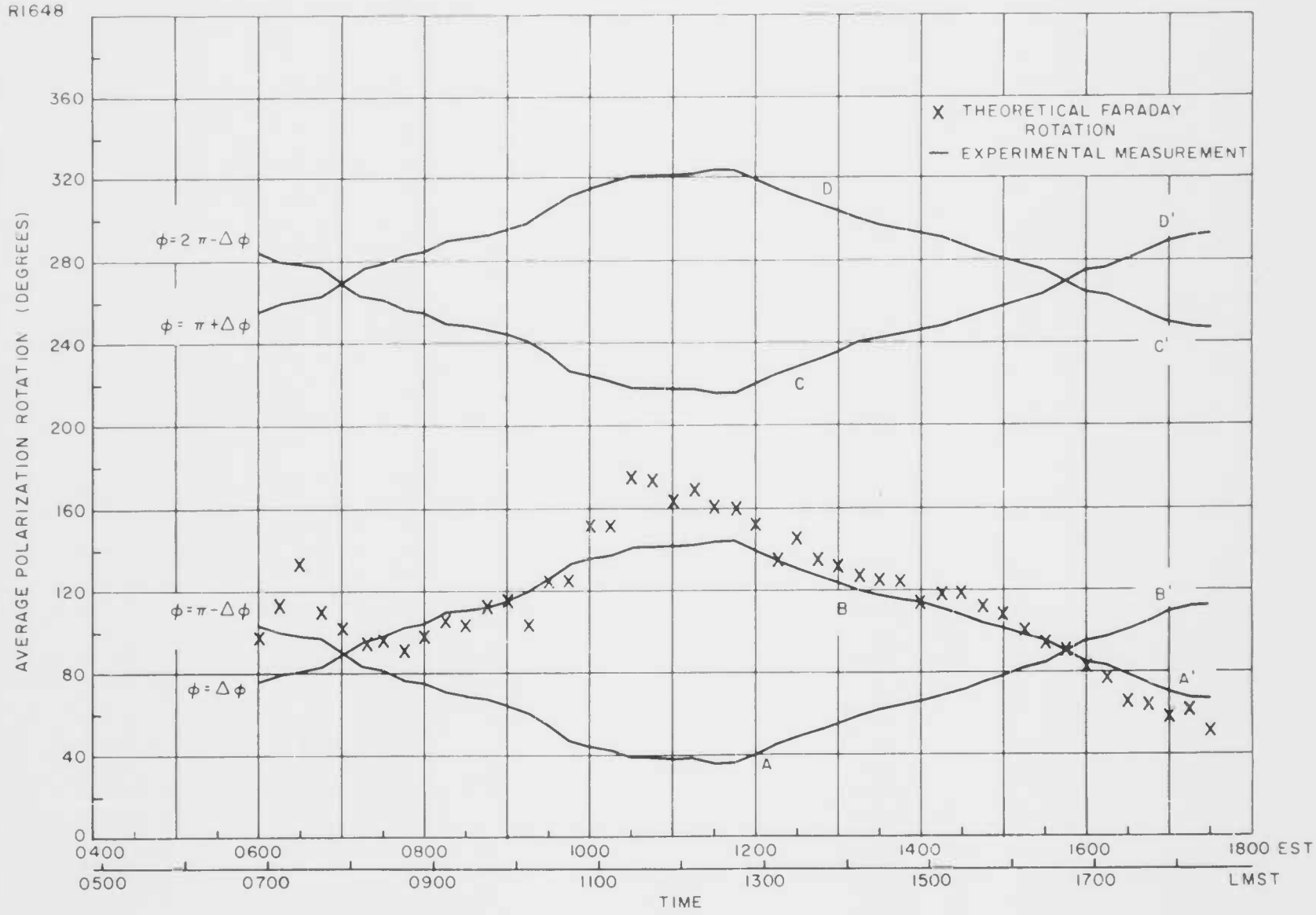

Figure 20. Average Faraday Rotation From Trinidad Radar-Lunar Observation, 26 May 1960

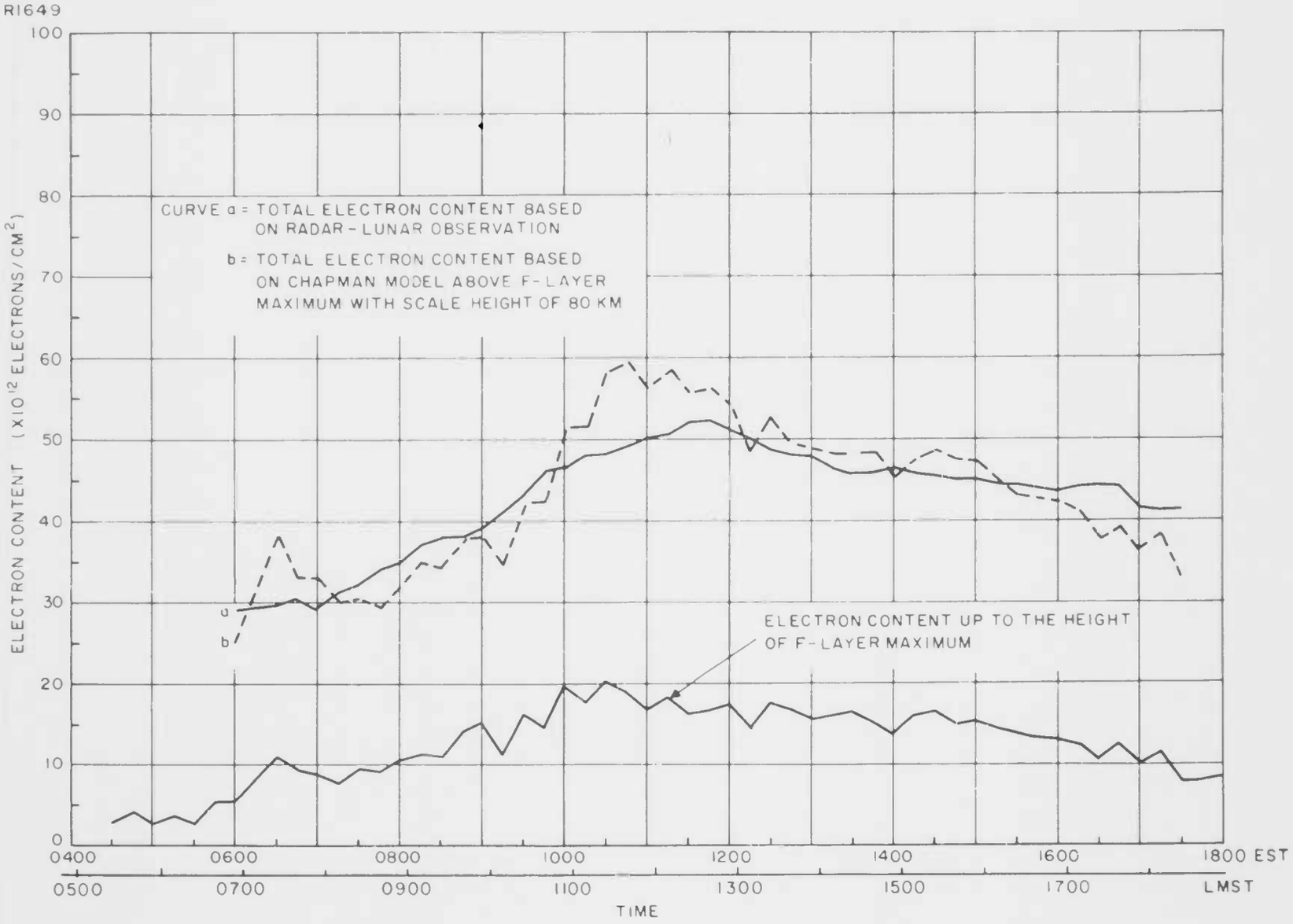

Figure 21. Comparison of the Measured Total Electron Content in a One Square Centimeter Vertical Column Through the Ionosphere with Theoretical Estimate, 26 May 1960

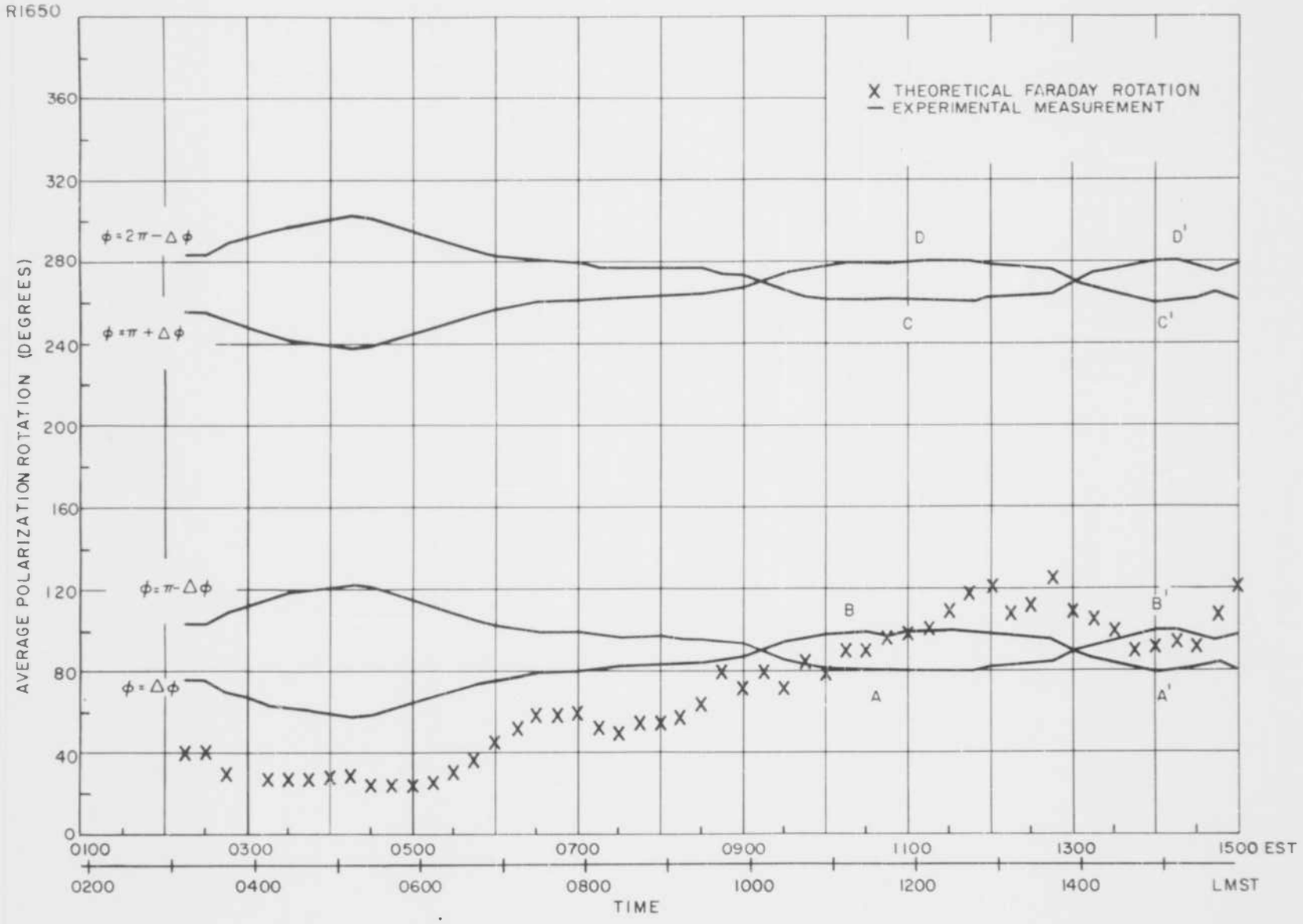

Figure 22. Average Faraday Rotation from Trinidad Radar-Lunar Observation, 20 July 1960

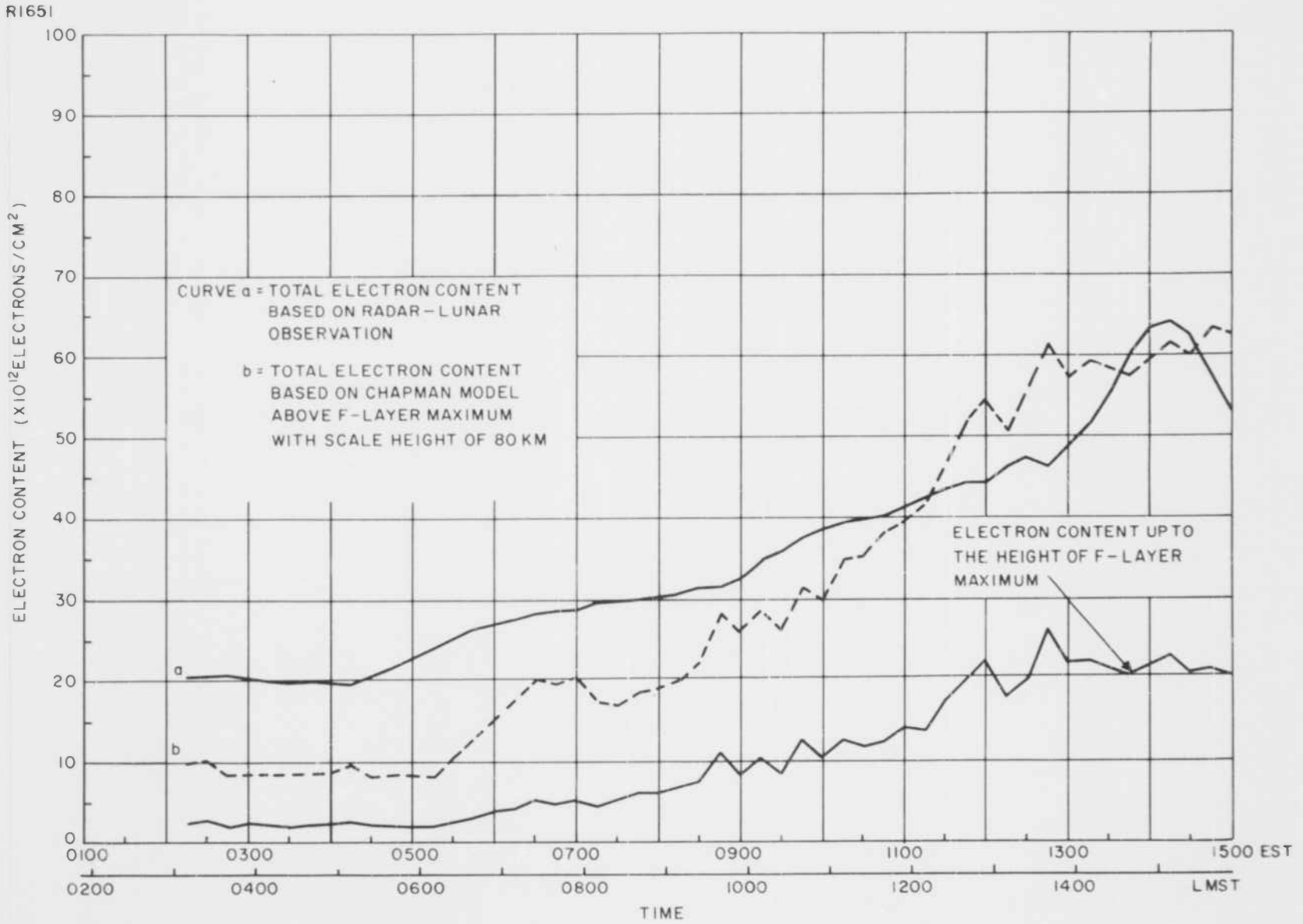

Figure 23. Comparison of the Measured Total Electron Content in a One Square Centimeter Vertical Column Through the Ionosphere with Theoretical Estimate, 20 July 1960

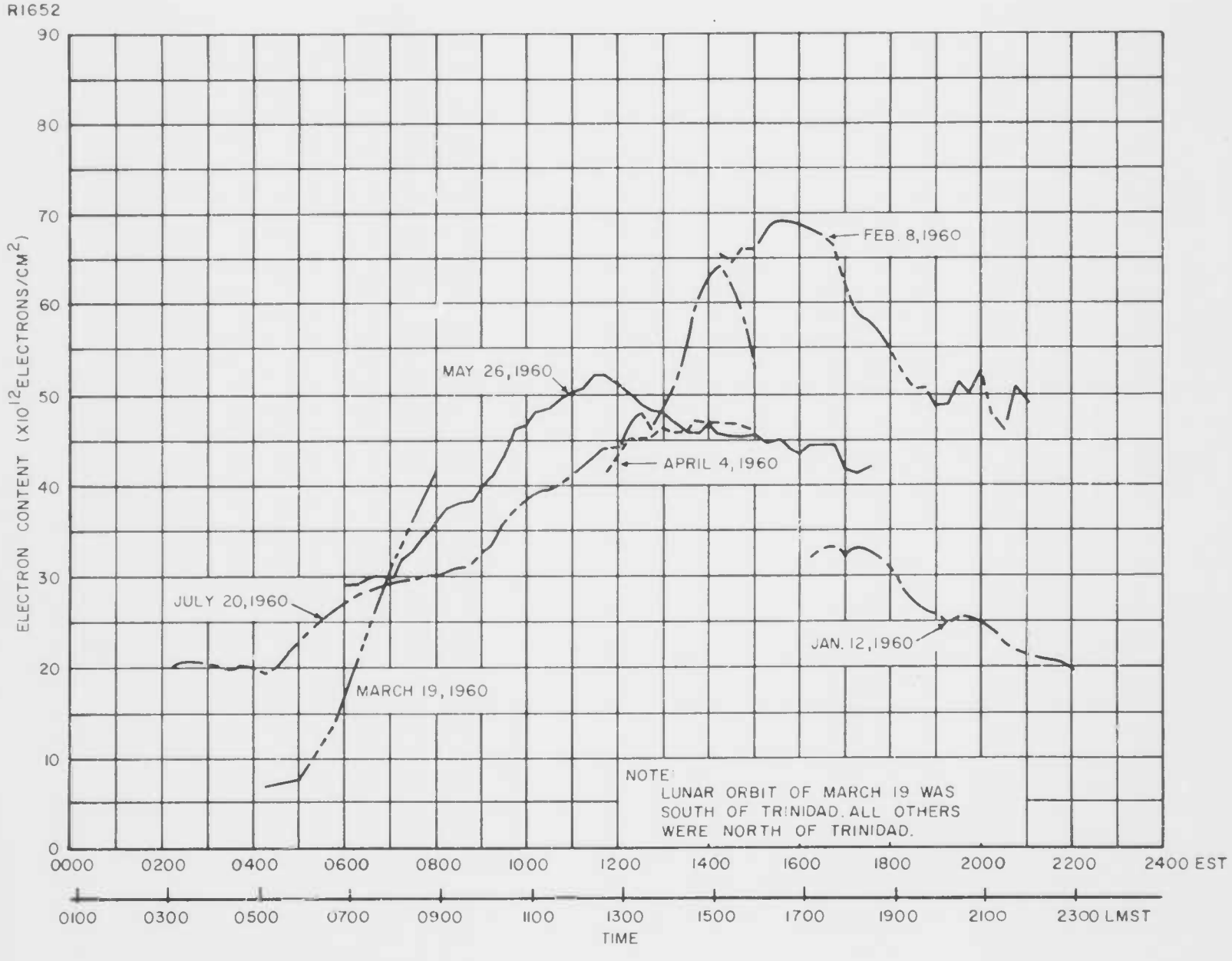

Figure 24. Total Electron Content in a One Square Centimeter Vertical Column Through the Ionosphere Based on Trinidad Radar-Lunar Observations

scale height gradient of about 0.2 km/km for the region above the peak of the F-layer may be more representative of an ionospheric model than one with a constant scale height.[45] Rocket sounding measurement of electron densities, as reported by Berning[20], has disclosed a linear scale height gradient of 0.22 km/km for the neutral gas.

3. Ratio of the Electron Content Above the F-Layer Maximum to That Below

The diurnal variation of the ratio of the integrated electron density above the peak of the F-layer to that below, based on all the radar-lunar measurements recorded at Trinidad, is summarized in Figure 25. It is seen that the ratio, K, as defined by Equation (12), is a variable function of time, attaining a minimum of about 1.5 (average value) at approximately 1300 to 1400 hours local time. At night there is a wide scatter of values ranging between four and 11. It is estimated that these results could have an rms error as high as 15 per cent.

The ratios of the electron content as measured by Bauer and Daniels[15] compare rather favorably with the data presented in this paper. They found the ratio to be on the order of four to five during three nights in June before sunrise and about equal to three after sunrise. In addition, for two days in November, the ratio was about three both before and after sunrise.

Evans and Taylor[40] have reported that, for the months of January and February 1960, the daytime ratio, as determined in England, appears to be about three while the nighttime ratios were in the range between 2.5 and 10. Their daytime results are slightly higher than those obtained at Trinidad, but this perhaps may be attributed to the difference in geographic latitude of the observation sites. Evan's early results[14] are in agreement with his recent work.[40]

The measurements of Hill and Dyce[16] indicate that the ratio of the electron content above to below the F-layer maximum during the night is on the order of 1.5 and during the day about 2.5. It is obvious that the nighttime result is considerably lower than the Trinidad data. This discrepancy could be brought about by their assumption that the function, $f(h)\ H \cos\theta$, can be considered a constant in the evaluation of the electron content integral.

4. Equivalent Slab Thickness and Scale Height of the Ionosphere

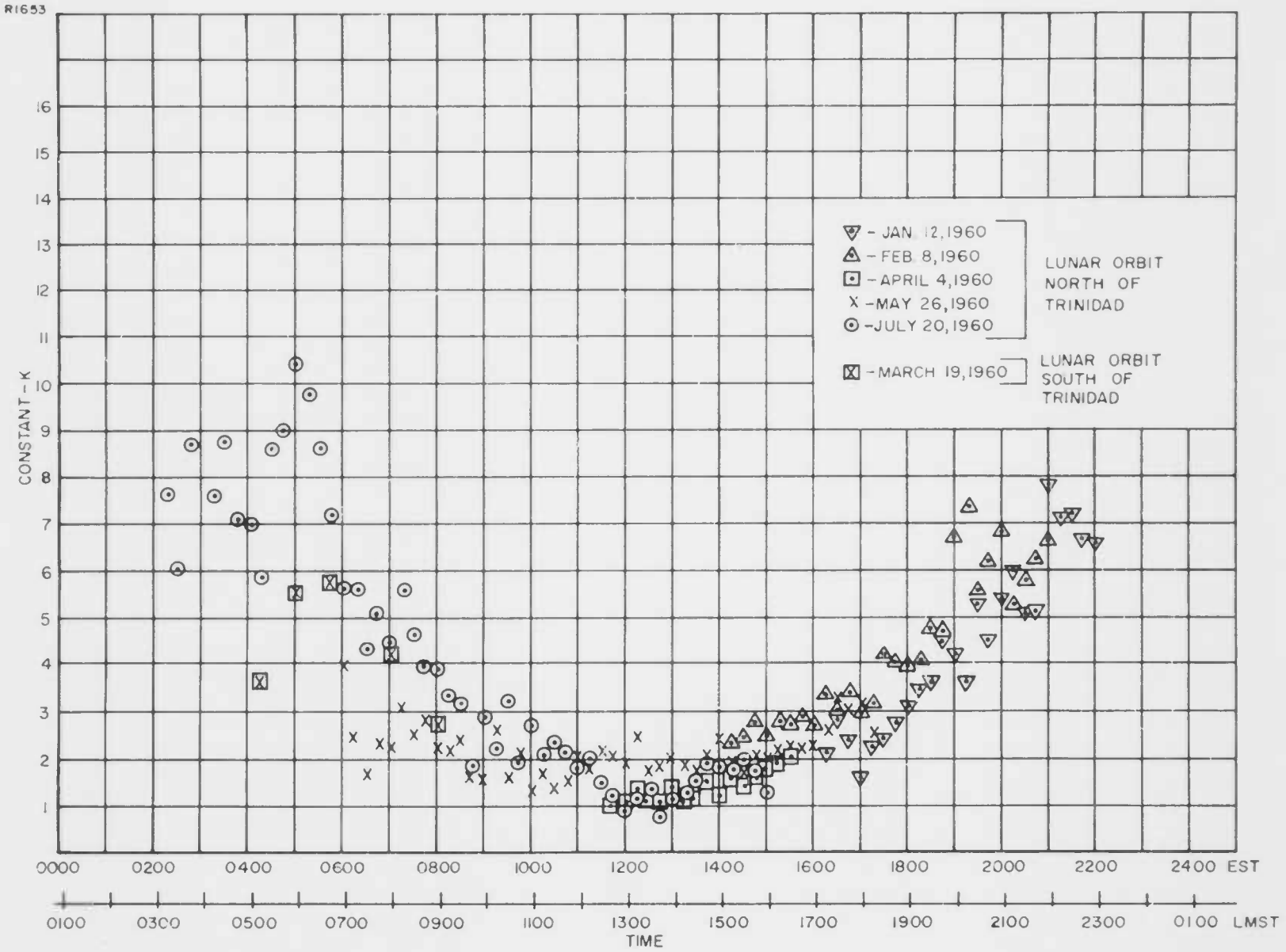

Figure 25. Diurnal Variation of the Ratio of the Electron Content Above the F-layer Maximum to the Electron Content Below the F-layer Maximum Based on Trinidad Radar-Lunar Observations

A parameter presently employed to describe the ionospheric medium is the equivalent slab thickness, τ, defined by Equation (13), which is merely the ratio of the total integrated electron content in the ionosphere to the maximum electron density at the peak of the F-layer.

A plot of the diurnal variation of the maximum electron density of the F-layer, recorded at Puerto Rico and Bogota, Colombia, during the time of the Trinidad lunar observations, is given in Figure 26. The Puerto Rico data corresponds to the times when the moon was at its maximum northern declination, while the Bogota data applies to the moon's southerly orbit of 19 March 1960.

A comparison of the total electron content evaluated from the Faraday rotation data, shown in Figure 24, with the maximum electron density (from vertical incidence ionospheric soundings) Figure 26, reveals that both parameters attain a maximum value in the afternoon.

It is evident from Figure 27 that there is a noticeable diurnal influence on the magnitude of the equivalent slab thickness of the ionosphere (or F-layer).

The equivalent slab thickness is a minimum between 200 and 370 kilometers during the daytime and attains a value as high as 800 kilometers at night.

The analysis of satellite doppler radio signals by Ross and Anderson[46] indicates a slight diurnal influence on the parameter, τ. The noon values of τ, however, do show a pronounced seasonal variation which can be fitted by a sinusoidal function of mean value 290 kilometers at the equinoxes and of amplitude 100 kilometers which maximizes near the summer solstice.[31, 46]

With regard to the presence of seasonal variations in the equivalent slab thickness of the Trinidad results, insufficient data are available to determine this effect.

Assuming that the electron densities in the ionosphere at the time of the Trinidad radar-lunar measurements were distributed in accordance with the Chapman model, the scale height can then be readily computed from Equation (14). The daytime values of scale height vary between 50 and 90 kilometers with a mean of about 75 kilometers, as shown in Figure 27. At night, there is a wide scatter

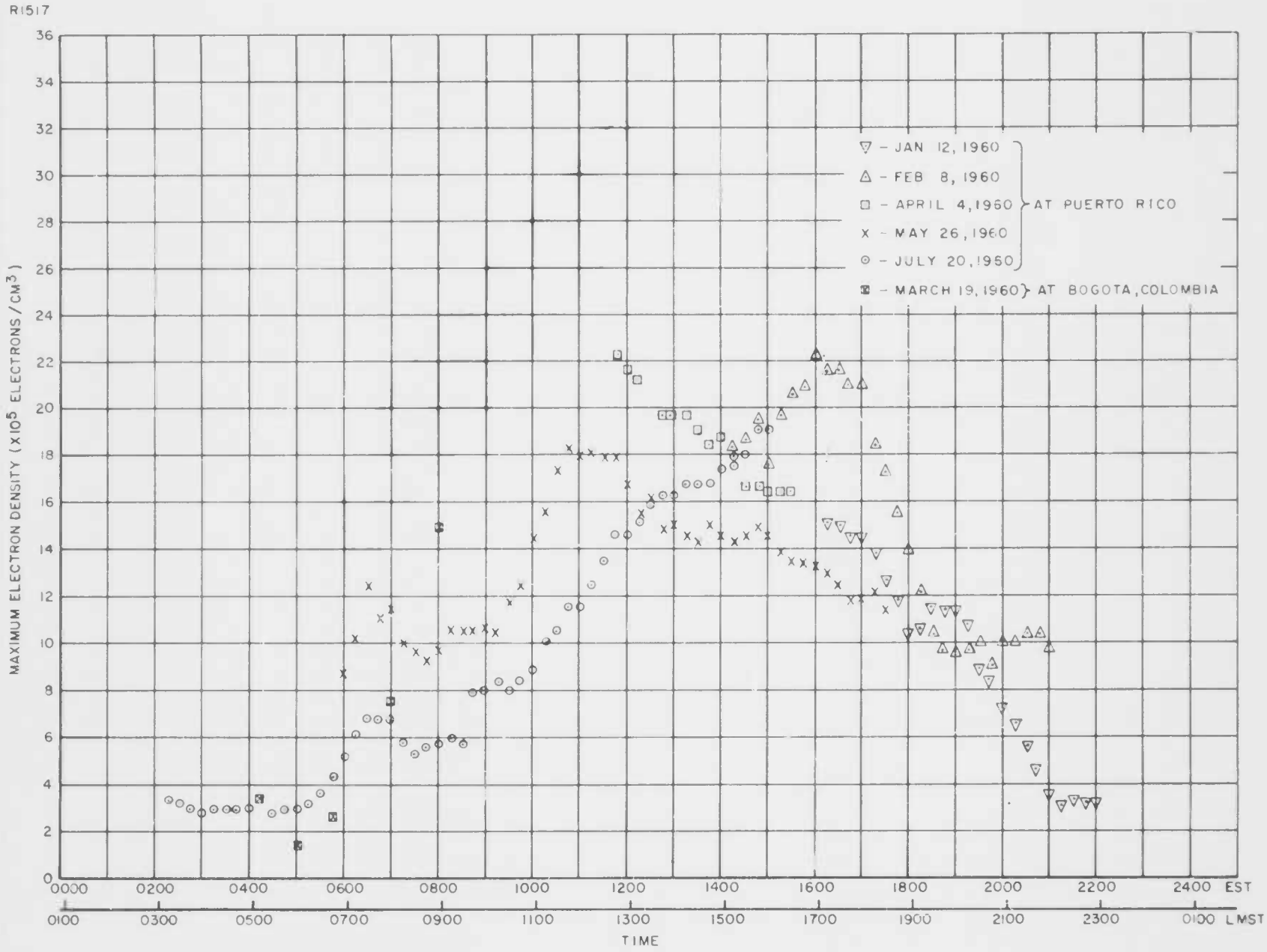

Figure 26. Diurnal Variation of the Maximum Electron Density of the F-layer During the Time of the Trinidad Radar-Lunar Observations.

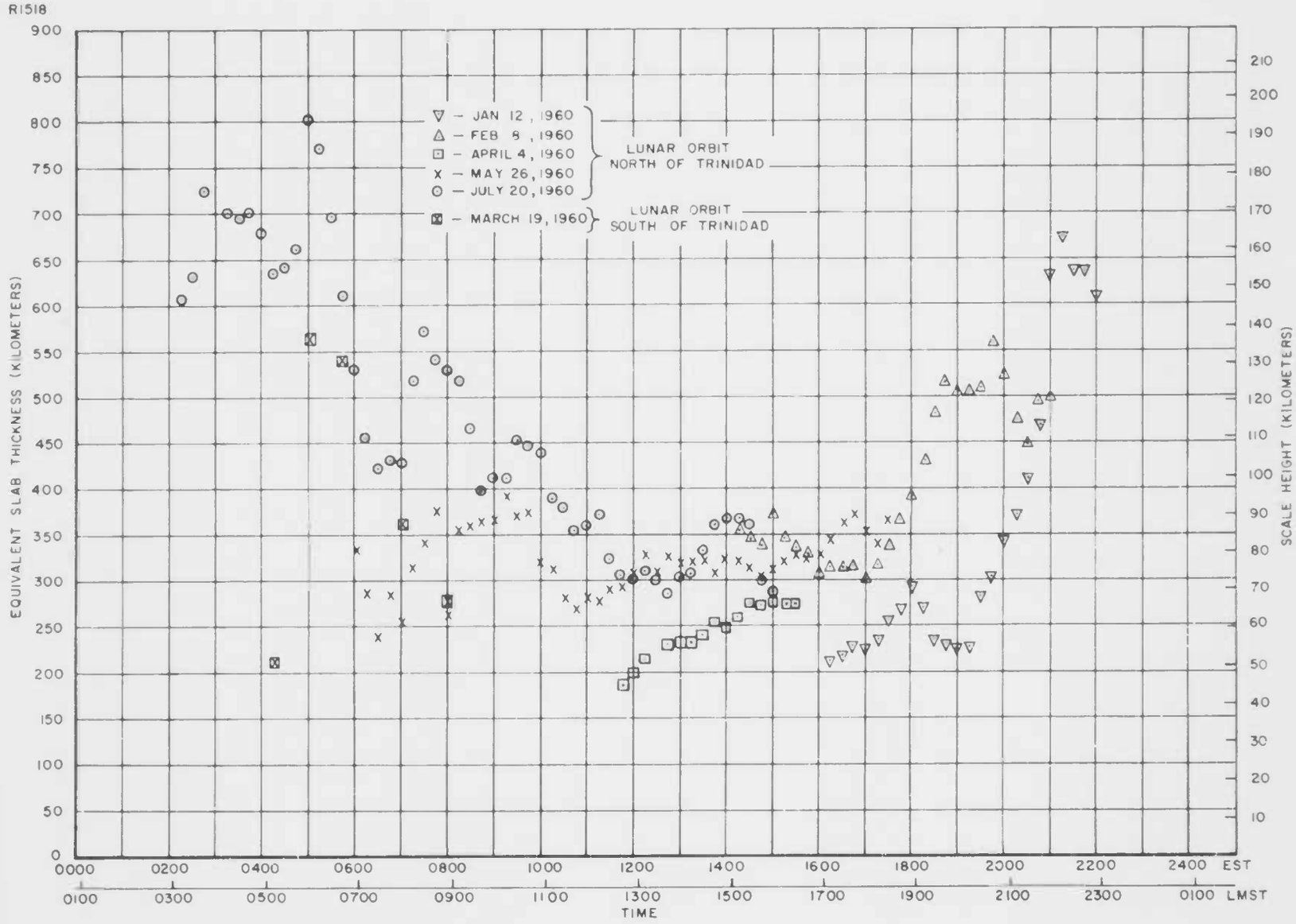

Figure 27. Diurnal Variation of the Equivalent Slab Thickness and Scale Height of the Ionosphere Based on Trinidad Radar-Lunar Observations

of values ranging from 50 to 200 kilometers.

It should be noted that the Trinidad daytime evaluations of the scale height of the neutral particles are in close agreement with Kallmann's estimate from rocket and satellite data.[47]

5. Data Correlation

An attempt was made to determine whether there was any correlation between the calculated ionosphere's parameters, i.e., the total electron content, the electron density ratios, the equivalent slab thickness and the scale height, and the solar and geophysical conditions existing during the time of the experimental measurements.

The various solar and geophysical data, which were considered and are tabulated in Table 2, were obtained from the bulletins published by the National Bureau of Standards.[48]

The geomagnetic planetary index, k_p, is a mean three-hourly magnetic reading based on an arbitrary scale of zero to nine where zero refers to a very quiet day and nine to an extremely disturbed day. The relative sunspot number is an index of the activity of the entire visible disk. It is defined as $R = K(10g + s)$ where g is the number of sunspot groups, s is the total number of distinct spots and K is a scale factor usually less than unity, its value being dependent upon the observer. The solar flux at 2800 megacycles is the daily value measured at noon in Ottawa, Canada.

Because of the lack of sufficient experimental data, this analysis did not disclose evidence of any correlation.

B. CHARACTERISTICS OF THE LUNAR SURFACE

1. Lunar Reflection Laws

The supposition that the moon is a rough body at radar frequencies has led to the speculation of various scattering laws and functions to describe the manner in which radio waves would scatter from the moon's surface. A method of investigating an applicable scattering law is to characterize the decay rate of the trailing edge of a lunar echo.

TABLE 2

SOLAR AND GEOPHYSICAL CONDITIONS DURING THE TIME OF THE TRINIDAD RADAR-LUNAR OBSERVATIONS

Date	Time (EST)	Planetary Magnetic Index - K_p	American Relative Sunspot Number R_A'	Zurich Provisional Relative Sunspot Number - R_z	Daily Values of Solar Flux at 2800 mc*
12 January 1960	1615-1745	4-	127	108	184
	1900-2145	2o			
	2200- -	2o			
8 February 1960	1415-1545	2-	118	116	183
	1600-1845	1o			
	1900-2100	3o			
19 March 1960	0415-0645	3+	93	102	137
	0700-0900	3+			
4 April 1960	1145-1245	4o	161	162	188
	1300-1530	4-			
26 May 1960	0600-0645	3-	122	130	158
	0700-0945	2+			
	1000-1245	3o			
	1300-1545	3o			
	1600-1730	4o			
20 July 1960	0215-0345	2+	126	137	152
	0400-0645	4-			
	0700-0945	5o			
	1000-1245	4o			
	1300-1500	4+			

* Watts Meter^{-2} (cycles/sec)$^{-1}$

In order to reduce the effect of short term fluctuations in the envelope of a lunar echo, 130 A-scope photographs, consisting of 65 different pulse returns received on the two orthogonal polarizations, were averaged to obtain a representative sample for analysis purposes. The resultant lunar echo, shown in Figure 28, was obtained by dividing each pulse into 0.25-millisecond intervals. At each interval along the pulse, an average amplitude was calculated from the 130 different data points.

It is seen that the trailing edge of the pulse can be described in terms of the trigonometric function, $A \cos \left[B (\theta + C)\right] + D$, where the constants $A = 2.5$, $B = \pi/55$, $C = -30$ and $D = -1.6$. The variable, θ, is the angle of incidence with respect to the normal to the surface of the moon. The relationship expressing θ in terms of the radio depth of the moon is contained in Appendix D.

The power distribution of the trailing edge of the average lunar echo is compared with other functions in Figure 29. The third degree polynomial, $\alpha + \beta \theta + \gamma \theta^2 + \delta \theta^3$, where $\alpha = 39.06$, $\beta = 74.33$, $\gamma = 39.09$ and $\delta = -3.38$, also accurately represents the shape of the pulse. It is obvious, however, that the angular scattering law, $A_1 \left[\sin 2 \theta/2 \theta\right]^{20}$, where the constant A_1 is equal to 163, suggested by Leadabrand[11] does not seem to apply to this example.

The trigonometric functions, $A_2 \cos \theta$ and $A_3 \cos^2 \theta$, where $A_2 = 11.2$ and $A_3 = 13.65$, also shown in Figure 28, are representative of the Lommel-Seeliger and the Lambert scattering law, respectively. When the relative echo power is plotted as a function of the cosine of the angle of incidence, as in Figure 30, it is found that the Lommel-Seeliger law and the Lambert law reduce to straight lines and that the pulse decay rate follows the slope of the Lommel-Seeliger scattering law displaced by approximately a factor of 1/8.

It should be mentioned that Pettengill[10] has reported that, following the decay of the initial specular component, the angular distribution of power in the moon echo obeyed the Lambert-type law except for a small amount of limb brightening at the extreme ranges. Since the Trinidad and Millstone Hill

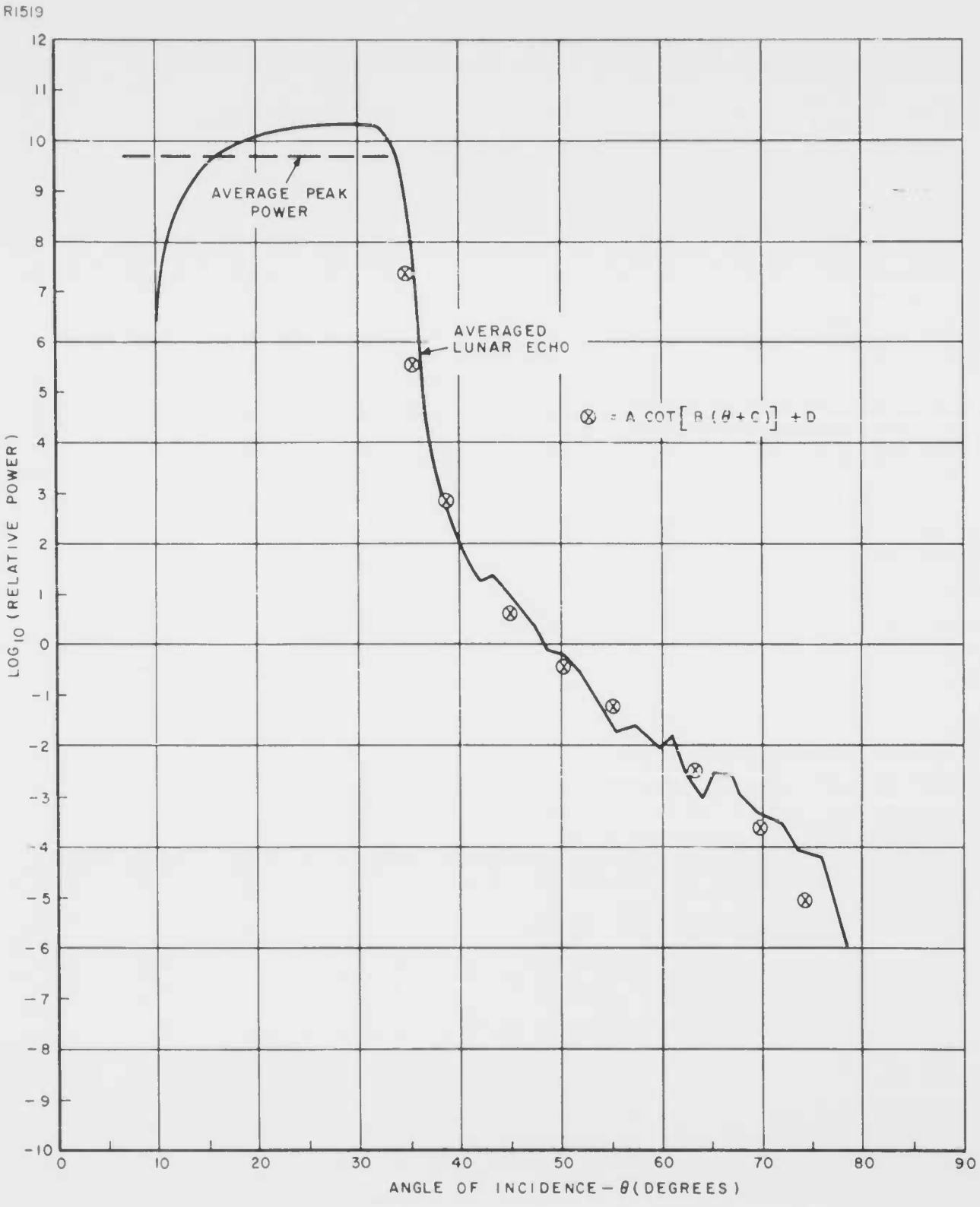

Figure 28. Mean Lunar Echo Recorded at Trinidad

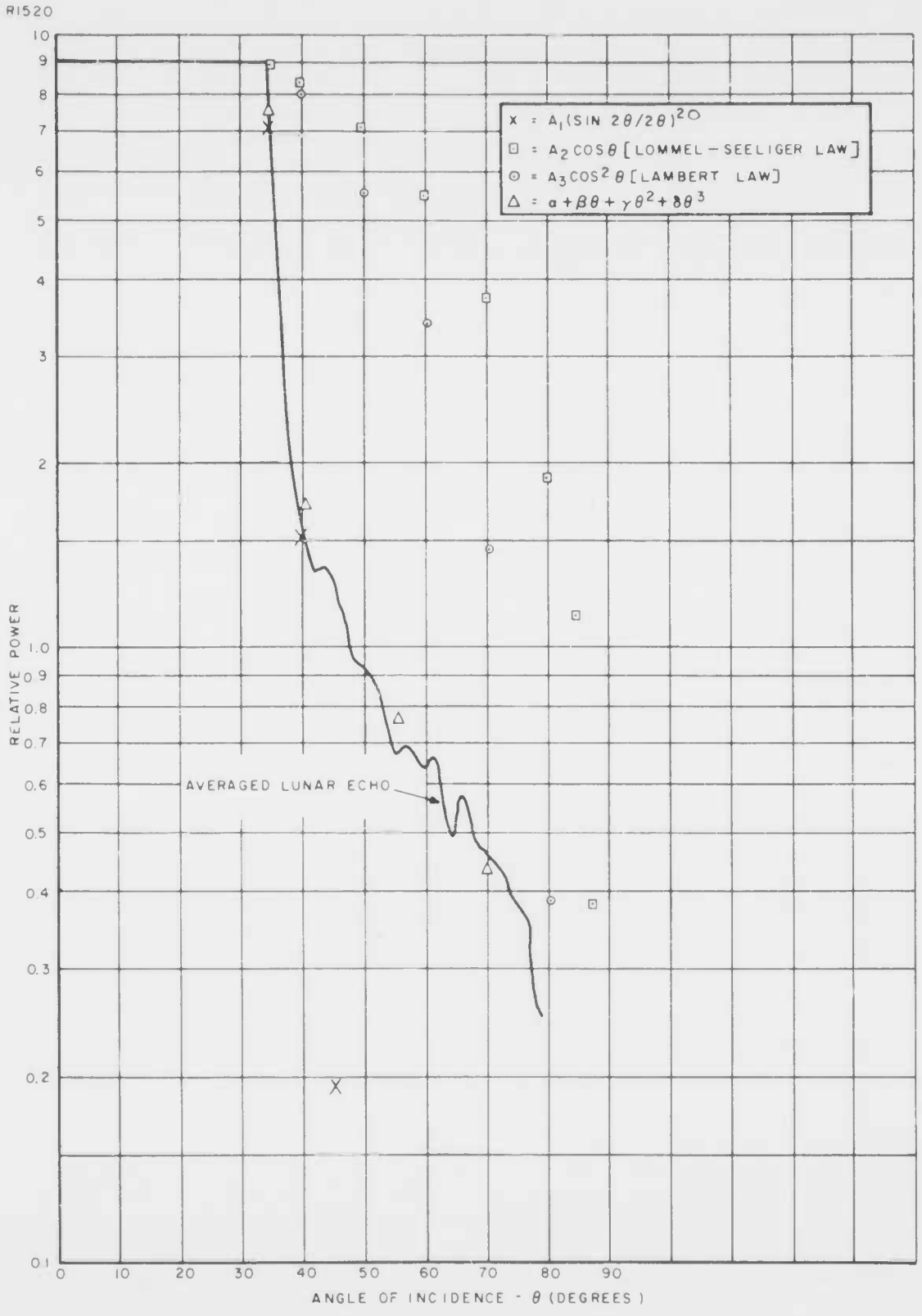

Figure 29. Scattering Laws Applied to Lunar Echo as a Function of the Angle of Incidence

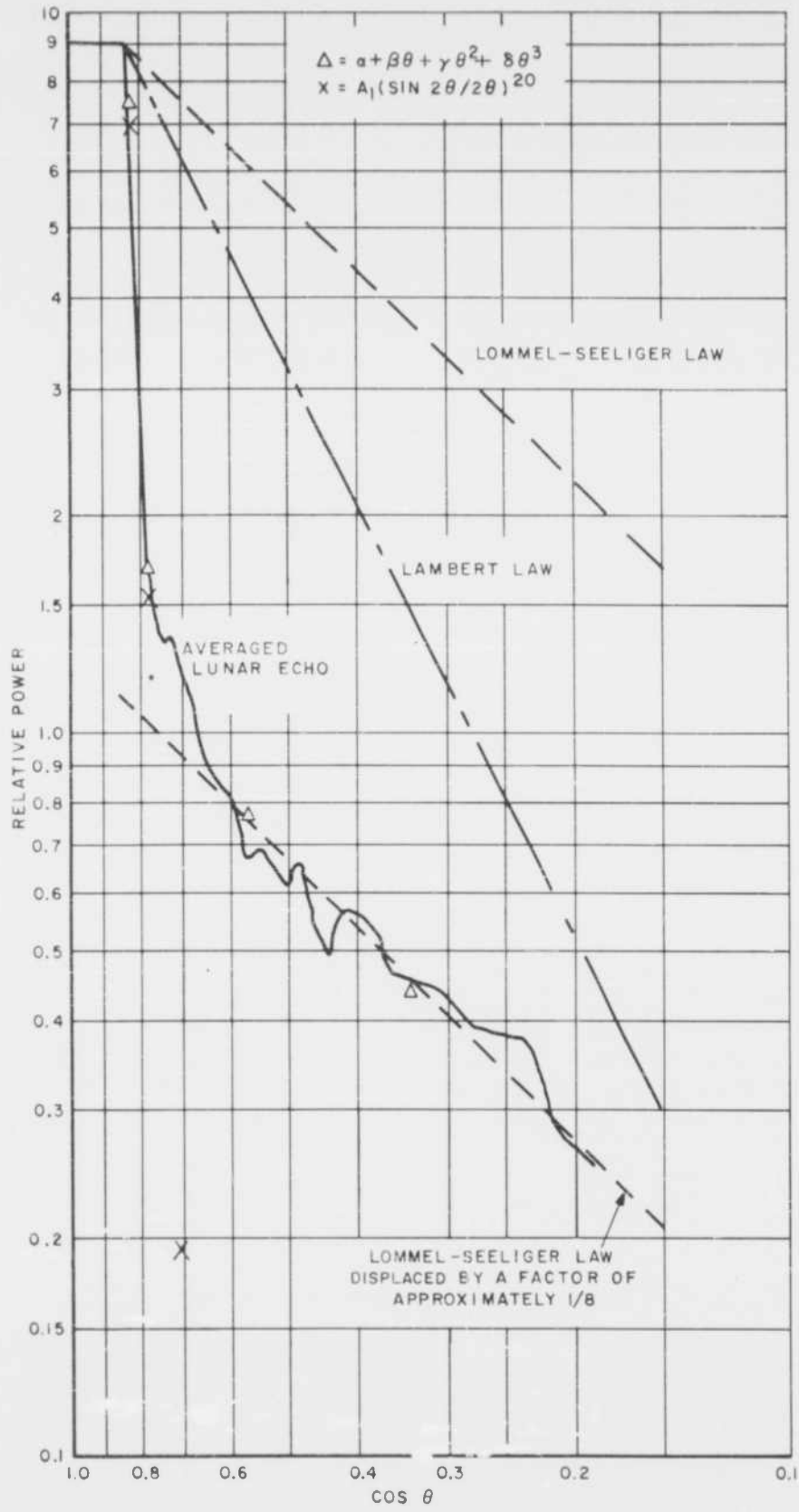

Figure 30. Scattering Laws Applied to Lunar Echo as a Function of the Cosine of the Angle of Incidence

investigations were conducted at approximately the same frequency, i.e., the transmission frequency at Millstone Hill was 440 megacycles compared to 425 megacycles at Trinidad, the discrepancy in the results may be attributed to the fact that the lunar echo analyzed by Pettengill was a composite of 24,000 pulses, integrated at each 500-microsecond range increment.

However, Browne[12], on the other hand, has found that an analysis of lunar echo data, observed at a frequency of 120 megacycles, gives best agreement with the Lommel-Seeliger scattering model.

2. Cross Section and Reflection Coefficient of the Moon

In analyzing the cross sectional area of the moon and the statistical distribution of the amplitudes of lunar signals, as discussed in the next section, the magnitude of the amplitude of the received echoes was measured at a constant position within the pulse, i.e., at one millisecond after the beginning of the pulse which corresponds in range to a lunar depth of 150 kilometers.

The cumulative probability distributions of the total cross section of the moon measured on 12 January 1960 during two 10-minute periods are shown in Figure 31. The total lunar cross section is merely the vectorial addition of cross sections obtained on the orthogonal polarization receiver channels. Each cumulative distribution curve was calculated from over 5000 individual data points. The interval between 1630-1640 EST corresponds to the time when the moon was oriented at an azimuth angle of about 72.5 degrees and elevation angles of 4.7 -6.7 degrees, while between 2215-2225 EST it was at an azimuth angle varying from 29 to 15 degrees and elevation angle of about 82 degrees.

It is seen that, for the low angle measurements, 50 per cent of the total cross sections were equal to or less than 8.5×10^{11} square meters, while, at transit, the value reduced to 6.0×10^{11} square meters.

The lunar observations of 2 February 1960, shown in Figure 32, reveal that 50 per cent of the total cross sections between 1430-1440 EST were equal to or less than 5.0×10^{11} square meters, while, during the interval 2025-2035 EST, they increased to 7.5×10^{11} square meters.

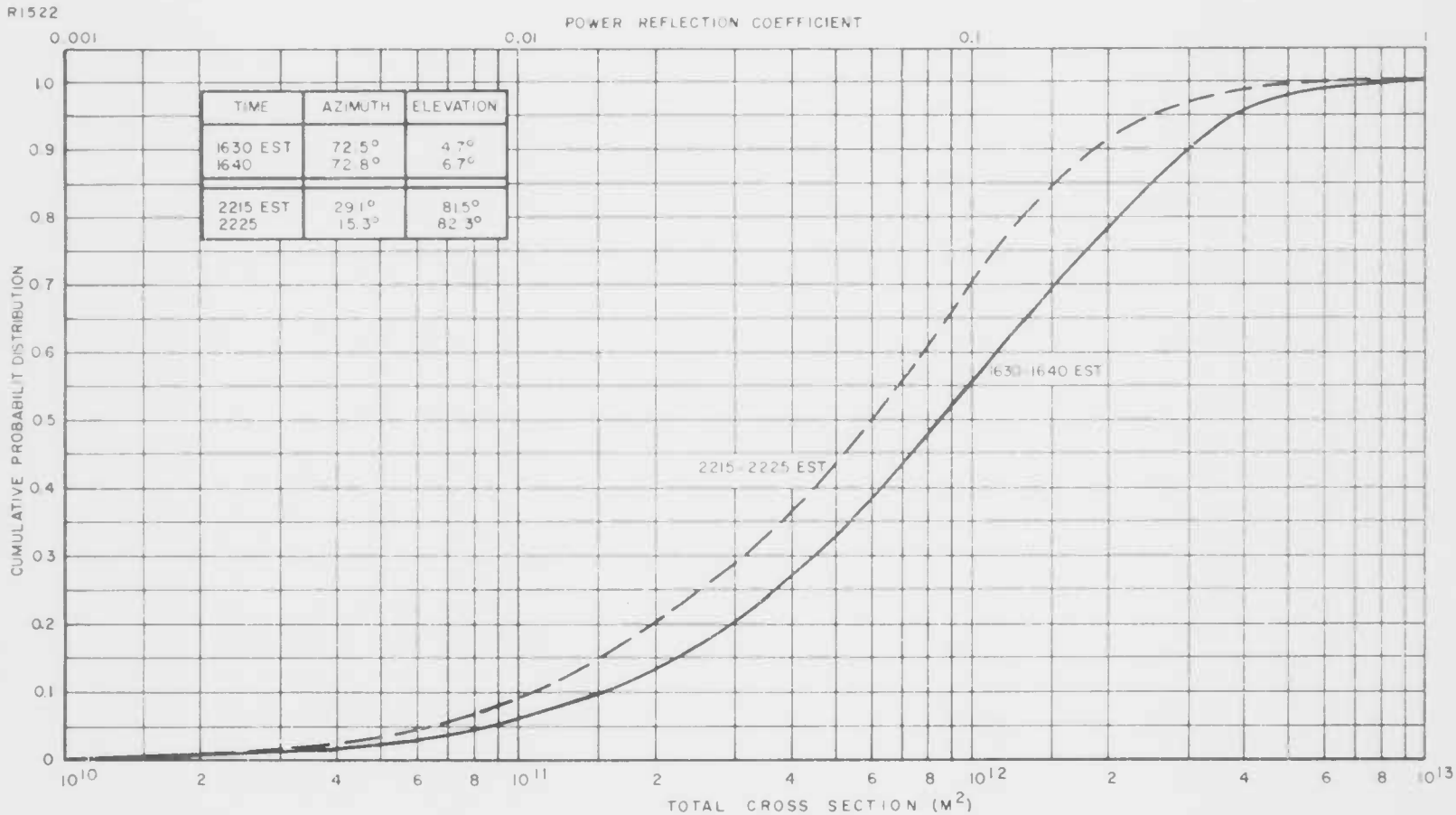

Figure 31. Cumulative Probability Distribution of the Total Cross Section of the Moon, 12 January 1960

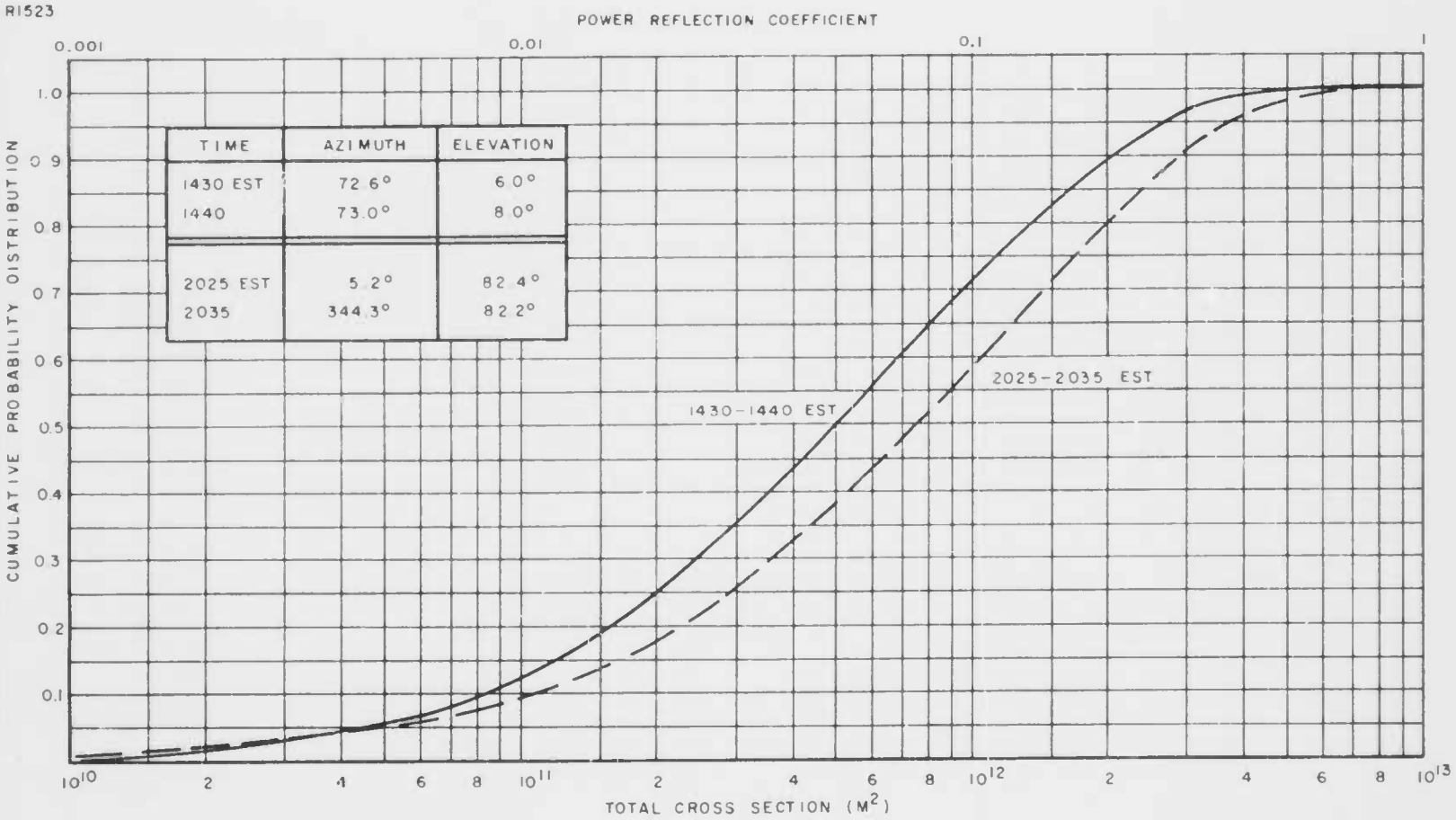

Figure 32. Cumulative Probability Distribution of the Total Cross Section of the Moon, 8 February 1960

Assuming that the moon is a perfectly conducting sphere, its radar cross section is then the projected geometric area of the whole disk or 9.5×10^{12} square meters. It follows from Equation (17) and Figures 31 and 32 that, for 50 per cent of the observations, the power reflection coefficient of the moon's surface appeared to lie between 0.05 and 0.085. It is estimated that the experimental error incurred in this analysis should be less than 3 db.

Measurements made by Fricker[44] at a frequency of 412 megacycles using a cw system, indicated a lunar power reflection coefficient of 0.074. According to Blevis and Chapman[49], radar observations of the moon at 488 megacycles, also made with a cw system, revealed a power reflection coefficient of about 0.05. The uncertainty in both experimental results are reported to be less than 3 db.

Since the Trinidad results, obtained by pulsed radar techniques having a pulse length less than the radio-depth of the moon, are in excellent agreement with other experimental data taken with cw systems in the same frequency range, it would appear that the moon must be sufficiently smooth for Fresnel type reflection to take place.

It should be mentioned that values of 0.1 to 0.15 have often been quoted for the power reflection coefficient of the moon's surface. The Trinidad measurements and those reported by Fricker[44] and Blevis and Chapman[49] would indicate that these values are somewhat high.

3. Statistical Analysis of Lunar Echo Amplitudes

According to theory, the amplitudes of pulses reflected from an irregular surface which scatters electromagnetic waves randomly, i.e., with random phases and amplitudes, should be Rayleigh distributed. For a surface which contains both one large smooth area and many rough scatters, the amplitude distribution should tend toward Gaussian.

In order to test this hypothesis for determining the surface characteristics of the moon, the lunar echo amplitudes recorded in two 10-minute intervals between 1430-1440 EST and 2025-2035 EST on 8 February 1960 were selected. It should be noted that the amplitude data from these time periods, considered

in this analysis, are identical with the lunar cross section data discussed in Figure 32. The statistical analysis was made on the total signal amplitude in order to reduce the effect of ionospheric Faraday rotation.

The probability density function of the total lunar amplitude, recorded during moonrise when the libration fading rate was normally low, is illustrated in Figure 33. The theoretical curves were calculated from Equation (27) with the parameter ψ, defined by Equation (25), equal to 28.0, this constantbeing evaluated from the experimental data.

The presence of a strong steady signal would be indicated by a probability density function which would be of the form of the b = 2 curve. It is seen that the experimental points coincide, to some degree, with the theoretical Rayleigh distribution (b = o) for low amplitude values, but commence to diverge for a normalized amplitude of 12 and greater. This is clearly evident if the natural logarithm of the ratio of the probability density function to the normalized amplitude is plotted as a function of the square of the normalized amplitude as shown in Figure 34. It is noted, from Equation (23), that for this type of a plot, the slope of the Rayleigh distribution is $1/2\ \psi$.

The experimental and theoretical probability density functions of the total amplitude of the lunar echoes observed for 10 minutes near transit are shown in Figure 35. After normalization, the parameter, ψ, for this time period was found to be 40.0

It is interesting to note that the experimental data appear to tend toward the b = 1 probability density curve except for the slight displacement at the maximum. It is definitely seen, from Figure 36, that the experimental points do not correlate with the Rayleigh distribution curve.

A comparison of the experimental points in Figures 33 and 35 indicate that, at high elevation angles where libration fading is a maximum,[44] the amplitude signals were observed more often having greater magnitudes than those detected near moonrise. This is based on the fact that the number of pulse returns considered in both analyses was the same.

An amplitude record of one minute in duration (2026:20 - 2027:20 EST)

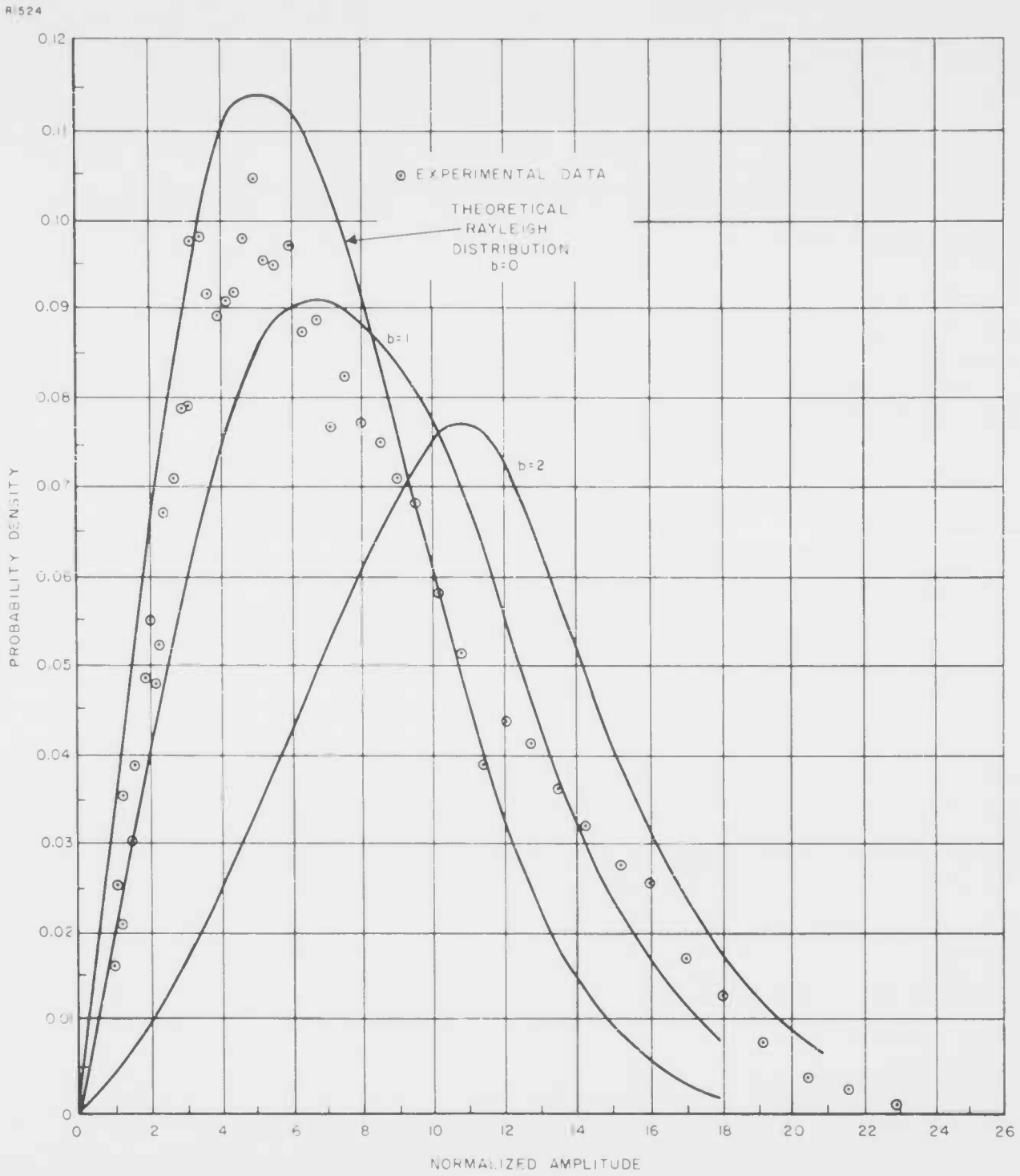

Figure 33. The Probability Density Function of the Total Amplitude of the Lunar Echo, 8 February 1960, 1430-1440 EST

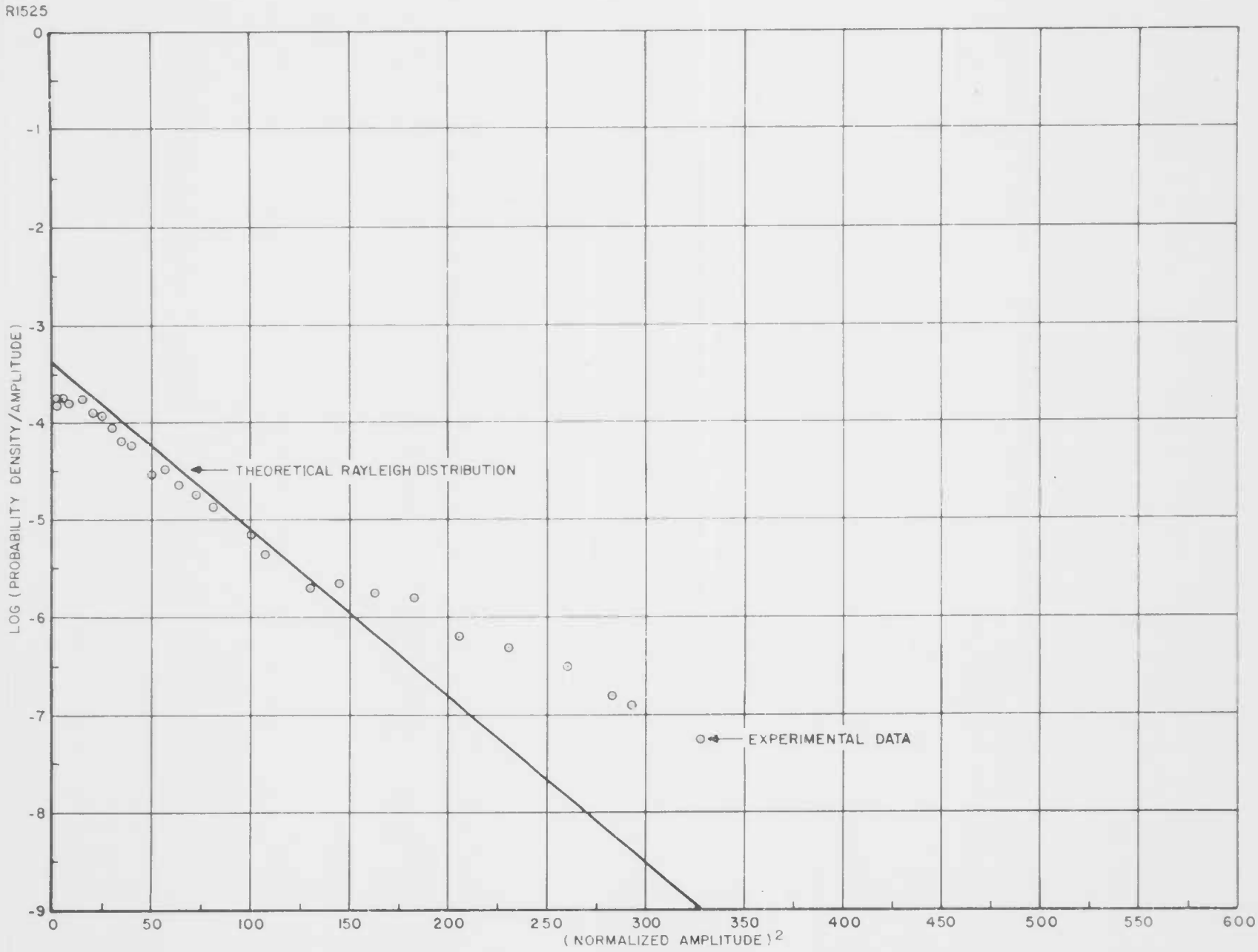

Figure 34. The Natural Logarithm of the Probability Density Function of the Total Amplitude of the Lunar Echo, 8 February 1960, 1430-1440 EST.

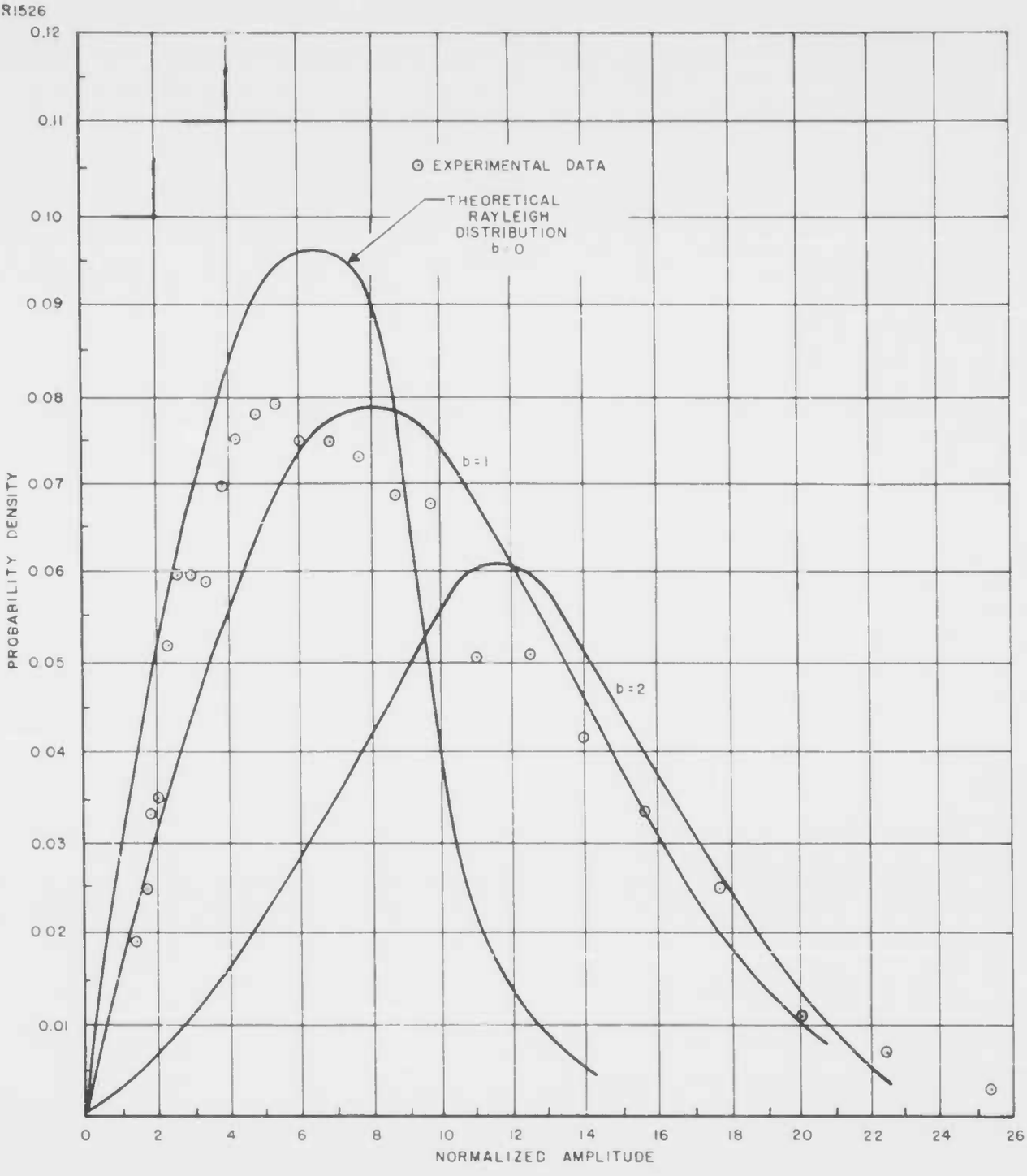

Figure 35. The Probability Density Function of the Total Amplitude of the Lunar Echo, 8 February 1960, 2025-2035 EST.

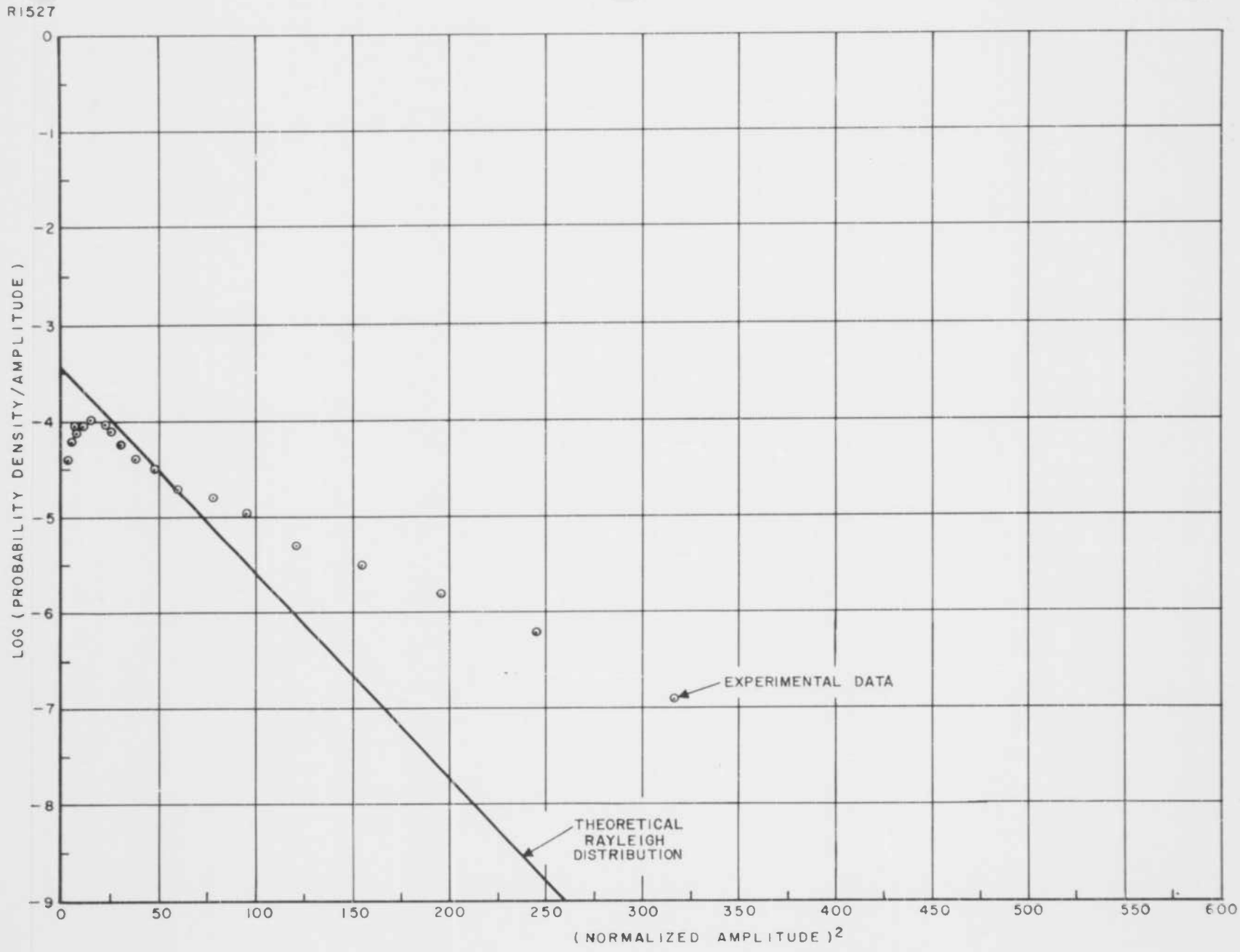

Figure 36. The Natural Logarithm of the Probability Density Function of the Total Amplitude of the Lunar Echo, 8 February 1960, 2025-2035 EST.

taken from the same statistical population, was also analyzed to determine the effect of a shortened sample size on the experimental distribution. In general, it was found that the amplitudes of the one-minute sample were distributed in a somewhat similar fashion to those of the 10-minute sample.

The results of this analysis reveal evidence of the presence of a slight specular component reflected from the lunar surface during the time when the moon was near transit. This was not the case, however, for observations conducted at moonrise.

It is possible that, instead of one large smooth region on the surface of the moon, there are many smooth areas which give rise to specular reflection. Thus, this would have the effect of imposing a random phase and random amplitude fluctuation on the resultant specular component. It would follow that the steady signal, which would be normally expected if the moon consisted of only one large smooth reflecting area, would, in essence, be washed out or smeared.

4. Doppler Frequency Shift

Because of the relative motion of the moon with respect to the earth, radio waves reflected from the moon are shifted in frequency.

The doppler frequency shifts measured during the partial lunar orbits of 12 January 1960 and 8 February 1960 are shown in Figure 37. It is quite evident that the experimental observations are in agreement with the theoretical predictions. The theoretical curves were computed according to the method proposed by Fricker[44], the mathematical relationships being given by Equations (34) through (39).

The doppler shift is a maximum of approximately +1130 cps at moonrise and a minimum at the moon's transit, as shown in Figure 37.

The doppler frequency shift at 120 megacycles, as reported by Browne[12], was on the order of ±50 cps for observations taken when the hour angle of the moon was less than 30 minutes of time. Doppler shifts as large as ±1000 cps at 412 megacycles have been recorded by Fricker[50].

5. Doppler Frequency Spread

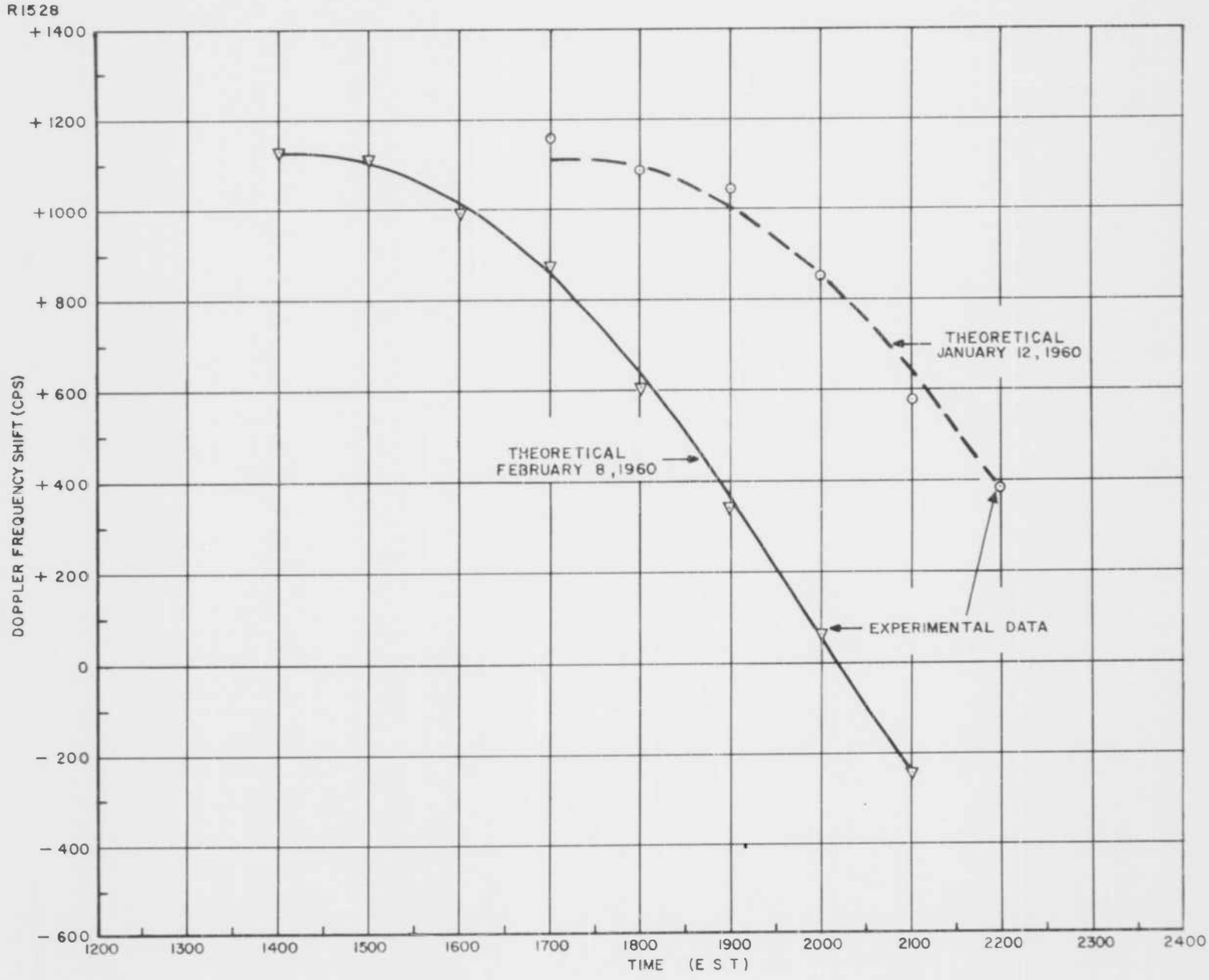

Figure 37. Doppler Frequency Shift of Lunar Echoes Recorded at Trinidad

Radio waves when reflected from the moon experience a doppler spread in frequency in addition to undergoing a doppler shift. The former phenomenon is predominantly the result of the moon's libration.

Fricker[44] has shown that the frequency spread at transit is always a maximum, while at moonrise, it could have any value depending upon the moon's effective total libration rate in latitude and longitude (see Equation (40)).

The moon's libration has the effect of imposing a rapid fluctuation on the amplitude of the signal reflected from its surface. Sample amplitude vs. time film records illustrating the presence of libration fading are displayed in Figure 38. An examination of Figure 38a reveals a dominant low periodic structure which is indicative of the minimum libration fading prevalent at the time of observation. Figure 38c represents data collected later in the same day during the moon's transit. The higher frequency variation of signal amplitude, evident in this record, corresponds to a time of comparatively high libration rates. The lunar echoes observed at an elevation angle of about 46.5 degrees, Figure 38b, show a mixture of both low and high fading rates. It should be noted that the relative difference of signal amplitudes on the horizontal and vertical polarizations from moonrise to transit was caused by the change in the rotation of the plane of polarization by the ionosphere, i.e., Faraday effect.

In an attempt to determine the correlation with the "effective-libration rate" doppler, the power spectrum for the two lunar observations were obtained and compared with the theoretical doppler spread.

As discussed in Appendix E, the power density spectrum is the Fourier transform of the autocorrelation function which is computed from an amplitude vs. time function. In this analysis, the autocorrelation function is obtained from the total lunar cross section which is proportional to the square of the signal amplitude. The power density spectrum, discussed in this section, in essence defines the frequency-power content of the time variation of the total echoing area of the moon.

A portion of the sample of the 8 February 1960 lunar data selected for this analysis is shown in Figure 38a. The total signal power for each pulse, i.e., sum of the power received on the two orthogonal polarizations, was

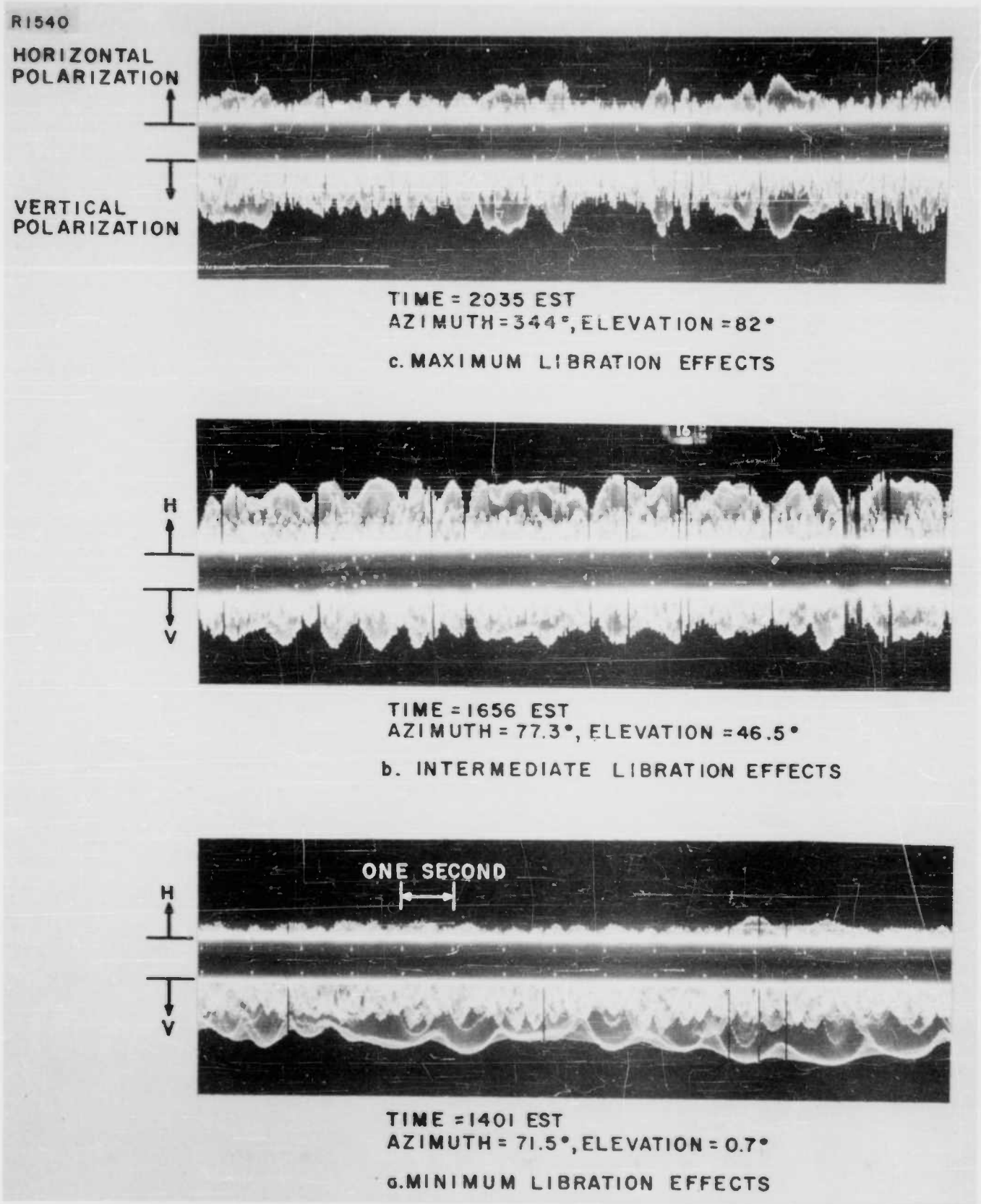

Figure 38. Amplitude vs. Time Film Records Showing the Influence of Lunar Libration, 8 February 1960

measured one millisecond after the rise of the pulse. This corresponds to the coverage of a spherical cap on the moon with a fractional radius of 0.404 (see Appendix D).

The autocorrelation function of the total cross section for a one-minute interval at moonrise is presented in Figure 39. The power density spectrum corresponding to this function is given in Figure 40. It is seen that the principle frequencies are all less than one cps, i.e., 0.27, 0.53, 0.69, and 0.94 with the dominant frequency being 0.27 cps.

It should be mentioned that a graphical Fourier analysis [51] of the film record for the same period revealed frequencies of 0.23, 0.82, and 1.73 cps.

The theoretical maximum doppler spread for this particular time was found to be 2.21 cps for the fractional radius of 0.404. This calculation was based on the lunar libration rate constants presented in Table 3 and applied to Equations (40) and (41).

A similar analysis of the 4 April 1960 lunar data, also at moonrise, revealed the autocorrelation function and the power density spectrum given in Figures 41 and 42, respectively. The principle frequencies present in the power density spectrum are 0.14, 0.27, 0.49, 0.98, 1.38, 1.62, 1.77, 2.00, 2.30, 2.50, 2.65, 3.20 and 3.50 cps, the dominant being 0.14 cps.

Utilizing the libration constants tabulated in Table 3, it can be shown that the theoretical maximum doppler spread for the fractional radius of 0.404 was 0.66 cps.

It is evident that, for the two lunar observations that were analyzed, the theoretical maximum doppler spreads exceed the dominant frequency of the power density spectrums deduced from the experimental data.

At a frequency of 425 megacycles, the first Fresnel zone on the moon has a fractional radius of approximately 0.007. This value differs from the fractional radius of 0.404 employed in the calculations by a factor of 0.017. The experimental dominant frequency of the 8 February 1960 observation, 0.27 cps, is 0.12 times smaller than the theoretical estimate of 2.21 cps. In addition,

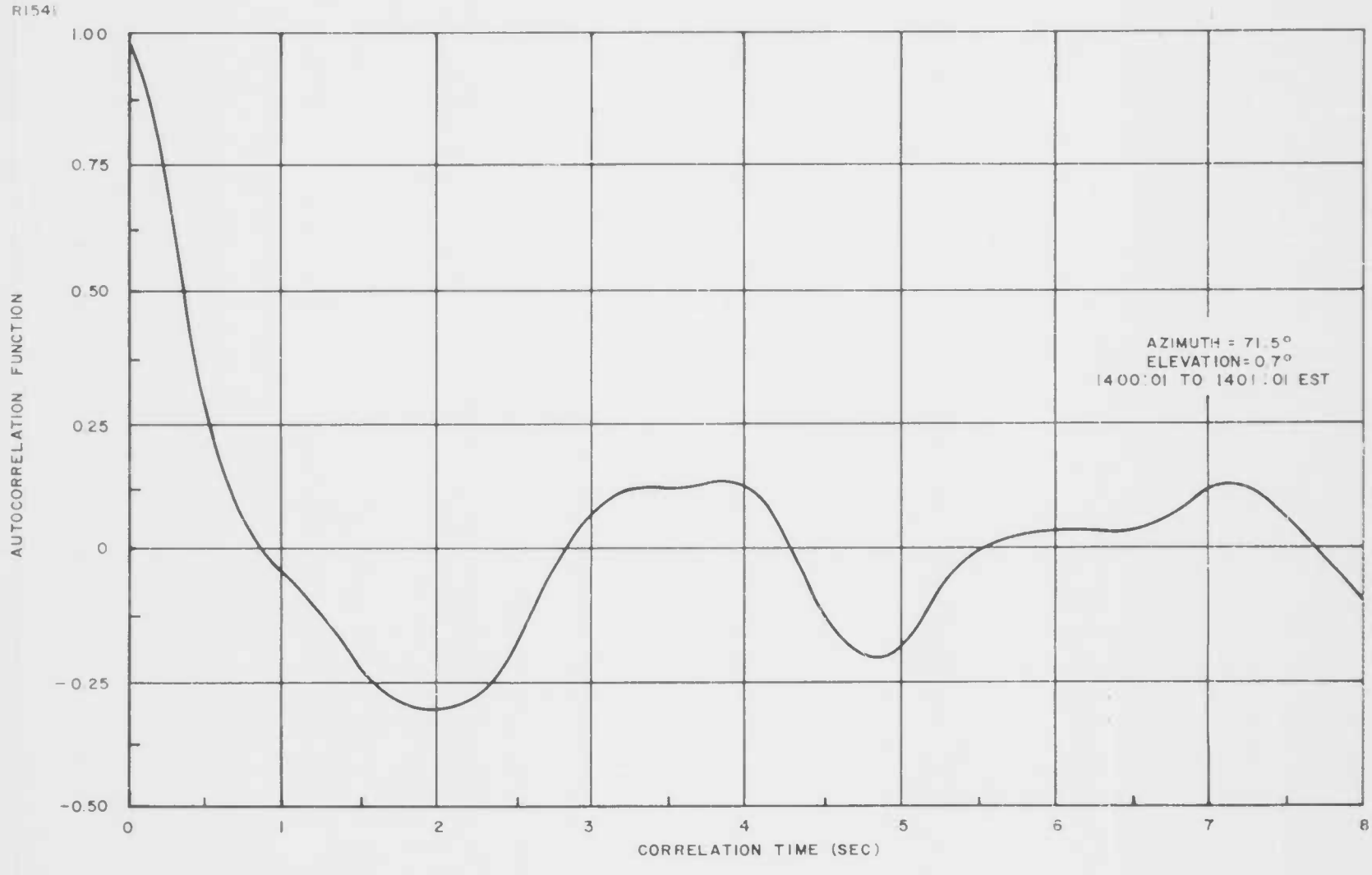

Figure 39. Autocorrelation Function of Total Cross Section, Moon Data, 8 February 1960

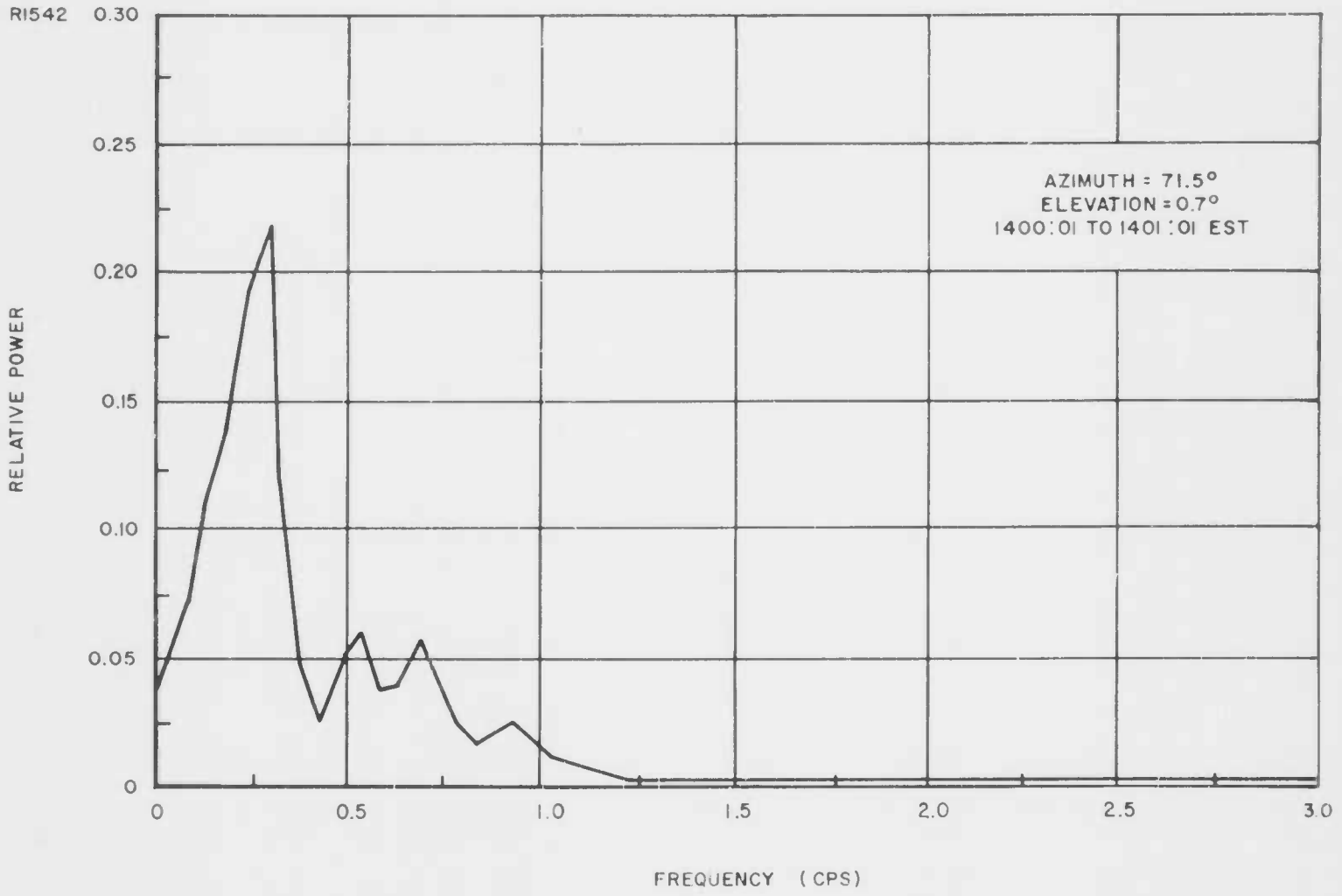

Figure 40. Power Density Spectrum of Total Cross Section, Moon Data, 8 February 1960

TABLE 3

LIBRATION RATE CONSTANTS FOR THE EVALUATION OF DOPPLER FREQUENCY SPREAD

Date	Time (EST)	Azimuth Angle (Degrees)	Elevation Angle (Degrees)	Total Libration Rate in Latitude $\dot{\ell}_{TB}$ (Radians/Sec.)	Total Libration Rate in Longitude $\dot{\ell}_{TL}$ (Radians/Sec.)	$\nu_o = \tan^{-1}\left[\frac{\dot{\ell}_{TB}}{\dot{\ell}_{TL}}\right]$ (Degrees)	Maximum Doppler Spread (cps)
8 Feb. 1960	1401	71.5	0.7	-1.34796×10^{-6}	-5.14733×10^{-7}	69.1	5.460 K*
4 Apr. 1960	1124	72.5	0.3	-5.59171×10^{-7}	-3.21373×10^{-7}	60.2	1.639 K

* K = Fractional radius of the moon

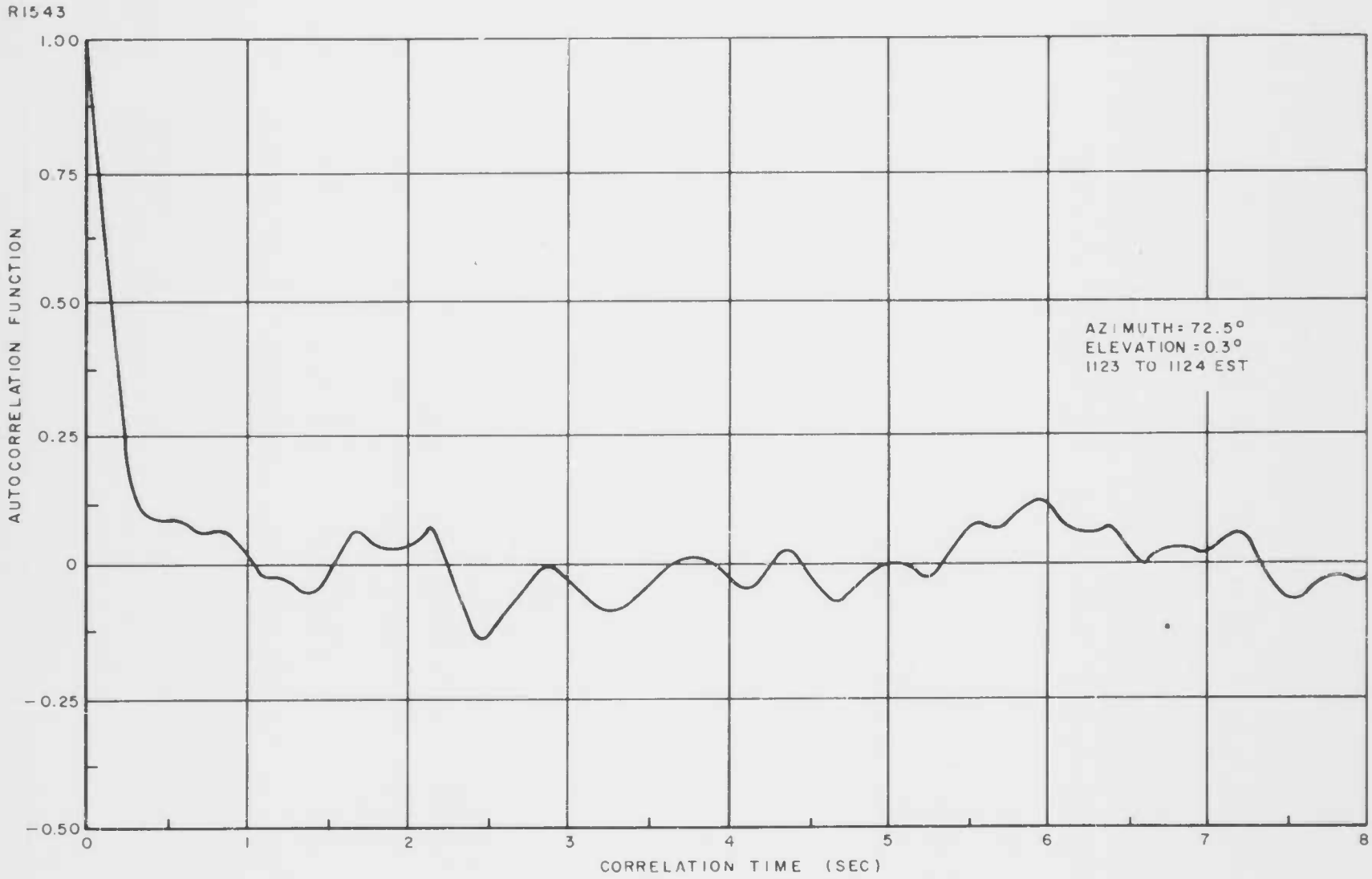

Figure 41. Autocorrelation Function of Total Cross Section, Moon Data, 4 April 1960

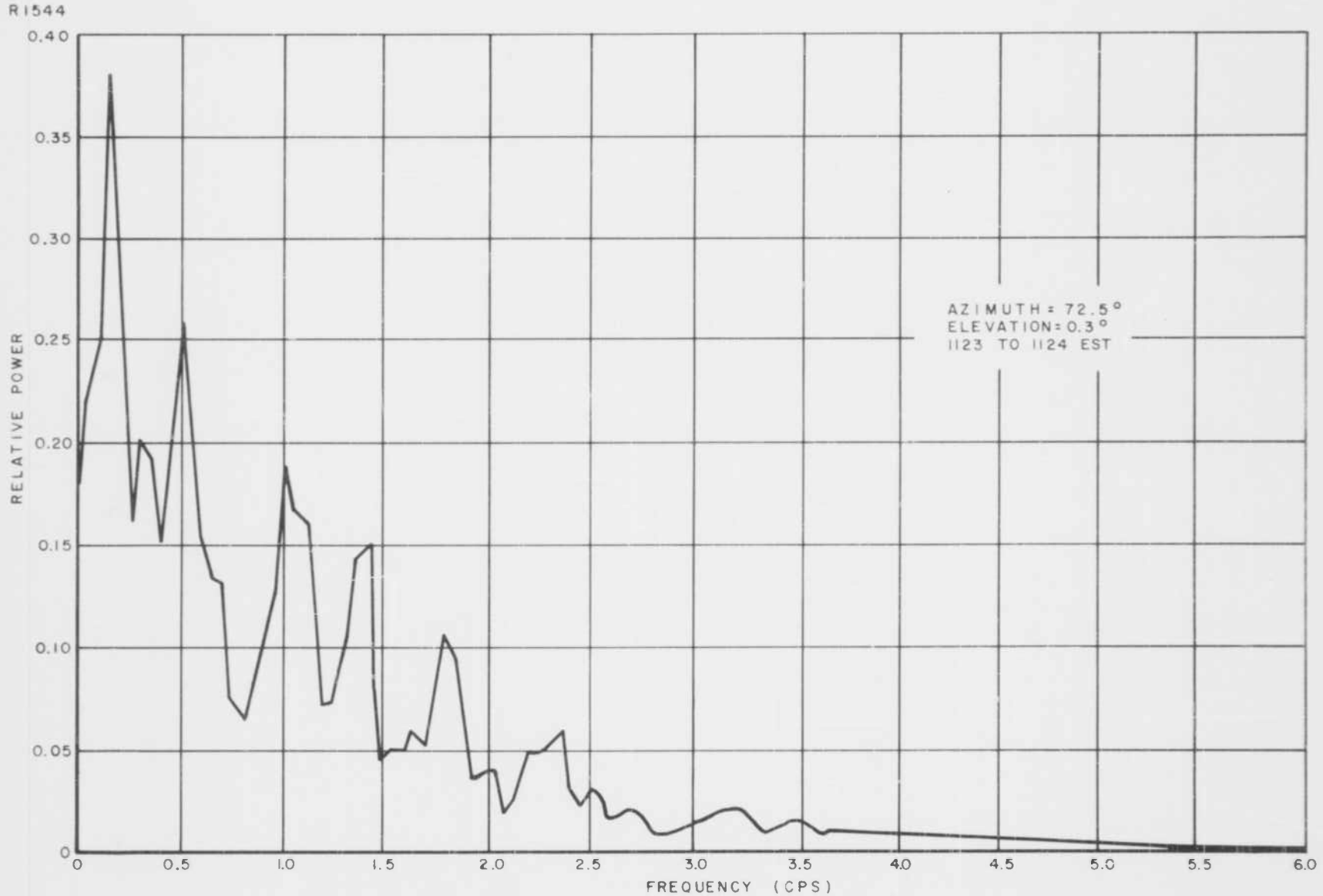

Figure 42. Power Density Spectrum of Total Cross Section, Moon Data, 4 April 1960

the dominant frequency of 0.14 cps measured on 4 April 1960, differs from the theoretical calculations of 0.66 cps by a factor of 0.22. It appears, therefore, that while the effective radius responsible for most of the amplitude variation is smaller than 713 kilometers, the radius of the spherical cap corresponding to a fractional radius of 0.404, it is larger than the radius of the first Fresnel zone, 11.7 kilometers, by approximately 10 times.

As shown in the photograph of the front portion of the moon's face, Figure 43, there is a comparatively smooth area in the center of the moon, Sinus Medii, large enough to encompass at least 10 Fresnel zones. This region is surrounded by a number of mountain peaks that rise 5000 to 8000 feet.[52] It could be possible that the librational motion of these peaks account for the higher frequency terms obtained in the power density spectrum. For example, the mountain range, Rhaeticus, with a fractional radius of approximately 0.08-0.09, could have imparted at its location, a fading rate of about 0.84-0.95 cps on 8 February 1960. It is interesting to note that the fading rate, possibly due to Rhaeticus, compares favorably with one of the frequencies, 0.94 cps, present in the power density spectrum of that date. This calculation is based on Equation (40) for $\nu = 30°$.

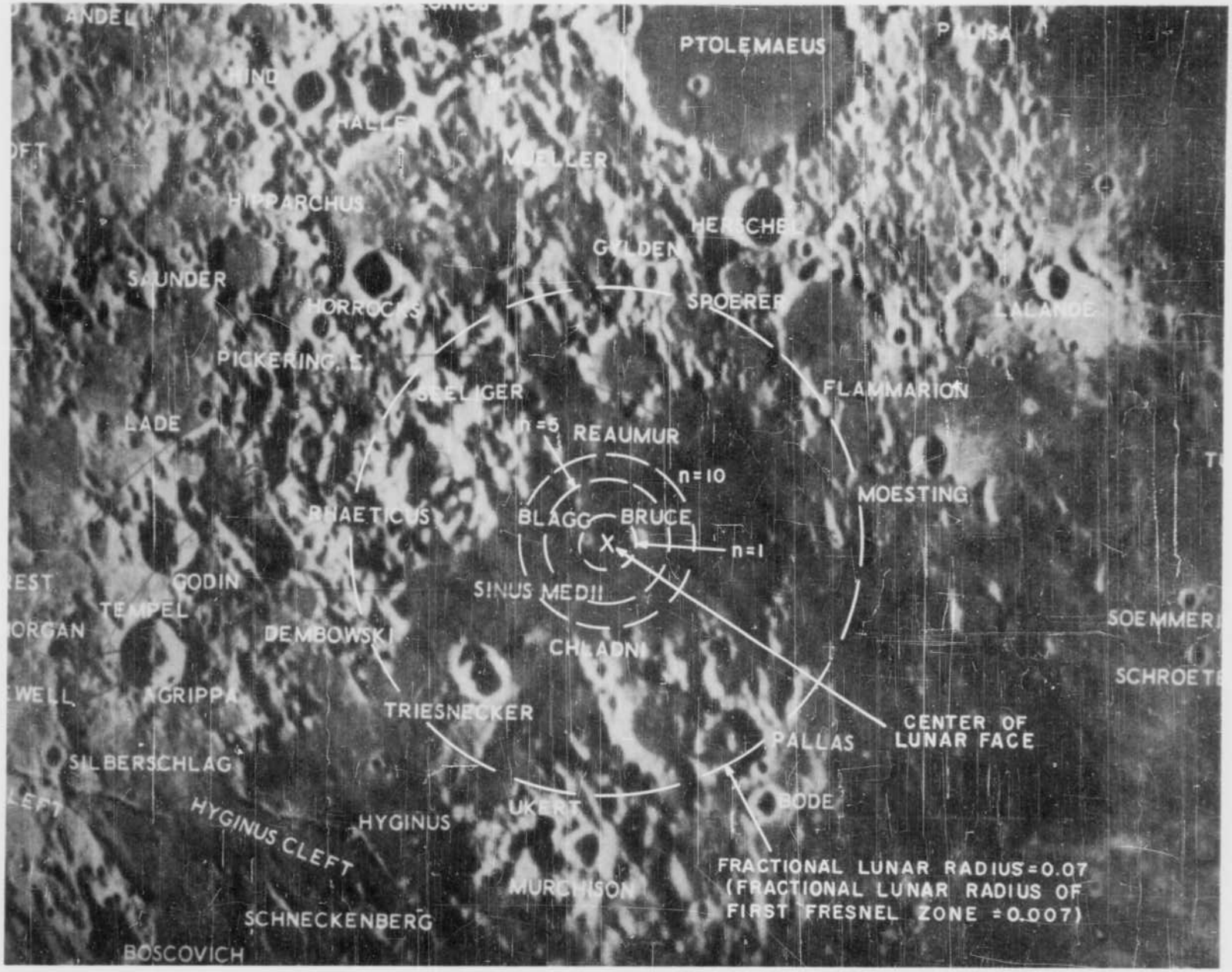

Figure 43. Fresnel Zones on the Face of the Moon

VI. CONCLUSIONS

Radar reflections from the moon afford a method for investigating the characteristics of the ionosphere.

It is shown that the polarization ambiguity problem of radar-lunar reflections, prevailing when only one frequency is employed on transmission, can be resolved by the comparison of the experimental measurements of the angular rotation (of the plane of polarization), introduced by the ionospheric Faraday effect, with theoretical estimates.

It appears that the electron density distribution above the peak of the F-layer can be represented, to a first approximation, by a Chapman model with a constant scale height of less than about 80 kilometers for the neutral particles, during the daytime and more than about 80 kilometers during the nighttime. This is based on the high degree of correlation between the total ionospheric electron content deduced from radar-lunar observations and that predicted from ionosonde data and the theoretical model.

The ratio of the integrated electron density above F-layer maximum to that below undergoes a diurnal variation, attaining a minimum average value of approximately 1.5 between 1300-1400 hours local time. At night, there is a scatter of values ranging from four to 11.

Evidence is presented which indicates the presence of diurnal influence on the equivalent slab thickness of the ionosphere which is defined as the ratio of the total ionospheric electron content to the electron density at F-layer maximum. The equivalent slab thickness is a minimum of 200 to 370 kilometers during the daytime, while, during the nighttime, its magnitude increases, attaining a value as high as 800 kilometers.

The scale height of the F-region deduced from the total electron content by the method proposed by Wright[41] also reveals a diurnal influence. The daytime values vary between 50 and 90 kilometers with a mean of 75 kilometers while during the nighttime, the scatter is from 50 to 200 kilometers.

Lack of sufficient experimental radar-lunar data has prevented a thorough analysis to determine the correlation of solar and geophysical phenomena with the

ionospheric parameters reduced from the total integrated electron density.

An analysis of radar pulses reflected from the moon has revealed pertinent data regarding the characteristics of its surface.

It appears that, at a frequency of 425 megacycles, the front portion of the moon is comparatively smooth and is the region where specular reflection takes place. The following experimental evidence is the basis of this conclusion.

1. Radar-pulse measurements of the cross section and the power reflection coefficient of the moon are approximately the same as those determined by cw systems operating at a frequency of 418 megacycles[41] and 488 megacycles[19]. This indicates that a pulsed radar system covering a sufficient number of Fresnel zones measures the same echoing area as a cw system covering the entire surface of the moon.

2. The probability density function of the total amplitude of the lunar echoes, for a one 10-minute sample, reveals the possible presence of a steady signal which may be indicative of a specular reflected signal. The analysis is based on Rice's theory of random noise.[43]

3. The envelope or fading pattern of the amplitude versus time photographs of the main lunar echo received on two linear orthogonal polarizations are always identical. This implies that the polarizations of the incident pulses are not altered on reflection from the front portion of the moon's surface.

4. The rotation of the plane of polarization of the radar-lunar echoes is found to be entirely due to the Faraday effect of the ionosphere. The polarization of the received signal often attains an acute angle of zero degrees and 90 degrees whereas, according to Senior and Siegel[33,34] a rough body can be expected to yield a minimum signal, containing at least 30 per cent of the total received energy. In other words, the polarization angle of signals reflected from a rough body should vary between 18 and 73 degrees and not between zero and 90 degrees.

5. The pulse shape of the main reflected echo most often resembles the transmitted pulse.

The experimental evidence, indicating that the back portion of the moon behaves as rough scatter, is based on the following:

1. A-scope photographs of lunar echoes show that the pulses are stretched out in length to approximately the radio-depth of the moon, i.e., 11.6 milliseconds.

2. It is found that the decay of the trailing edge of a composite lunar echo which is the average of 130 echoes, obeys the Lommel-Seeliger scattering law displaced by a factor of approximately 1/8.

VII. REFERENCES

1. Webb, H.D., "Project Diana - Army Radar Contacts the Moon," Sky and Telescope, Vol. 5, pp. 3-6, April 1946.
2. DeWitt J.H. and Stodola, B.K., "Detection of Radio Signals Reflected From the Moon," Proceedings of IRE, Vol. 37, pp. 229-242, March 1949.
3. Bay, Z., "Reflections of Microwaves from the Moon," Hungarian Acta Physica, Vol. 1, pp. 1-22, April 1946.
4. Kerr, F.J., Shain, C.A., and Higgins, C.S., "Moon Echoes and Penetration of the Ionosphere," Nature, Vol. 163, pp. 310-313, February 1949.
5. Kerr, F.J., Shain, C.A., "Moon Echoes and Transmission Through the Ionosphere," Proceedings of IRE, Vol. 39, pp. 230-242, March 1951.
6. Sulzer, P.G., Montgomery, G.F. and Gerks, I.H., "An UHF Moon Relay," Proceedings of IRE, Vol. 40, p. 361, March 1952.
7. Evans, J.V., "The Scattering of Radio Waves by the Moon," Proceedings of Physical Society, B., Vol. 70, p. 1105, 1957.
8. Trexler, J.H., "Lunar Radio Echoes," Proceedings of IRE, Vol. 46, pp. 286-292, January 1958.
9. Yaplee, B.S., Bruton, R.H., Craig, K.J. and Roman, N.G., "Radar Echoes from the Moon at a Wavelength of 10 cm," Proceedings of IRE, Vol. 46, pp. 293-297, January 1958.
10. Pettengill, G.H., "Measurements of Lunar Reflectivity Using the Millstone Radar," Proceedings of IRE, Vol. 48, pp. 933-934, May 1960.
11. Leadabrand, R.L., Dyce, R.B., Fredricksen, A., Presnell, R.I. and Schlobohm, J.C., "Evidence that the Moon is a Rough Scatterer at Radio Frequencies," Journal of Geophysical Research, Vol. 65, pp. 3071-3078, October 1960.
12. Browne, I.C., Evans, J.V., Hargreaves, J.K., and Murray, W.A.S., "Radio Echoes from the Moon," Proceedings of Physical Society, B., Vol. 69, pp. 901-920, September 1956.
13. Evans, J.H., "The Measurement of the Electron Content of the Ionosphere by the Lunar Radio Echo Method," Proceedings of Physical Society, B., Vol. 69, pp. 953-955, September 1956.
14. Evans, J.H., "The Electron Content of the Ionosphere," Journal of Atmospheric and Terrestrial Physics, Vol. 11, pp. 259-271, 1957.
15. Bauer, S.J. and Daniels, F.B., "The Measurement of Ionospheric Electron Content by the Lunar Radio Technique," Journal of Geophysical Research, Vol. 64, pp. 1371-1376, October 1959.
16. Hill, R.A. and Dyce, R.B., "Some Observations of Ionospheric Faraday Rotation on 106.1 mc/sec.," Journal of Geophysical Research, Vol. 65, pp. 173-176, January 1960.

17. Smith, F.G., "Ionospheric Refraction of 81.5 mc/sec Radio Waves from Radio Stars," Journal of Atmospheric and Terrestrial Physics, Vol. 2, pp. 350-355, 1952.

18. Jackson, J.E. and Seddon, J.C., "Ionospheric Electron Density Measurements with Navy Aerobee-Hi Rocket," Journal of Geophysical Research, Vol. 63, pp. 197-208, March 1958.

19. Pfister, W. and Ulwick, J.C., "The Analysis of Rocket Experiments in Terms of Electron Density Distributions," Journal of Geophysical Research, Vol. 63, pp. 315-332, June 1958.

20. Berning, W.W., "A Sounding Rocket Measurement of Electron Densities to 1500 Kilometers," Journal of Geophysical Research, pp. 2589-2594, September 1960.

21. Nisbet, J.S. and Bowhill, S.A., "Electron Densities in the F Region of the Ionosphere from Rocket Measurements; Part 1, Method of Analysis," Journal of Geophysical Reserach, Vol. 65, pp. 3601-3607, November 1960.

22. Nisbet, J.S. and Bowhill, S.A., "Electron Densities in the F Region of the Ionosphere from Rocket Measurements; Part 2, Results of Analysis," Journal of Geophysical Research, Vol. 65, pp. 3609-3614, November 1960.

23. Garriott, O.K., "The Determination of Ionospheric Electron Content and Distribution from Satellite Observations; Part 1. Theory of Analysis," Journal of Geophysical Research, Vol. 65, pp. 1139-1150, April 1960.

24. Garriott, O.K., "The Determination of Ionospheric Electron Content and Distribution from Satellite Observations; Part 2, Results of the Analysis," Journal of Geophysical Research, Vol. 65, pp. 1151-1158, April 1960.

25. Jackson, J.E. and Kane, J.A., "Measurements of Ionospheric Electron Densities Using an RF Probe Technique," Journal of Geophysical Research, Vol. 64, pp. 1074-1075, August 1959.

26. Jackson, J.E. and Kane, J.A., "Performance of an RF Impedance Probe in the Ionosphere," Journal of Geophysical Research, Vol. 65, pp. 2209-2210, July 1960.

27. Pineo, V.C., Kraft, L.G. and Briscoe, H.W., "Some Characteristics of Ionospheric Backscatter Observed at 440 mc/sec," Journal of Geophysical Research, Vol. 65, pp. 2629-2633, September 1960.

28. Bowles, K.L., "Incoherent Scattering by Free Electrons as a Technique for Studying the Ionosphere and Exosphere; Some Observations and Theoretical Considerations," Journal of Research, NBS, Vol. 65, D, pp. 1-14, June-February 1961.

29. Millman, G.H., "Observations of Ionospheric Faraday Rotation by Incoherent Backscatter Technique," paper presented at the NATO Advanced Study Institute on Electron Density Profiles in the Ionosphere and Exosphere, Skeikampen, Norway, April 1961.

30. Ross, W.J., "The Determination of Ionospheric Electron Content from Satellites Doppler Measurements: 1. Method of Analysis," Journal of Geophysical Research, Vol. 65, pp. 2601-2606, September 1960.

31. Ross, W.J., "The Determination of Ionospheric Electron Content from Satellite Doppler Measurement; 2. Experimental Results," Journal of Geophysical Research, Vol. 65, pp. 2607-2615, September 1960.

32. Yeh, K.C. and Sevenson, G.W., "Ionospheric Electron Content and Its Variation Deduced from Satellite Observations," Journal of Geophysical Research, Vol. 66, pp. 1061-1067, April 1961.

33. Millman, G.H., Sanders, A.E. and Mather, R.A., "Radar-Lunar Investigations at a Low Geomagnetic Latitude," Journal of Geophysical Research, Vol. 65, pp. 2619-2626, September 1960.

34. Budden, K.A., "A Method for Determining the Variation of Electron Density with Height (N (Z) Curves) from Curves of Equivalent Height Against Frequency," The Physics of the Ionosphere, pp. 332-339, The Physical Society, London, 1955.

35. Millman, G.H., "The Geometry of the Earth's Magnetic Field at Ionospheric Heights," Journal of Geophysical Research, Vol. 64, pp. 717-726, July 1959.

36. Vestine, E.H., LaPorte, L., Lange, I., Scott, W.E., "The Geomagnetic Field, Its Description and Analysis," Department of Terrestrial Magnetism, Carnegie Institution of Washington, Publication 580, 1947.

37. Chapman, S., and Bartels, J., "Geomagnetism," Volumes I & II, Oxford University Press, 1940.

38. Millman, G.H., "Atmospheric and Extraterrestrial Effects on Radio Wave Propagation," General Electric Technical Information Series Report No. R60EMH36, December 1960. (Lecture notes presented at the "Modern Radar Techniques" course conducted at the Moore School of Electrical Engineering, University of Pennsylvania, June 1960.)

39. Nisbet, J.S., "Electron-Density Distribution in the Upper Ionosphere From Rocket Measurements," Journal of Geophysical Research, Vol. 65, pp. 2597-2599, September 1960.

40. Evans, J.V. and Taylor, C.N., "The Electron Content of the Ionosphere in Winter," submitted for publication to the Proceedings of the Royal Society.

41. Wright, J.W., "A Model of the F Region Above h_{max} F2", Journal of Geophysical Research, Vol. 65, pp. 185-191, January 1960.

42. Grieg, D.D., Metzger, S., and Waer, R., "Considerations of Moon-Relay Communication", Proceedings of IRE, Vol. 36, pp. 652-663, May 1948.

43. Rice, S.O., "Mathematical Analysis of Random Noise", Bell System Technical Journal, Vol. 23, pp. 282-332, July 1944; Vol. 24, pp. 46-156, January 1945.

44. Fricker, S.J., Ingalls, R.P., Mason, W.C., and Swift, D.W., "Computation and Measurement of the Fading Rate of Moon-Reflected UHF Signals", Journal of Research NBS, Vol. 64D, pp. 455-465, September-October 1960.

45. Wright, J.W., "Comment on Model of the Ionosphere above h_{max} F2", Journal of Geophysical Research, Vol. 65, pp. 2595-2596, September 1960.

46. Ross, W.J. and Andreson, D.S., "The Variation of Ionospheric Profile with Season and Solar Cycle", paper presented at the NATO Advanced Study Institute on Electron Density Profiles in the Ionosphere and Exosphere, Skeikampen, Norway, April 1961.

47. Kallmann, H.K., "A Preliminary Model Atmosphere Based on Rocket and Satellite Data", Journal of Geophysical Research, Vol. 64, pp. 615-623, June 1959.

48. "Solar-Geophysical Data", CRPL-F, Part B, U.S. Department of Commerce, National Bureau of Standards, Central Radio Propagation Laboratory, Boulder, Colorado.

49. Blevis, B.C. and Chapman, J.H., "Characteristics of 400 Megacycles per Second Radio Signals Reflected from the Moon", Journal of Research NBS, Vol. 64D, pp. 331-334, July-August 1960.

50. Fricker, S.J., Ingalls, R.P., Mason, W.C., Stone, M.L., Swift, D.W., "Characteristics of Moon-Reflected UHF Signals", MIT Lincoln Laboratory, Technical Report No. 187, December 1958.

51. Kerchner, R.M. and Corcoran, G.F., "Alternating Current Circuits", John Wiley & Sons, Inc., New York, 1955.

52. Nelson, E., "The Moon and the Condition and Configuration of its Surface", London, 1876.

53. Senior, T.B.A. and Siegel, K.M., "Radar Reflection Characteristics of the Moon", Paris Symposium on Radio Astronomy, Edited by R.N. Bracewell, pp. 29-45, Stanford University Press, 1959.

54. Senior, T.B.A. and Siegel, K.M., "A Theory of Radar Scattering by the Moon", Journal of Research NBS, Vol. 64D, pp. 217-229, May-June, 1960.

55. Mitra, S.K., "The Upper Atmosphere", The Asiatic Society of Calcutta, 1952.

56. Jenkins, F.A., and White, H.E., "Fundamentals of Optics", McGraw-Hill Book Co., Inc., New York, 1957.

57. Blackman, R.B., and Tukey, J.W., "The Measurement of Power Spectra", Dover Publications, Inc., 1958.

APPENDIX A

IONOSPHERIC FARADAY EFFECT

A. INTRODUCTION

When a linearly polarized electromagnetic wave enters an ionized medium in the presence of an external magnetic field, such as encountered in the ionosphere, the wave separates into two independent components both, in the general case, elliptically polarized with opposite senses of rotation. For frequencies in the UHF range, the two components, which are referred to as the ordinary and the extraordinary waves, are circularly polarized.[38]

As the ionosphere is traversed, the two waves progress with different velocities of propagation which result in the phase relationship between them to be continuously changing. On leaving the ionosphere, the circularly polarized components recombine to form a linearly polarized wave which is rotated with respect to the original linear wave. This phenomenon is commonly referred to as the Faraday effect.

B. THEORETICAL CONSIDERATIONS

Since a circularly polarized wave is basically composed of two harmonic orthogonal signals which are 90 degrees out of phase with one another, only one of the linearly polarized waves from each of the two circularly polarized components, i.e., the ordinary and the extraordinary waves, need be considered in analyzing the polarization rotational effects of the ionosphere.

The differential phase shift that each of the components undergoes in an element of path length, ds, is given by

$$d\phi_o = \frac{2\pi}{\lambda_o} ds \qquad (A\text{-}1)$$

and

$$d\phi_e = \frac{2\pi}{\lambda_e} ds \qquad (A\text{-}2)$$

where the subscripts, o and e, refer to the ordinary and extraordinary modes of propagation, respectively, and λ_o and λ_e are the wavelengths associated with the phase velocity, V_{Po} and V_{Pe}, of the waves.

As illustrated in Figure A-1, the angular rotation of the plane of polarization of the wave, $d\phi$, as it travels the distance, ds, is therefore

$$d\phi = 1/2 \, (d\phi_o - d\phi_e) \tag{A-3}$$

By definition,

$$\lambda_{o,e} = \frac{V_{Po,e}}{f} \tag{A-4}$$

and

$$V_{Po,e} = \frac{c}{n_{o,e}} \tag{A-5}$$

where c is the free space velocity; f, the transmission frequency; and $n_{o,e}$, the refractive indices of the medium. It follows that Equation (A-3) can be written in the form

$$d\phi = \frac{\omega}{2c} \, \Delta n \, ds \tag{A-6}$$

where ω is the angular transmission frequency and $\Delta n = n_o - n_e$.

This relationship defines the angular rotation of the wave for a one-way propagation path. Thus, the total polarization shift for a two-way propagation path becomes

$$\phi(s) = \frac{\omega}{c} \int_{s_1}^{s_2} \Delta n \, ds \tag{A-7}$$

where s_1 and s_2 are the limits of the path.

In terms of a vertical height variable, this expression is modified to

$$\phi(h) = \frac{\omega}{c} \int_{h_1}^{h_2} \Delta n \, f(h) \, dh \tag{A-8}$$

where

$$f(h) = \frac{r_o + h}{\left[(r_o + h)^2 - (r_o \operatorname{Cos} E)^2 \right]^{1/2}} \qquad \text{(A-9)}$$

and r_o is the radius of the earth and E is the elevation angle of the antenna beam.

According to the magneto-ionic theory, i.e., the theory of propagation of electromagnetic waves through an ionized medium in the presence of an external magnetic field, the complex index of refraction of the medium, M, is given by [55]

$$M^2 = 1 + \frac{2}{2(\alpha + j\beta) - \frac{(\gamma_T)^2}{1 + \alpha + j\beta} \pm \left[\frac{(\gamma_T)^4}{(1 + \alpha + j\beta)^2} + 4(\gamma_L)^2 \right]^{1/2}} \qquad \text{(A-10)}$$

where

$$\alpha = -\frac{\omega^2}{\omega_c^2} \qquad \gamma_T = \frac{\omega \omega_H}{\omega_c^2} \operatorname{Sin} \theta$$

$$\beta = \frac{\omega \nu}{\omega_c^2} \qquad \omega_H = \frac{H e}{m c} \qquad \text{(A-11)}$$

$$\gamma_L = \frac{\omega \omega_H}{\omega_c^2} \operatorname{Cos} \theta \qquad \omega_c^2 = \frac{4\pi N e^2}{m}$$

and where e is the electron charge (4.8×10^{-10} esu); m, the electron mass (9.1×10^{-28} gm); N, electron density (electrons/cm^3); ν the electron angular collision frequency; H, the earth's magnetic field strength (gauss); and θ, the propagation angle, i.e., the angle between the magnetic field vector and the direction of propagation. The quantity, He/mc, is the gyromagnetic frequency of the electron about the earth's magnetic field while ω_c is the critical frequency.

or plasma frequency, of the ionized medium.

It is noted that there are two possible values for the complex index of refraction which indicate two different modes of propagation. The waves travel independently in the ionized medium and each has a polarization vector associated with it. In the general case, at the low frequencies, the waves are elliptically polarized with opposite senses of rotation. At frequencies on the order of 100 megacycles, the waves are circularly polarized.[38]

It can be shown that, under ordinary ionospheric conditions, for frequencies in the 100-mc range, it is valid to assume $\omega^2 >> \nu^2$ and $\omega^2 > \omega_c^2$.[38] Thus, the complex index of refraction reduces to a real quantity given by

$$n_{c,e}^2 = 1 - \frac{1}{\frac{\omega^2}{\omega_c^2} - \frac{\omega_H^2}{2\omega_c^2}\,\mathrm{Sin}^2\theta \pm \frac{\omega\omega_H}{\omega_c^2}\left[\left(\frac{\omega_H\,\mathrm{Sin}^2\theta}{2\omega}\right)^2 + \mathrm{Cos}^2\theta\right]^{1/2}} \qquad \text{(A-12)}$$

where the positive sign is associated with the ordinary mode of propagation while the negative sign with the extraordinary mode of propagation.

Assuming quasi-longitudinal mode of propagation which is represented by the condition

$$4\frac{\omega^2}{\omega_H^2} >> \mathrm{Sin}^2\theta\ \mathrm{Tan}^2\theta \qquad \text{(A-13)}$$

it follows that the difference in the index of refraction between the ordinary and extraordinary waves is

$$\Delta n \approx \frac{Ne^3 H}{2\pi^2 m^2 c f^3}\,\mathrm{Cos}\,\theta \qquad \text{(A-14)}$$

This approximation is valid at a frequency of 400 megacycles for values of θ between $0 \leq \theta \leq 89.6°$.

According to Equation (A-8), the total two-way polarization rotation (in radians) evaluates to

$$\phi(h) = \frac{4.7233 \times 10^{4}}{f^{2}} \int_{h_1}^{h_2} f(h)\, H \cos\theta\, N\, dh \qquad \text{(A-15)}$$

where the altitude limits, h_1 and h_2, are in centimeter units and f in cps.

It is evident that, for quasi-longitudinal propagation, the magnitude of the angular rotation is inversely proportional to the square of frequency and directly proportional to the magnetic field strength.

The condition for quasi-transverse propagation is denoted by the inequality

$$\sin^2\theta \tan^2\theta >> \frac{4\omega^2}{\omega_H^2} \qquad \text{(A-16)}$$

By simple manipulation, it can be shown from Equation (A-12) that the difference in the refractive indices for the two modes of propagation is, therefore, given by

$$\Delta n \approx \frac{Ne^4 H^2}{8\pi^3 m^3 c^2 f^4} \sin^2\theta \qquad \text{(A-17)}$$

Referring to Equation (A-8), it follows that the two-way polarization rotation becomes

$$\phi(h) = \frac{6.6087 \times 10^{10}}{f^{3}} \int_{h_1}^{h_2} f(h)\, H^2 \sin\theta\, N\, dh \qquad \text{(A-18)}$$

It is noted that, for the quasi-transverse case, the angular rotation is directly proportional to the magnetic field squared and inversely proportional to the cube of frequency.

APPENDIX B

DETERMINATION OF SIGNAL POWER REFLECTED FROM A ROUGH SPHERE

Any calculation of the theoretical power reflected from a rough sphere must include such factors as the increment of surface contributing energy at a given instant of time and a scattering law describing the surface characteristics.

In order to formulate a relationship incorporating all the necessary parameters, the geometric relation of the incident pulse with respect to the sphere must be considered.

A plane wave is assumed incident on the surface of the sphere with zero range (or time) taken at the point of tangency. For a pulse of length, p (in units of distance), less than the radius of the sphere, r, the incremental zone, dA, around the sphere contributing to the reflected pulse at a given zone depth, d, is as shown in Figure B-1, defined by the angular limits

$$\theta_1 = \cos^{-1}\left[\frac{r - (d-p)}{r}\right] \tag{B-1}$$

and

$$\theta_2 = \cos^{-1}\left[\frac{r - d}{r}\right] \tag{B-2}$$

Since $p = cT/2$ and $d = ct/2$, it follows that

$$\theta_1 = \cos^{-1}\left[\frac{r - \frac{c}{2}(t-T)}{r}\right] \tag{B-3}$$

and

$$\theta_2 = \cos^{-1}\left[\frac{r - \frac{ct}{2}}{r}\right] \tag{B-4}$$

where c is the free space velocity; T, the pulse width in units of time; and t, the time associated with the zone depth.

For $t \leq T$, the contributions to the received pulse originate within the surface area bounded by $\theta_1 = 0$ and θ_2 defined by Equation (B-4).

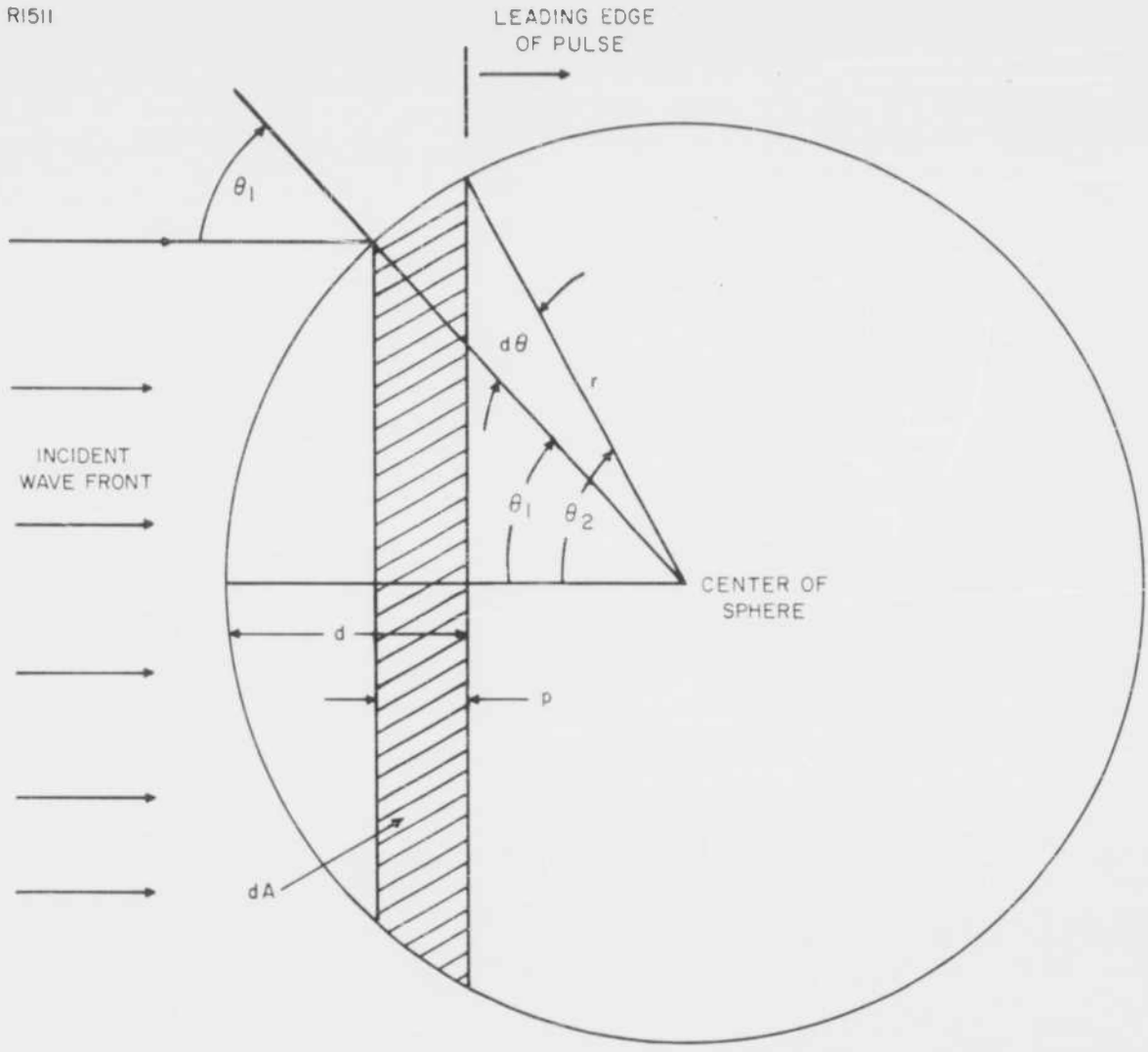

p = PULSE WIDTH (UNITS OF DISTANCE)

d = ZONE DEPTH

r = RADIUS OF SPHERE

dA = INCREMENTAL AREA

Figure B-1. Geometry of a Pulse Incident on a Rough Sphere

The method for determining the magnitude of the signal reflected from a rough sphere, as described below, is similar to that developed by Grieg, Metzger, and Waer.[41]

If P_o is the power per unit area incident on an incremental area, dA, of a rough surface, then the effective incident power, P_I , is

$$P_I = P_o \text{ Cos } \theta \text{ dA} \tag{B-5}$$

where θ is the angle between the normal to the surface and the direction of the incident wave. The angle, θ_1 , in Figure B-1 corresponds to θ in this expression.

If the surface is not perfectly reflecting, the reflected power, P_R, is given by

$$P_R = \rho P_o \text{ Cos } \theta \text{ dA} \tag{B-6}$$

where ρ is the power reflection coefficient of the surface.

It is convenient to define P_N as the power per unit solid angle reflected normal to the area dA. For Lambert scattering, the power radiated in any direction is proportional to the cosine of the angle between the scattered ray and the normal to the surface. Thus, the power scattered per unit solid angle is simply P_N Cos γ where γ is any angle measured from the normal to dA.

The unit solid angle $d\Omega$ enclosed by dA, as shown in Figure B-2, is given by

$$d\Omega = \frac{dA}{r^2} \tag{B-7}$$

It can be readily shown from spherical geometry that

$$dA = 2\pi r^2 \text{ Sin } \gamma \text{ } d\gamma \tag{B-8}$$

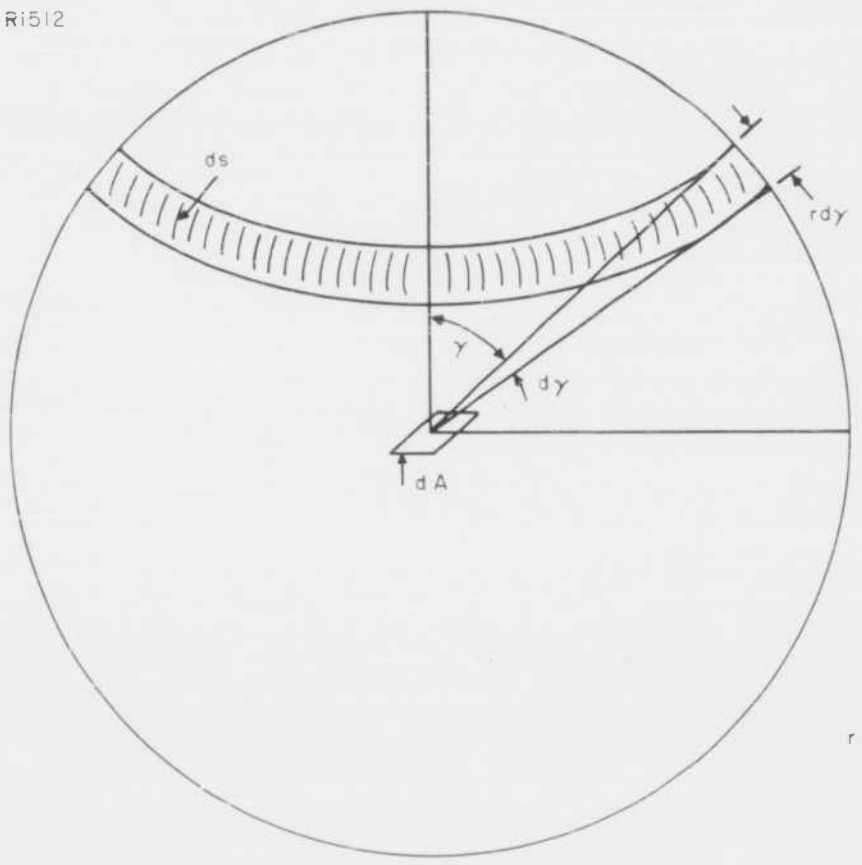

Figure B-2. Scattering from a Diffuse Surface

It follows that the total power intercepted (or reflected) by the upper hemisphere of Figure B-2 is, therefore,

$$P_R = 2\pi P_N \int_0^{\pi/2} \text{Sin}\,\gamma\,\text{Cos}\,\gamma\; d\gamma \tag{B-9}$$

or simply

$$P_R = \pi P_N \tag{B-10}$$

Since the reflected power is also defined by Equation (B-6), it is evident that

$$P_N = \frac{\rho P_o \text{Cos}\,\theta\; dA}{\pi} \tag{B-11}$$

Taking into account Lambert's law once again, it follows that the power per unit solid angle scattered back in the direction of θ, i.e., incident direction, becomes

$$P_\theta = \frac{\rho P_o \text{Cos}^2\,\theta\; dA}{\pi} \tag{B-12}$$

If P_t is the transmitted power and G_t is the gain of the transmitting antenna relative to an isotropic antenna, then

$$P_o = \frac{P_t G_t}{4\pi R^2} \tag{B-13}$$

where R is the distance from the transmitting source to the sphere.

The power intercepted at the receiving antenna, P_r, is simply

$$P_r = P_\theta \left(\frac{A_e}{R^2} \right) \tag{B-14}$$

where A_e is the effective antenna area defined by

$$A_e = \frac{G_r \lambda^2}{4\pi} \tag{B-15}$$

and where G_r is the gain of the receiving antenna and λ is the transmitted wavelength.

Since the element of area, dA, can be expressed in terms of the angle θ by (assuming $\theta_1 = \theta$ in Figure (B-1))

$$dA = 2\pi r^2 \operatorname{Sin} \theta \, d\theta \tag{B-16}$$

on substituting Equations (B-12), (B-13), (B-15), and (B-16) in Equation (B-14), it is seen that the total received power for a monostatic system can be expressed by the integral

$$P_r = \left(\frac{P_t G^2 \lambda^2 \sigma_s}{(4\pi)^3 R^4} \right) 8 \int_{\theta_1}^{\theta_2} \operatorname{Sin} \theta \operatorname{Cos} \theta \, i\theta \tag{B-17}$$

where σ_s is the echoing area of a smooth reflecting body defined by

$$\sigma_s = \pi r^2 \rho \tag{B-18}$$

It is noted that the terms in the parenthesis of Equations (B-17) describe the general radar equation, i.e., the power intercepted from a target which reflects radiation isotropically.

On integrating between the limits, $\theta_1 = 0$ and $\theta_2 = \pi/2$, it is found that the total power received from a rough sphere, scattering in accordance with Lambert's law, is 8/3 times greater than that from a smooth body.

With regard to a rough surface obeying the Lommel-Seeliger scattering law, the power scattered per unit solid angle, P_N, is independent of the scattering angle, γ, i.e., the angle between the scattered ray and the normal to the surface. Thus, the total power intercepted by the upper hemisphere, shown in Figure B-2, becomes

$$P_R = 2\pi P_N \int_0^{\pi/2} \operatorname{Sin} \gamma \, d\gamma \tag{B-19}$$

or

$$P_R = 2\pi P_N \tag{B-20}$$

It can be readily shown that the power received from a rough sphere evaluates to

$$P_r = \left(\frac{P_t G^2 \lambda^2 \sigma_s}{(4\pi)^3 R^4} \right) \quad 4 \int_{\theta_1}^{\theta_2} \text{Sin}\, \theta \, \text{Cos}\, \theta \; d\theta \qquad \text{(B-21)}$$

Integration between the limits $\theta_1 = 0$ and $\theta_2 = \pi/2$ reveals that the power scattered from a Lommel-Seeliger type spherical surface is twice that of a smooth sphere.

The theoretical shape of pulses reflected from a rough moon are depicted in Figure B-3. The relative power scale has been normalized with respect to the Lommel-Seeliger law. It is seen that, for short pulse lengths, more energy is scattered back from the limb of the moon for the Lommel-Seeliger scattering case than for Lambert scattering. On this particular plot, a smooth moon would reflect a constant relative power of 0.5, irrespective of pulse width.

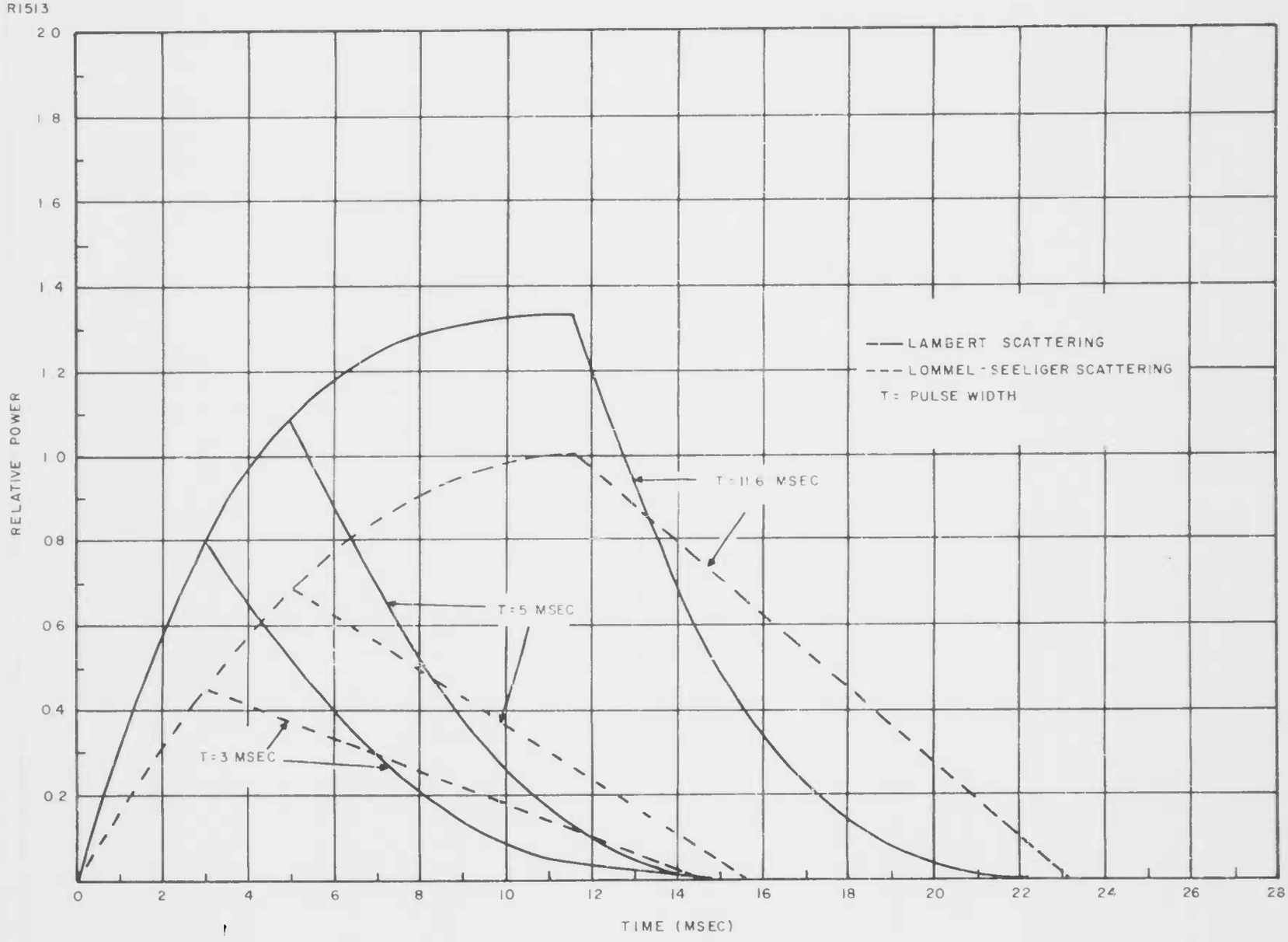

Figure B-3. Shape of Pulses Reflected From a Rough Moon

APPENDIX C

ORBIT OF A CELESTIAL BODY

The relationship of the celestial coordinate system with the geographic coordinate system is illustrated in Figures C-1 and C-2. The declination, D, of a point on the celestial sphere is analogous to geographic latitude since it is the angular displacement from the equatorial plane measured positive northward. The right ascension, RA, which corresponds to geographic longitude is the angular position about the celestial pole. It is measured positive east from the meridian containing the Vernal Equinox (or the First Point of Aries) which is the intersection of the plane of the ecliptic, i.e., the plane of the sun's orbit about the earth, with the celestial equator. The Greenwich Hour Angle of Aries, GHA^{γ}, is the angular distance measured positive westward along the celestial equator from the Greenwich meridian to the Vernal Equinox. The local hour angle, $\emptyset$, is the angular displacement between the meridians containing the observation site and the point of the celestial sphere, and is measured positive westward.

It can be readily shown by applying the law of cosines to the spherical triangle of Figure C-3 that the function relating the geographic and celestial coordinates is given by.

$$\text{Sin } D = \text{Sin } E \text{ Sin } L + \text{Cos } E \text{ Cos } L \text{ Cos } A \qquad \text{(C-1)}$$

where L is the latitude of the observation sight, and A and E are the azimuth and elevation angles of the celestial body as observed at the site, respectively. For the special case when $A = 180°$, this equation simplifies to

$$E = \frac{\pi}{2} + D - L \qquad \text{(C-2)}$$

For $A = 0°$

$$E = L \pm \left(\frac{\pi}{2} - D \right) \qquad \text{(C-3)}$$

where the two solutions exist only when the condition, $L > \left[(\pi/2) - D \right]$, is satisfied.

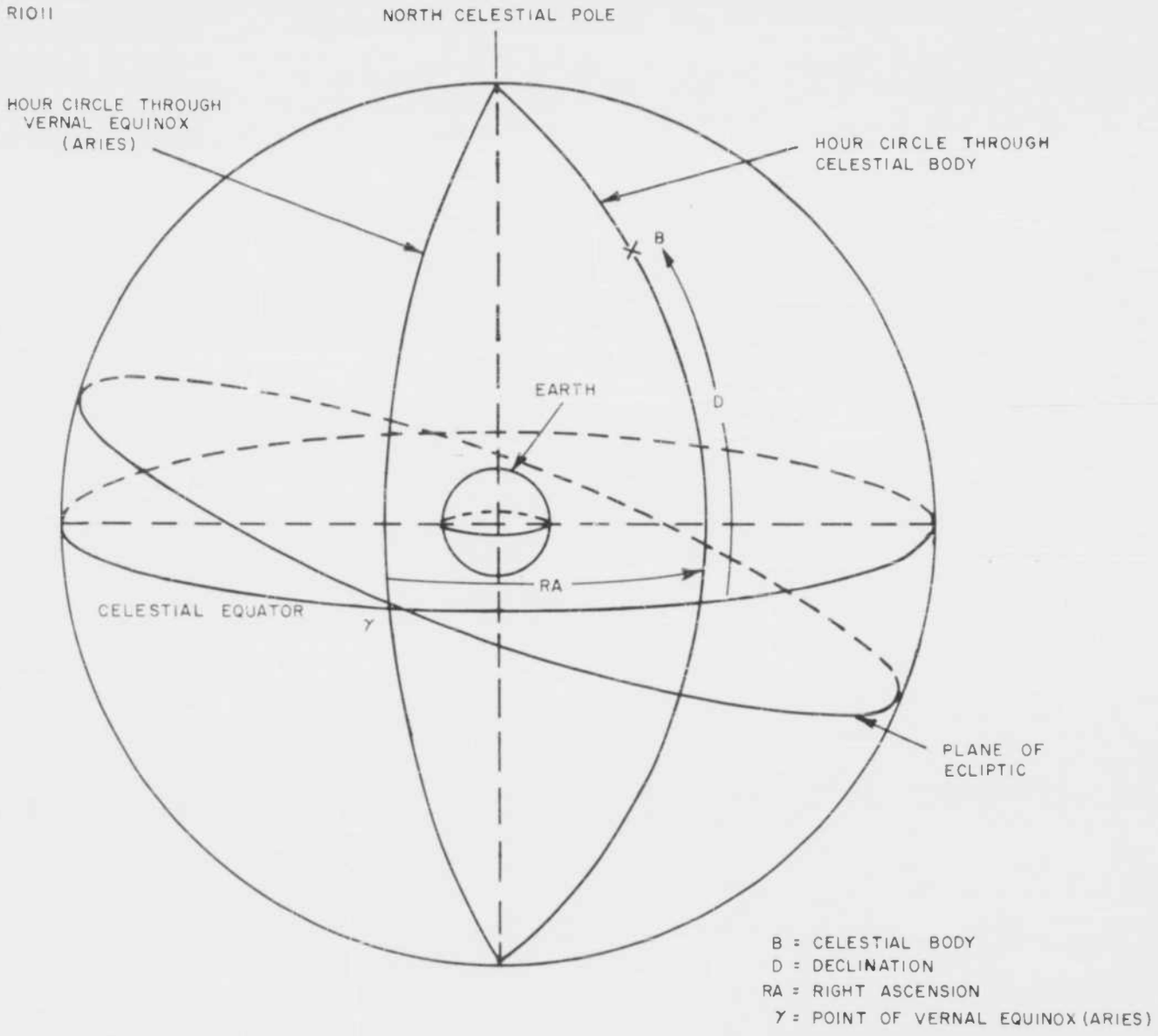

Figure C-1. Celestial Coordinate System

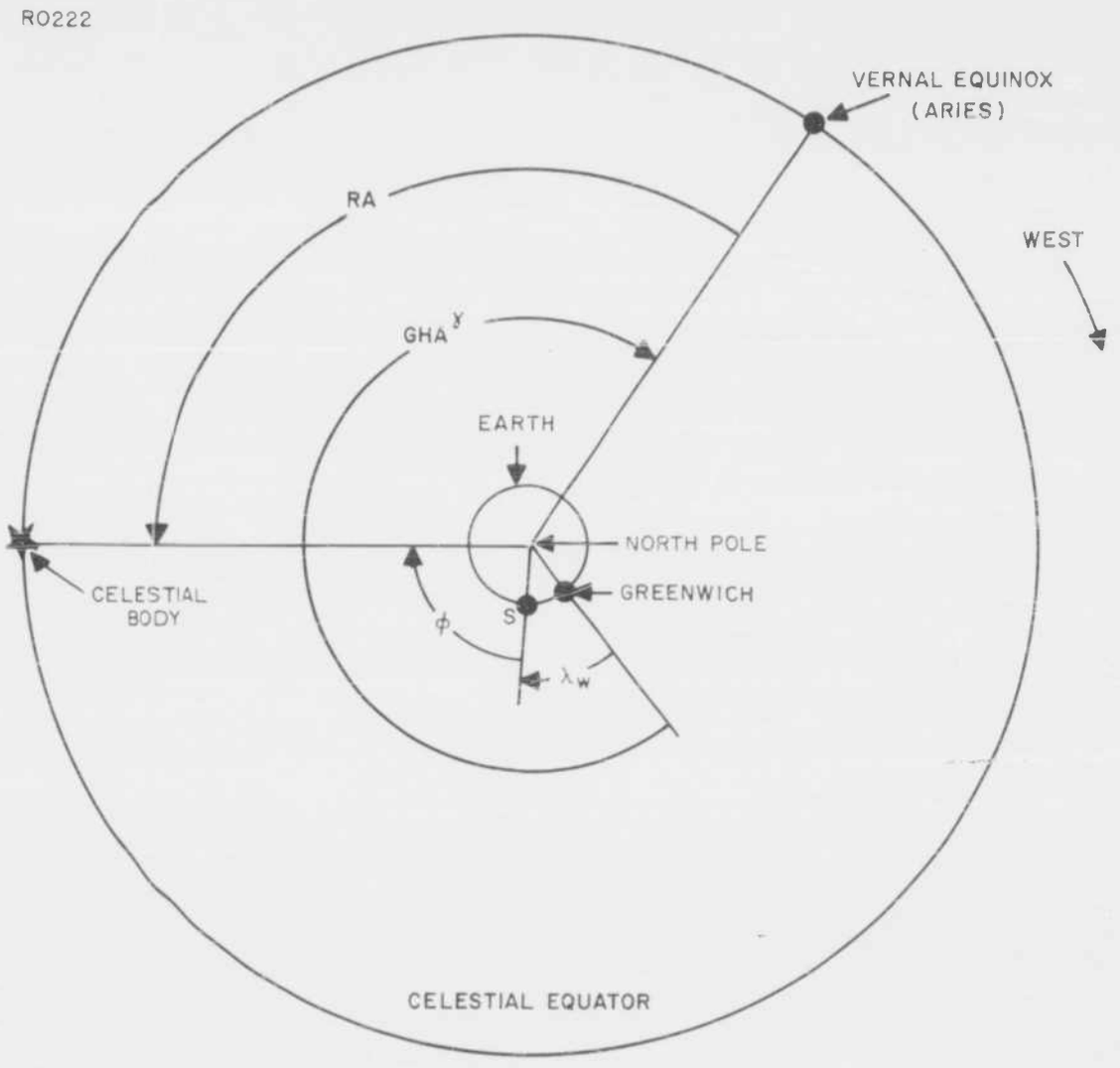

Figure C-2. Celestial Time Coordinates

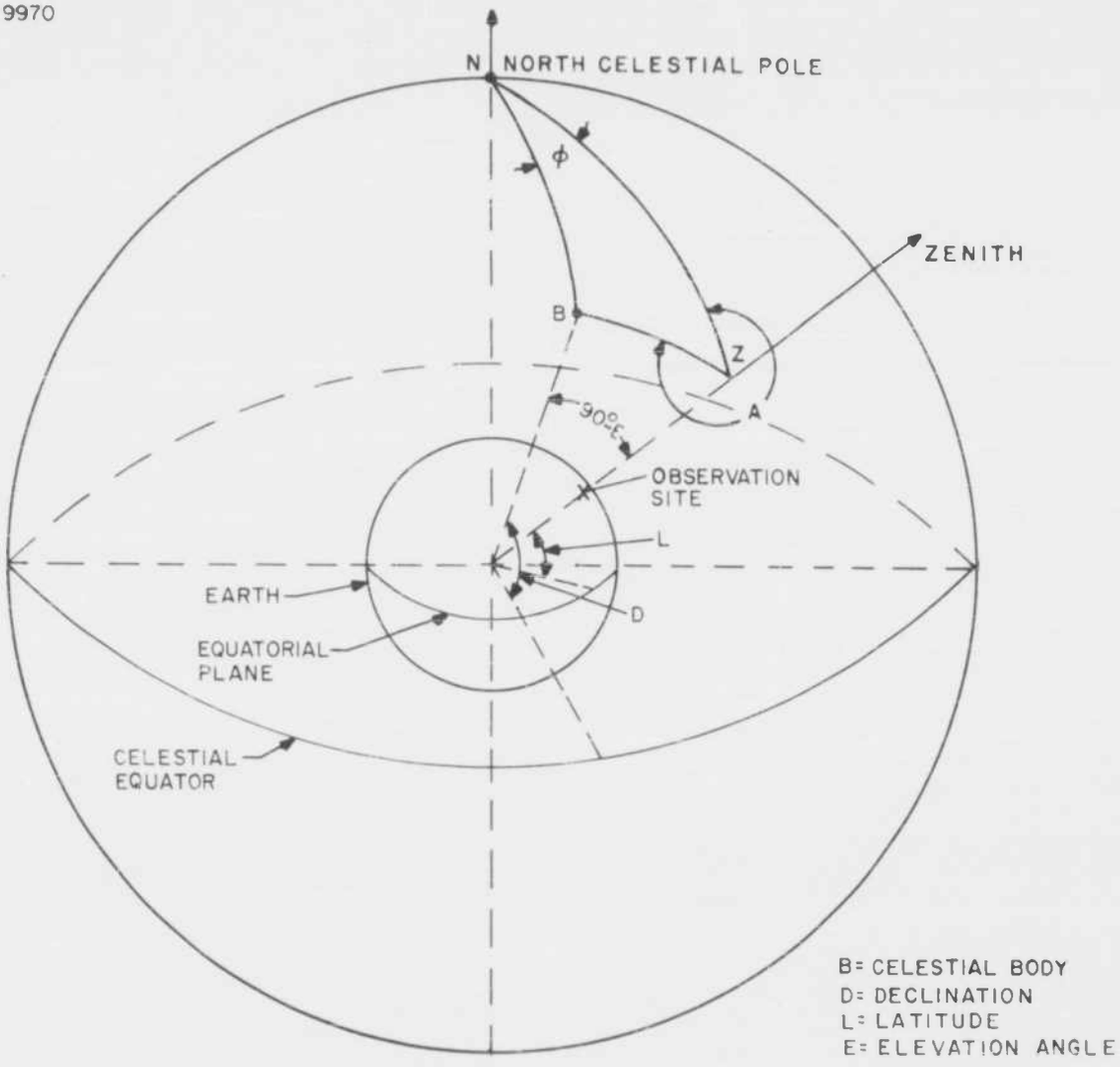

Figure C-3. Astronomical Configuration

According to Equation (C-1), it is seen that the azimuth and elevation orientations of a celestial body are only dependent upon the observer's latitude and the declination. Since the declination of a star is relatively constant, its orbit as observed from a fixed location on the earth's surface, remains the same from day-to-day and is symmetrical about the observer's meridian. With regard to the sun and the moon, however, both orbital paths are not constant since their declinations are variable functions of time.

The duration of time that a celestial body will remain above the horizon at any latitude can be readily determined. Referring to Figure C-3, it can be shown from spherical trigonometry that, in terms of units of time, the azimuth and elevation coordinates can also be expressed by

$$\text{Sin } E = \text{Cos } \emptyset \text{ Cos L Cos D} + \text{Sin L Sin D} \qquad \text{(C-4)}$$

and

$$\text{Tan } A = \frac{\text{Sin } \emptyset}{\text{Tan D Cos L} - \text{Sin L Cos } \emptyset} \qquad \text{(C-5)}$$

It should be noted that the local hour angle, $\emptyset$, is expressed in sidereal time units and not in solar time. Since the sidereal day is shorter than the solar day, a star will cross an observer's meridian approximately three minutes, 55.91 seconds earlier every day.

The time at which a celestial body such as a star crosses a given angular position can be determined by utilizing Equations (C-4) and (C-5) in conjunction with

$$\emptyset = 360^\circ + GHA^\gamma - RA - \lambda_w \qquad \text{(C-6)}$$

where λ_w is the longitude of the observer measured positive westward. This expression is derivable from Figure C-2. The parameter, GHA^γ, is listed as a function of time of day in the Nautical Almanac.

With regard to determining the time of passage of the moon or the sun, Equation (C-6) is modified to the form

$$\emptyset = GHA - \lambda_w \qquad \text{(C-7)}$$

where GHA, the Greenwich Hour Angle, is, in essence, the local hour angle. This angle, which is also tabulated in the Nautical Almanac, is measured positive westward from Greenwhich meridian.

APPENDIX D

THE GEOMETRY OF THE MOON

According to the theory of Fresnel diffraction as pertaining to physical optics[56], the radius of the n'th Fresnel zone, a_n, is expressed by

$$n \lambda = a_n^2 \left[\frac{1}{S} + \frac{1}{R} \right] \tag{D-1}$$

where λ is the wavelength of the transmitted monochromatic light and S and R are the distances between the diffracting aperture and the light source and the observing screen, respectively.

For a source at infinite distance, the dimension of the n'th zone reduces to

$$a_n = \left[n \lambda R \right]^{1/2} \tag{D-2}$$

With regard to the concept of specular reflection from a smooth spherical surface as applied to the radar problem, the radius of the n'th zone is modified to

$$a_n = \left[\frac{n \lambda R}{2} \right]^{1/2} \tag{D-3}$$

This relationship implies that the transmitter and receiver are situated at the same location and that the target dimensions are large compared to the wavelength of the incident radiation.

A plot of the radius of the Fresnel zones on the surface of the moon at a frequency of 425 megacycles is given in Figure D-1. The average earth-moon separation, R, is assumed to be 385,000 kilometers for this calculation.

The fractional radius of the moon, K, also depicted in Figure D-1, is defined by

$$K = \frac{a_n}{r} \tag{D-4}$$

where r is the radius of the moon.

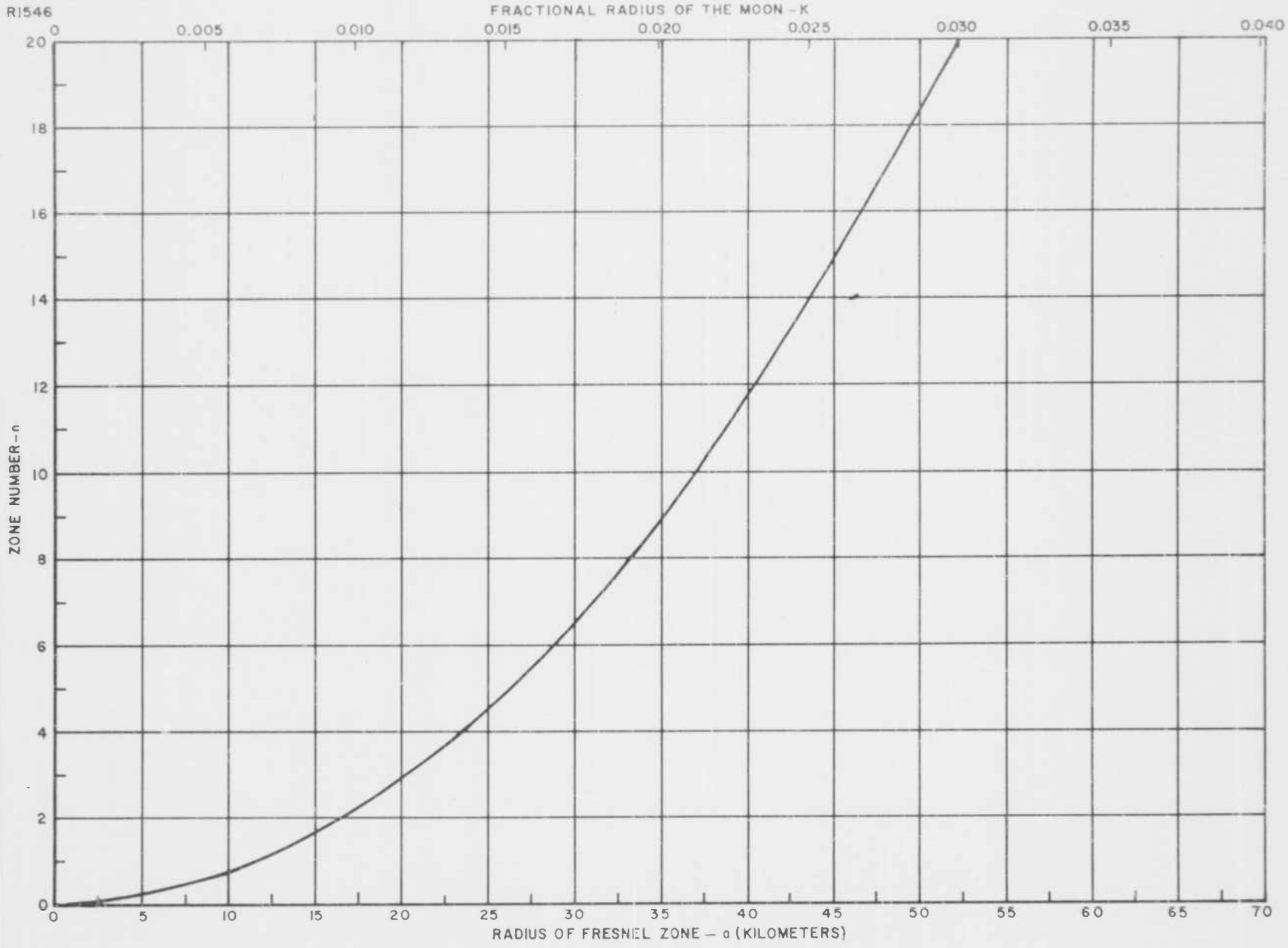

Figure D-1. Radius of Fresnel Zones on the Moon at 425 Mc

For an electromagnetic wave incident on the moon, the depth of penetration into the moon is given by

$$d = \frac{tc}{2} \tag{D-5}$$

where c is the free space velocity and t is the two-way travel time.

As shown in Figure D-2, the radius of the base of the spherical cap, a , defined by the penetration depth, is expressible by

$$a = \left[2\,rd - d^2 \right]^{1/2} \tag{D-6}$$

The angle of incidence, θ, with respect to the normal to the lunar surface is related to the fractional radius by

$$\theta = \mathrm{Sin}^{-1} \left[K \right] \tag{D-7}$$

A plot of the angle, θ, as a function of the travel time of the wave, the penetration depth and the fractional radius of the moon is given in Figure D-3. A photograph of the face of the moon illustrating the functional relationship between these various parameters is shown in Figure D-4.

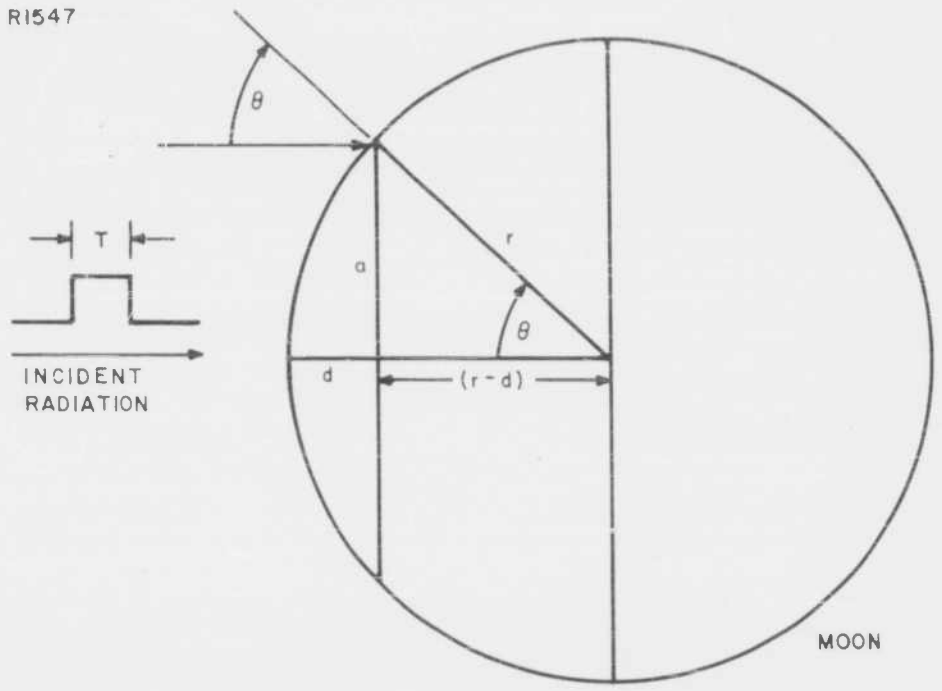

Figure D-2. Lunar Cross Section Geometry

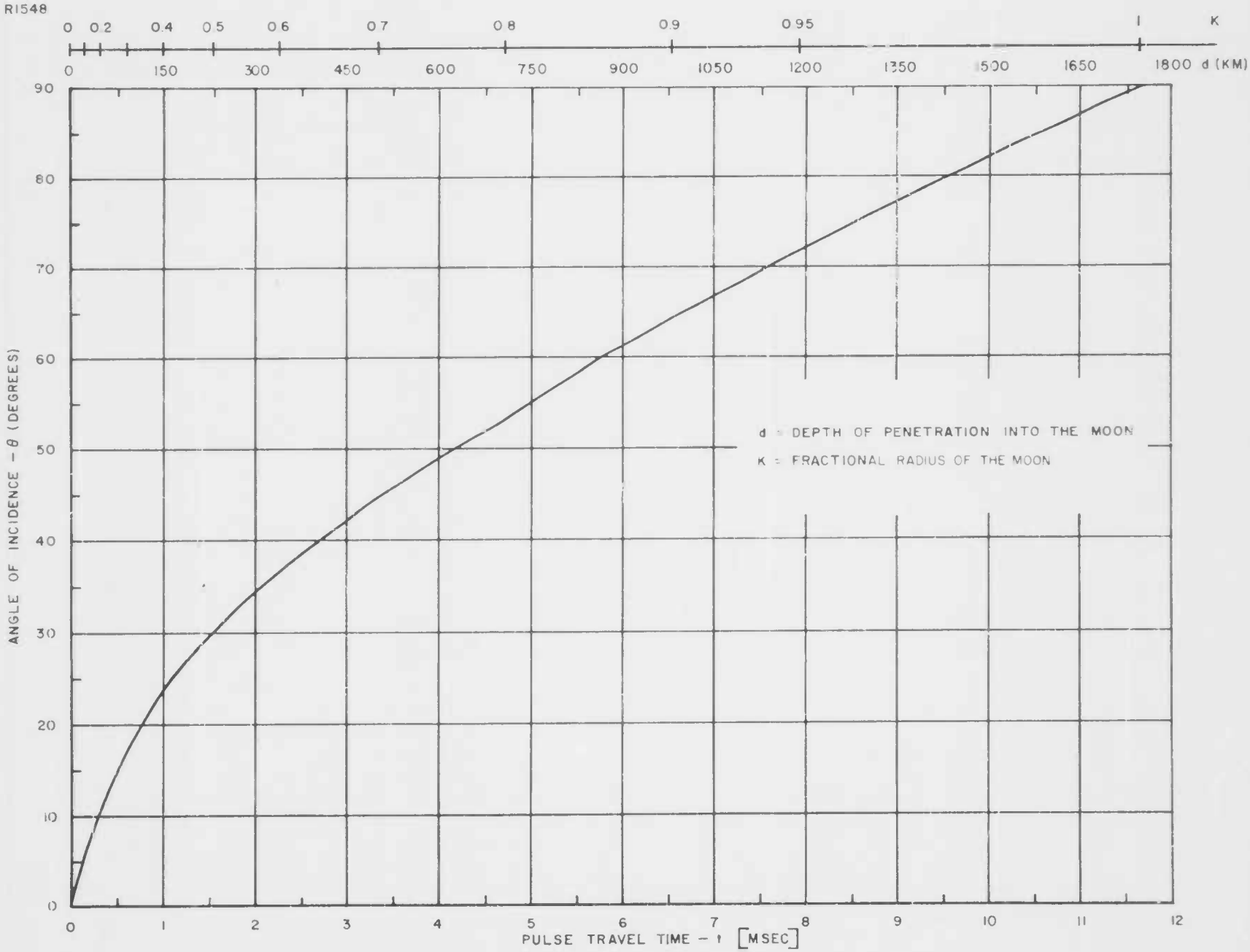

Figure D-3. The Angle of Incidence at the Surface of the Moon as a Function of Pulse Travel Time

Figure D-4. The Lunar Surface

APPENDIX E

AUTOCORRELATION FUNCTION AND POWER DENSITY SPECTRUM

A statistical or random function of time, $y(t)$, such as random noise current, is one in which the value of the function, $y(t)$, does not depend in a definite manner on the independent variable time. The function can best be described in terms of a statistical or probability distribution.

The autocorrelation function is a measure of the average correlation between two values of the same time series. It is similar to the correlation coefficient, often used in statistical analysis, which is a measure of the linearity between two variables.

The autocorrelation function is defined by [57]

$$\psi(\tau) = \lim_{T \to \infty} \frac{1}{T} \int_{-T/2}^{T/2} y(t)\, y\,(t + \tau)\, dt \qquad \text{(E-1)}$$

For a random process which is stationary in time, i.e., the causes of the random fluctuations do not change with time so that the process is independent of the time of origin, $\psi(t)$ is an even function with respect to τ.

The autocorrelation function, in normalized form, can also be written as

$$\psi(\tau) = \frac{\overline{\left[y(t) - \overline{y(t)} \right] \left[y\,(t + \tau) - \overline{y(t)} \right]}}{\overline{\left[y(t) - \overline{y(t)} \right]^2}} \qquad \text{(E-2)}$$

Some of the properties of the normalized autocorrelation function are namely;

$\psi(0) = 1$; $\psi(\tau) \leq \psi(0)$; and for a random phenomenon without the presence of a steady signal, $\psi(\tau) \longrightarrow 0$ as $\tau \to \infty$.

The power density spectrum, $\omega(f)$ of the function $y(t)$ is the Fourier transform of the autocorrelation function. In other words,

$$\omega(f) = \int_{-\infty}^{\infty} \psi(\tau)\, e^{-j\,\omega\,\tau} d\tau \qquad \text{(E-3)}$$

and similarly the autocorrelation function is derived from the Fourier transform of the power density spectrum.

In simpler form, the relationship between $\psi(\tau)$ and $\omega(f)$ can be expressed in terms of Fourier cosine transform by

$$\psi(\tau) = 2\int_{o}^{\infty} \omega(f) \operatorname{Cos} 2\pi f\tau \, df \qquad \text{(E-4)}$$

and

$$\omega(f) = 2\int_{o}^{\infty} \psi(\tau) \operatorname{Cos} 2\pi f\tau \, d\tau \qquad \text{(E-5)}$$

With reference to the analysis of the amplitude versus time function of lunar echoes, the resultant signal reflected from the surface of the moon undergoes a rapid fluctuation due to libration. Since the lunar libration rate changes continuously throughout the orbit, a statistical description of the amplitude record obtained at one particular time, is therefore, only valid for one portion of the orbit.

Radar data are usually acquired at equally spaced time intervals which are dependent upon the pulse repetition frequency of the transmitted signal. The autocorrelation function for this form of a discrete time series can be computed by [57]

$$\psi(r) = \frac{1}{n-rh} \sum_{i=o}^{n-rh} X_i \; X_{i+rh} \qquad \text{(E-6)}$$

where $X_o, X_1, \ldots X_n$ is the time series, and $r = 0,1 \ldots m$ where $mh < n$. The lag interval $\Delta\tau = h\,\Delta t$ for an integer $h > o$ where Δt is the time interval between adjacent values.

The computation of the power density spectrum can be represented by

$$V(r) = \Delta\tau \left[\psi(0) + 2 \sum_{i=1}^{m-1} \psi(i) \operatorname{Cos} \frac{i\,r\pi}{m} + \psi(m) \operatorname{Cos} r\pi \right] \qquad \text{(E-7)}$$

where $V(r)$ is the raw estimate of the smoothed power density at the nominal frequency $r/(2\,m\,\Delta t)$.